ANALYSIS OF COMPRESSIBLE AND INCOMPRESSIBLE FLOWS THROUGH SEE-THROUGH LABYRINTH SEALS

A Thesis

by

JENG WON WOO

Submitted to the Office of Graduate Studies of
Texas A&M University
in partial fulfillment of the requirements for the degree of

MASTER OF SCIENCE

May 2011

Major Subject: Mechanical Engineering

ANALYSIS OF COMPRESSIBLE AND INCOMPRESSIBLE FLOWS THROUGH SEE-THROUGH LABYRINTH SEALS

A Thesis

by

JENG WON WOO

Submitted to the Office of Graduate Studies of
Texas A&M University
in partial fulfillment of the requirements for the degree of

MASTER OF SCIENCE

Approved by

Chair of Committee,	Gerald L. Morrison
Committee Members,	Michael B. Pate
	Hamn-Ching Chen
Head of Department,	Dennis O'Neal

May 2011

Major Subject: Mechanical Engineering

ABSTRACT

Analysis of Compressible and Incompressible Flows Through See-through Labyrinth Seals.

(May 2011)

Jeng Won Woo, B.S., Yonsei University, Republic of Korea

Chair of Advisory Committee: Dr. Gerald L. Morrison

The labyrinth seal is a non-contact annular type sealing device used to reduce the internal leakage of the working fluid which is caused by the pressure difference between each stage in a turbomachine. Reducing the leakage mass flow rate of the working fluid through the labyrinth seal is desirable because it improves the efficiency of the turbomachine.

The carry-over coefficient, based on the divergence angle of the jet, changed with flow parameters with fixed seal geometry while earlier models expressed the carry-over coefficient solely as a function of seal geometry. For both compressible and incompressible flows, the Reynolds number based on clearance was the only flow parameter which could influence the carry-over coefficient. In the case of incompressible flow based on the simulations for various seal geometries and operating conditions, for a given Reynolds number, the carry-over coefficient strongly depended on radial clearance to tooth width ratio. Moreover, in general, the lower the Reynolds number, the larger is the divergence angle of the jet and this results in a smaller carry-over coefficient at lower Reynolds numbers. However, during transition from laminar to turbulent, the carry-over coefficient reduced initially and once the Reynolds number attained a critical value, the carry-over coefficient increased again. In the case of compressible flow, the carry-over coefficient had been slightly increased if radial clearance to tooth width ratio and radial clearance to tooth pitch ratio were increased. Further, the carry-

over coefficient did not considerably change if only radial clearance to tooth width ratio was decreased.

The discharge coefficient for compressible and incompressible flows depended only on the Reynolds number based on clearance. The discharge coefficient of the tooth in a single cavity labyrinth seal was equivalent to that in a multiple tooth labyrinth seal indicating that flow downstream had negligible effect on the discharge coefficient. In particular, for compressible fluid under certain flow and seal geometric conditions, the discharge coefficient did not increase with an increase in the Reynolds number. It was correlated to the pressure ratio, Pr. Moreover, it was also related to the fact that the flow of the fluid through the constriction became compressible and the flow eventually became choked.

At low pressure ratios (less than 0.7), Saikishan's incompressible model deviated from CFD simulation results. Hence, the effects of compressibility became significant and both the carry-over coefficient compressibility factor and the discharge coefficient compressibility factor needed to be considered and included into the leakage model.

The carry-over coefficient compressibility factor, φ, had two linear relationships with positive and negative slopes regarding the pressure ratios. This result was not associated with the seal geometry because the seal geometry ratios for each instance were located within the nearly same ranges. Further, the φ-Pr relationship was independent of the number of teeth regardless of single and multiple cavity labyrinth seals.

The discharge coefficient compressibility factor, ψ, was a linear relationship with pressure ratios across the tooth as Saikishan predicted. However, in certain flow and seal geometric conditions, Saikishan's model needed to be modified for the deviation appearing when the pressure ratios were decreased. Hence, a modified ψ-Pr relationship including Saikishan's model was presented in order to compensate for the deviation between the simulations and his model.

DEDICATION

To my parents, for their support, love, and faith

Out of the night that covers me,
Black as the pit from pole to pole,
I thank whatever gods may be
For my unconquerable soul.

In the fell clutch of circumstance
I have not winced nor cried aloud.
Under the bludgeoning of chance
My head is bloody, but unbowed.

Beyond this place of wrath and tears
Looms but the Horror of the shade,
And yet the menace of the years
Finds and shall find me unafraid.

It matters not how strait the gate,
How charged with punishments the scroll,
I am the master of my fate:
I am the captain of my soul."

– Invictus, William Ernest Henry (1849–1903)

ACKNOWLEDGEMENTS

I would like to deeply express my gratitude and appreciation to Dr. Gerald L. Morrison for providing me with fundamental ideas, considerate guidance, and authentic inspiration to make this thesis a priority. I am also grateful to Dr. Michael B. Pate and Dr. Hamn-Ching Chen for serving on my committee and for their precious guidance and support. Moreover, I would especially like to acknowledge thanks from the bottom of my heart to my parents for their ceaseless support, everlasting love, and genuine belief in me.

NOMENCLATURE

A	Clearance area, πDc
c	Radial clearance, *m*
$C_d^{1\ tooth}$	Discharge coefficient for seal with a single tooth
C_d	Discharge coefficient for given tooth of multi tooth labyrinth seal
D	Shaft diameter, *m*
h	Tooth height, *m*
k	Ratio of specific heats, C_p/C_v
L	Axial length of the seal, *m*
Ma	Mach number
$\dot{m}$	Mass flow rate of leakage flow, *kg/s*
P_i	Seal inlet pressure, *Pa*
P_e	Seal outlet pressure, *Pa*
p_i	Tooth inlet pressure, *Pa*
p_e	Tooth outlet pressure, *Pa*
Pr	Pressure ratio, p_e/p_i
Re	Reynolds number based on clearance, $\frac{\dot{m}}{\mu\pi D}$
s	Tooth pitch, *m*
w	Tooth width, *m*
x	Axial distance along seal, *m*
z	Ratio of discharge coefficient of a tooth following a cavity to the discharge coefficient of a single tooth with same tooth width and clearance with no preceding cavity at the same Reynolds number

α	Flow coefficient
β	Divergence angle of jet, *radians*
γ	Kinetic energy carry-over coefficient
ε	Dissipation of turbulent kinetic energy
κ	Turbulent kinetic energy
μ	Dynamic viscosity, *Pa-s*
ρ_i	Fluid density at seal inlet, kg/m^3
ρ	Fluid density at tooth inlet, kg/m^3
φ	Carry-over coefficient compressibility factor
χ	Percentage of kinetic energy carried over
ψ	Discharge coefficient compressibility factor

TABLE OF CONTENTS

Page

LIST OF FIGURES

FIGURE Page

FIGURE Page

FIGURE Page

FIGURE Page

FIGURE Page

FIGURE Page

FIGURE Page

LIST OF TABLES

CHAPTER I

INTRODUCTION

The labyrinth seal is a non-contact annular type sealing device used to reduce the internal leakage of the working fluid which is caused by the pressure difference between each stage in a turbomachine. Reducing the leakage mass flow rate of the working fluid through the labyrinth seal is desirable because it improves the efficiency of the turbomachine. It is also necessary to optimize the shape of the labyrinth seal to increase the flow resistance. In order to increase the flow resistance, it is best to minimize the clearance under each tooth, form various type of unevenness on the surface of the seal, and make the geometry of the seal complex.

The labyrinth seal consists of the rotor and the stator which includes a number of teeth. The labyrinth seal is the component which can reduce the leakage mass flow rate by throttling and then expanding the flow repeatedly. By arranging the sharp teeth in regular sequence on the stator, the labyrinth seal is made up of the constrictions under each tooth and the cavities in the path of the leakage as in Figure 1.1. When the leakage proceeds through the constriction it is throttled and in the section of cavity the decompression happens. While this behavior continues iteratively, the leakage mass flow rate consequently lessens because its pressure becomes equal with the pressure at the labyrinth seal outlet.

This thesis follows the style of Journal of Turbomachinery.

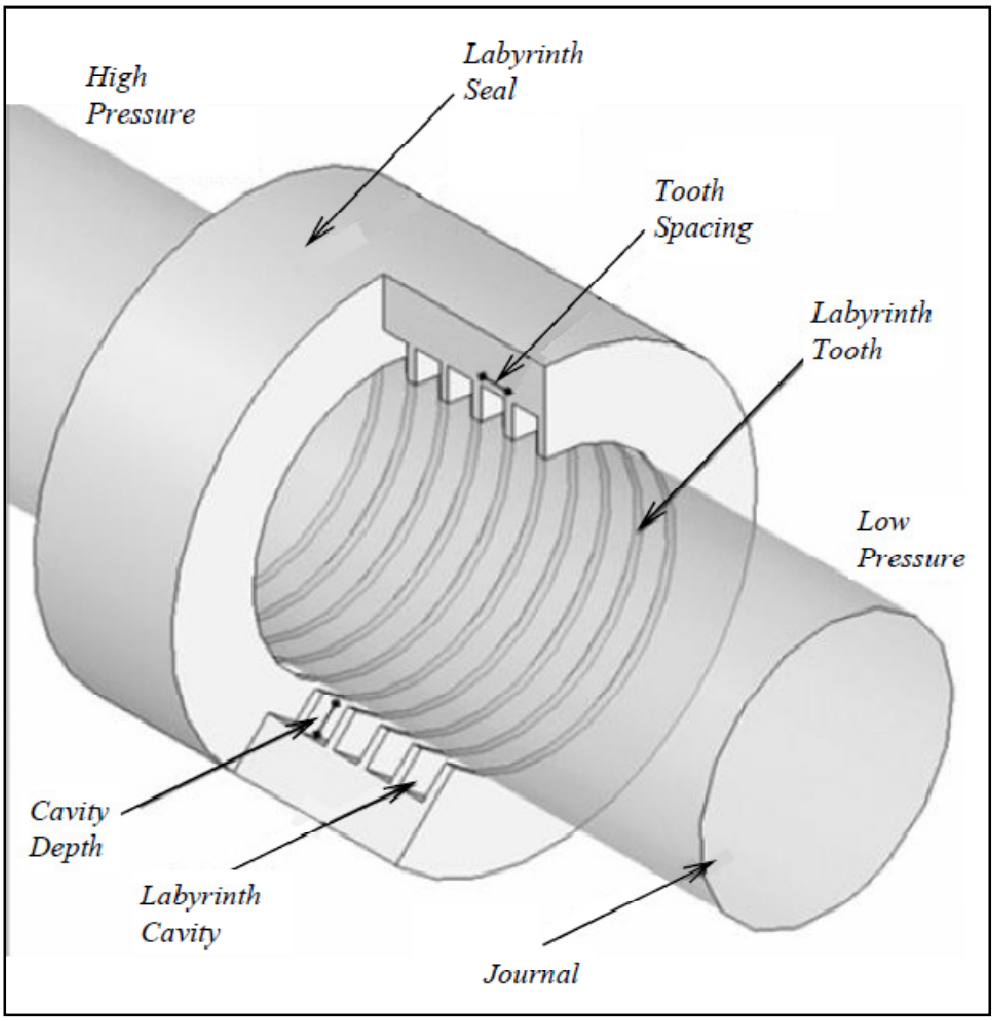

Figure 1.1. See-through labyrinth seal [1]

There are, as in Figure 1.2, basically three types of labyrinth seals: the see-through labyrinth seal which is the simplest type, the stepped labyrinth seal which makes the leakage passage more mazelike, and the staggered labyrinth seal which organizes the teeth on the rotor and stator alternately maintaining the same clearance under the teeth.

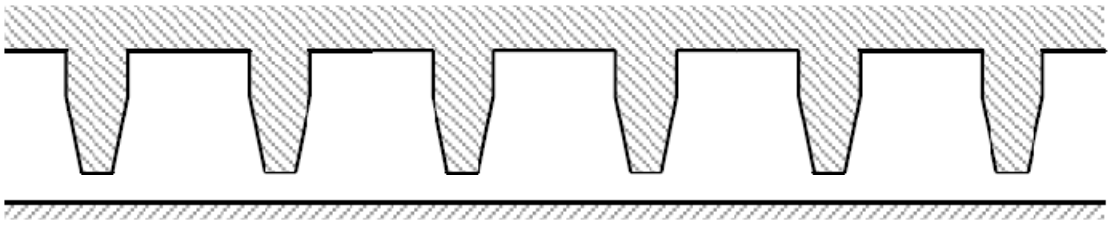

(a) See-through labyrinth seal

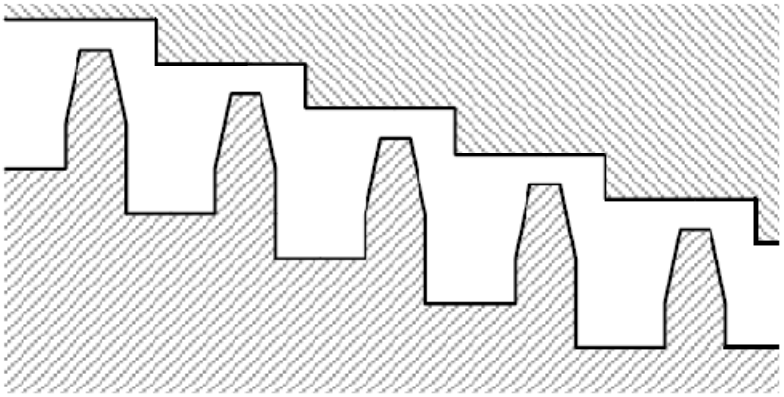

(b) Stepped labyrinth seal

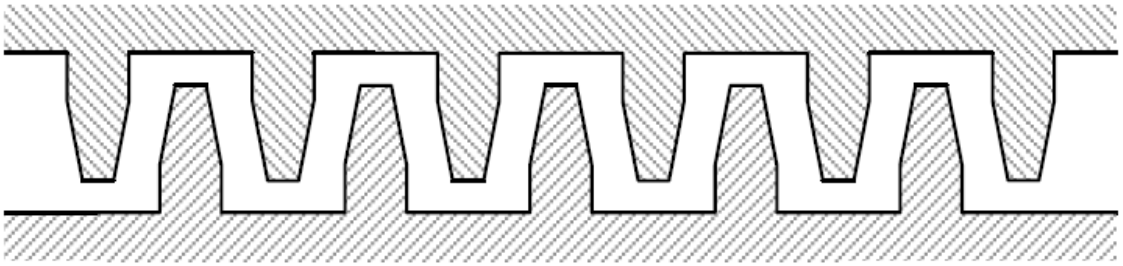

(c) Staggered labyrinth seal

Figure 1.2. Labyrinth seal configurations [1]

Among these types of the labyrinth seals, the see-through labyrinth seal is the most manufactured and assembled when compared with the stepped labyrinth seal and the staggered labyrinth seal. It is generally employed as a part of the turbomachine.

The carry-over coefficient can be defined as the portion of the undissipated kinetic energy in the cavity of the fluid exiting the seal clearance that is convected to the next cavity. It can be measured according to the divergence angle of the jet, β as defined in Figure 1.3. In other words, the carry-over coefficient stands for the turbulent dissipation of the kinetic energy which takes place in each cavity. The relationship of the carry-over coefficient, γ, and the percentage of the kinetic energy carried over into the next cavity, χ, is provided by Hodkinson [2].

$$\gamma^2 = \frac{1}{1-\chi} \tag{1.1}$$

$$tan\,\beta = c\frac{(1-\chi)}{\chi s} \tag{1.2}$$

$$\chi = \frac{c}{c + s\,tan\,\beta} \tag{1.3}$$

The rate of seal leakage is dependent upon how much energy is dissipated in each cavity. Therefore, one needs to study the discharge coefficient and its relationship to the carry-over coefficient in order to comprehend the influence of the carry-over coefficient. The discharge coefficient can be defined as both the flow losses occurring when the fluid flows through the cavity and as the frictional losses arising when the fluid flows under the tooth. The discharge coefficient can be expressed in terms of the mass flow rate, $\dot{m}$, the clearance area, $A(=\pi Dc)$, the fluid density, ρ, and the inlet and the outlet pressures across the tooth, p_i and p_e.

$$C_d = \frac{\dot{m}}{A\sqrt{2\,\rho\,(p_i - p_e)}} \tag{1.4}$$

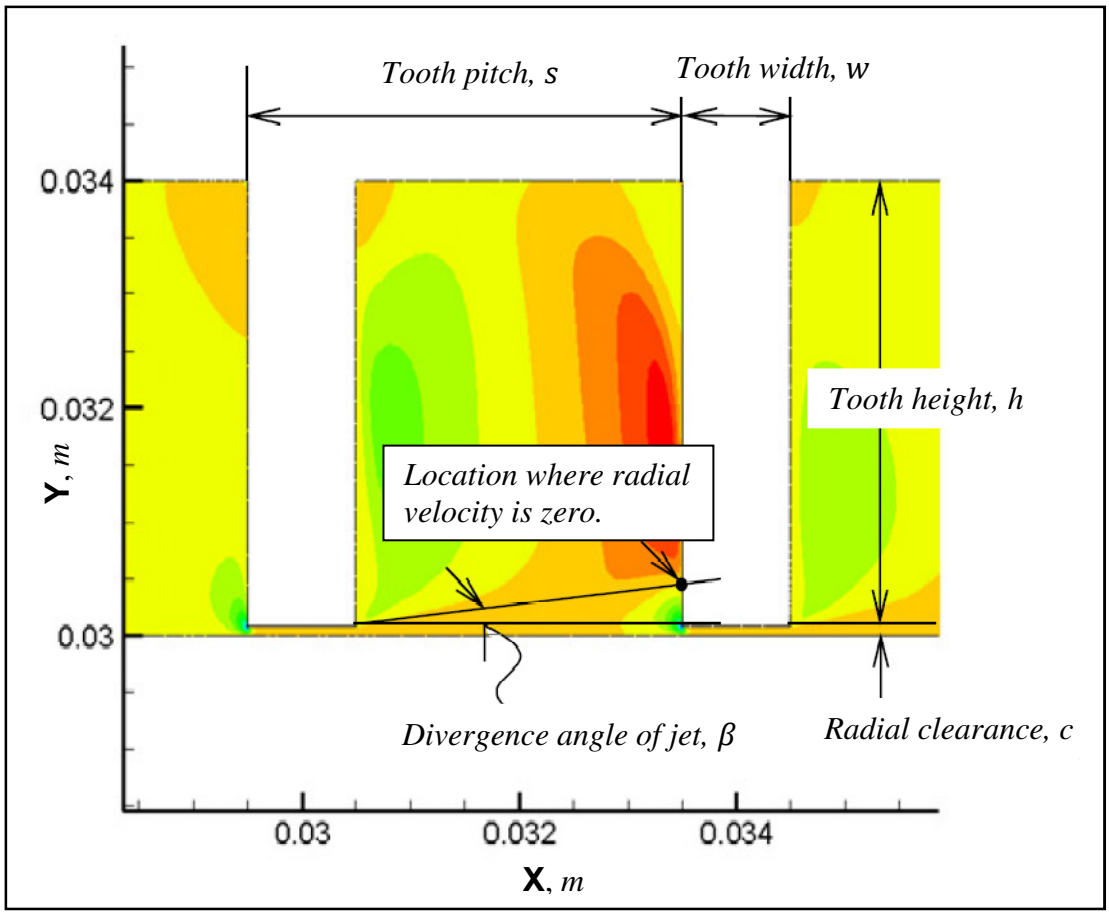

Figure 1.3. Flow pattern and geometry within labyrinth seal cavity

This thesis considers both compressible and incompressible fluids and compares them by using FLUENT CFD (Computational Fluid Dynamics) simulations in order to predict the leakage mass flow rate according to the various geometric configurations in the teeth of the see-through labyrinth seals. These labyrinth seals are non-contact annular type sealing devices that reduce the internal leakage mass flow rate of the working fluid. Also notable is the fact that air is utilized as the compressible fluid and water is employed as the incompressible fluid.

CHAPTER II

REVIEW OF LEAKAGE MODELS

Alford [3] first presented a seal leakage prediction technique by using the bulk flow model which employs the concept of mean velocity. He assumed that the velocity profile remained constant along the direction of flow in a labyrinth seal, i.e. the velocity gradient is zero. This bulk flow model has been utilized due to its small computational time. However, since the bulk flow model does not consider the consummate governing equations derived from the Navier-Stokes equations and the turbulence model, the model cannot predict the leakage mass flow rate in the various geometric configurations in the teeth.

Martin [4] attempted to attain the required pressure drop in order to fulfill more accurate estimation of the leakage mass flow rate through the labyrinth seal. However, he ignored the effect of the kinetic energy carry-over and his model is only applicable to incompressible flows. Moreover, his model was not verified against any experimental data and is completely based on certain theoretical assumptions.

$$\dot{m} = \frac{A\,P_i}{\sqrt{RT_i}}\sqrt{\frac{1-(p_e/p_i)^2}{n-ln(p_e/p_i)}} \tag{2.1}$$

Egli [5] modified Martin's model to evaluate the leakage mass flow rate through a labyrinth seal. He provided rational analytical treatment of flow in labyrinth seals based on the flow characteristics of a sharp-edged orifice. He also demonstrated how the effect of kinetic energy carried over from one cavity to the next cavity could be treated

rationally. As steam flows through a labyrinth seal, it passes through a series of expansion-compression processes resulting in a pressure drop from the inlet to the outlet. After each throttling process, a small portion of the kinetic energy of the steam jet is converted to pressure energy while the rest is dissipated into heat. Remaining kinetic energy will pass through the subsequent cavity and is represented by $\gamma_{emperical}$.

$$\dot{m} = \gamma_{emperical} \frac{A\ P_i}{\sqrt{RT_i}} \sqrt{\frac{1-(p_e/p_i)^2}{n - ln(p_e/p_i)}} \tag{2.2}$$

Hodkinson [2] modified Egli's model based on a semi-empirical approach. His approach relied on the geometry of the gas jet while Egli employed an empirical approach to explain kinetic energy carry-over. The fluid jet from the upstream tooth expands conically and diverges onto the downstream tooth forming a small angle, the divergence angle of the jet. This jet collides with the downstream tooth and re-circulates in the cavity dissipating the kinetic energy of the fluid while the rest of it is carried over to the next cavity. Hodkinson developed a model for the carry-over coefficient as a function of the real geometry.

$$\dot{m} = \gamma \frac{A\ P_i}{\sqrt{RT_i}} \sqrt{\frac{1-(p_e/p_i)^2}{n - ln(p_e/p_i)}} \tag{2.3}$$

$$\gamma = \sqrt{\frac{1}{1 - [(n-1)/n]\left[(c/s)/\left((c/s) + 0.02\right)\right]}} \tag{2.4}$$

Vermes [6] obtained his expression for kinetic energy carry-over by combining Martin's model. His kinetic energy carry-over was developed on the basis of the boundary layer theory.

$$\dot{m} = \gamma \frac{A\, P_i}{\sqrt{RT_i}} \sqrt{\frac{1-(p_e/p_i)^2}{n - ln(p_e/p_i)}} \tag{2.5}$$

$$\gamma = \sqrt{\frac{1}{1-\alpha}} \tag{2.6}$$

$$\alpha = \frac{8.52}{(s-w)/c + 7.23} \tag{2.7}$$

Neumann [7] developed a model for the prediction of the leakage mass flow rate based on the empirical approach. His model includes the semi-empirical flow coefficient determined from Chaplygin's formula, which is provided in Equation 2.9, as defined by Gurevich [8]. This parameter indicates further contraction of the flow after it has proceeded through the plane of the physical constriction. Since he considered each throttle independently, his leakage mass flow rate was expressed as a function of the upstream and downstream pressures through a single tooth.

$$\dot{m} = Cf_i \gamma_i A \sqrt{\frac{p_i^2 - p_{i+1}^2}{RT}} \tag{2.8}$$

$$Cf_i = \frac{\pi}{\pi + 2 - 5\beta_i + 2\beta_i^2} \tag{2.9}$$

$$\beta_i = \left(\frac{p_i}{p_{i+1}}\right)^{\frac{k-1}{k}} - 1 \tag{2.10}$$

$$\gamma_i = \sqrt{\frac{N}{N\,(1-\alpha_i) + \alpha_i}} \tag{2.11}$$

$$\alpha_i = 1 - \frac{1}{\left(1 + 16.6\,(c/s)\right)^2} \tag{2.12}$$

Zimmerman and Wolff [9] analyzed the leakage mass flow rate through a see-through labyrinth seal to suggest their calculation method which dealt with the first tooth individually. Their experimental data agreed with their analytical model. Their model applied St. Venant equation [10] to the first constriction and looks like Egli's model which modified Martin's model to the remaining part of the seal in order to compute carry-over coefficient.

$$\dot{m} = \frac{A\,P_i}{\sqrt{kRT_i}}\sqrt{\frac{2k^2}{k-1}\left(\left(\frac{P_{i+1}}{P_i}\right)^{\frac{2}{k}} - \left(\frac{P_{i+1}}{P_i}\right)^{\frac{k+1}{k}}\right)} \qquad for\ i = 1 \tag{2.13}$$

$$\dot{m} = \gamma_i \frac{A\,P_i}{\sqrt{RT_i}}\sqrt{\frac{1-(P_{i+1}/P_i)^2}{n - ln(P_{i+1}/P_i)}} \qquad for\ i > 1 \tag{2.14}$$

Childs and Scharrer [11] applied Neumann's model with non-constant kinetic energy carry-over coefficient developed from Vermes's model.

$$\dot{m} = Cf_i\gamma_i A\sqrt{\frac{p_i^2 - p_{i+1}^2}{RT}} \tag{2.15}$$

$$Cf_i = \frac{\pi}{\pi + 2 - 5\beta_i + 2\beta_i^2} \tag{2.16}$$

$$\beta_i = \left(\frac{p_i}{p_{i+1}}\right)^{\frac{k-1}{k}} - 1 \tag{2.17}$$

$$\gamma = \sqrt{\frac{1}{1-\alpha}} \tag{2.18}$$

$$\alpha = \frac{8.52}{(s-w)/c + 7.23} \tag{2.19}$$

Esser and Kazakia [12] also worked with Neumann's model but applied a constant semi-empirical flow coefficient unlike in Chaplygin's model. They studied motion of fluid under each tooth and then concluded that their model with the constant semi-empirical flow coefficient presented more precise results than Chaplygin's model.

$$\dot{m} = Cf_i \gamma_i A \sqrt{\frac{p_i^2 - p_{i+1}^2}{RT}} \tag{2.20}$$

$$Cf_i = 0.716 \tag{2.21}$$

$$\gamma_i = \sqrt{\frac{N}{N\,(1-\alpha_i) + \alpha_i}} \tag{2.22}$$

$$\alpha_i = 1 - \frac{1}{\left(1 + 16.6\,(c/s)\right)^2} \tag{2.23}$$

Gamal [1] described that these models were appropriate under certain flow conditions and were not applicable under certain other flow conditions. He argued that the fundamental assumption that the carry-over coefficient is independent of the flow conditions was not justified. Gerald L. Morrison and Adnan Al-Ghasem [13] discovered, while using Hodkinson' model to compute carry-over coefficients for windback seals, the carry-over coefficient did not remain constant for the seal geometry as suggested by Hodkinson but varied according to the flow conditions such as pressure ratio. Their study contrasted the existing assumption that the carry-over coefficient is a function of seal geometry only.

Saikishan [14], [15], [16], [17] developed his model by employing the models for the carry-over coefficient and the discharge coefficient. His model was developed to

predict not only the leakage mass flow rate for incompressible flow but also the pressure distribution across the seal provided that the inlet and the outlet pressures are known. His model can also be used for gases, provided $Pr > 0.7$. For such cases, the density for each cavity is calculated based upon the cavity pressure by applying the ideal gas equation. The pressure and density of the fluid upstream of a tooth is also used to compute the pressure drops across the tooth.

$$\dot{m} = \psi C_{d_n} A\sqrt{2\rho_n(p_n - p_{n+1})} \qquad (1 \le n \le N) \tag{2.24}$$

for $0.0075 < c/s < 0.0375$, $0.0075 < w/s < 0.5$, $2.67 < w/c < 66.67$,

$0.75 < h/s < 4$, *and* $250 < Re < 15000$

$$C_{d_n} = C_d^{1\,tooth} \qquad for\ first\ constriction \qquad (n = 1) \tag{2.25}$$

$$C_{d_n} = C_d^{1\,tooth}(0.925\,\gamma^{0.861}) \qquad for\ subsequent\ teeth \qquad (n > 1) \tag{2.26}$$

$$C_d^{1\,tooth} = \frac{0.7757 - 0.002051(w/c)}{(1 + 44.86(w/c)/Re)^{0.2157}} \tag{2.27}$$

$$\gamma = \left(1 - 6.5\,(c/s) - 8.638(c/s)(w/s)\right)(Re + R_0)^{\left(2.454(c/s)+2.268(c/s)(w/s)^{1.673}\right)} \tag{2.28}$$

$$R_0 = \left(1 - 6.5\,(c/s) - 8.638(c/s)(w/s)\right)^{\left(-\frac{1}{2.454(c/s)+2.268(c/s)(w/s)^{1.673}}\right)} \tag{2.29}$$

$$Re = \frac{\dot{m}}{\mu\pi D} \tag{2.30}$$

$$\psi = 0.558\left(\frac{p_{n+1}}{p_n}\right) + 0.442 \tag{2.31}$$

CHAPTER III

RESEARCH OBJECTIVES

The objective of this thesis is to analyze both compressible and incompressible flows and then collate them by using CFD (Computational Fluid Dynamics) simulations in order to predict the leakage mass flow rate according to the various geometric configurations in the teeth of the see-through labyrinth seals. These labyrinth seals are non-contact annular type sealing devices used to reduce the internal leakage of the working fluid. The main aims of this current thesis will be accomplished by the following:

1. Perform the simulations of the leakage mass flow rate through a labyrinth seal at different Reynolds numbers and geometric conditions by using the FLUENT program.
2. Study the carry-over coefficient in a cavity with different Reynolds numbers to assess the effects of various flow and geometric conditions.
3. Evaluate the effects of the geometric components such as radial clearance, tooth height, tooth pitch, and tooth width.
4. Research the discharge coefficient for a tooth with different Reynolds numbers to evaluate the effects of diverse flow and geometric conditions.
5. Extend the above results achieved from a single generic cavity to a labyrinth seal with multiple cavities.
6. Obtain the carry-over coefficient compressibility factor, which is determined as the ratio of the carry-over coefficient of a cavity that includes effect of kinetic

energy carry-over for compressible flow to that for incompressible flow with the same geometry and at the same Reynolds number.

7. Obtain the discharge coefficient compressibility factor, which is determined as the ratio of the discharge coefficient for compressible flow to the incompressible flow at the same Reynolds number regarding the pressure ratio across the tooth.
8. Analyze the above results against an earlier model for the carry-over coefficient and the discharge coefficient which can predict the leakage mass flow rate and the pressure distribution across the different cavities for the seal of a given seal geometry and the inlet and the outlet pressures.

CHAPTER IV

COMPUTATIONAL METHOD

The studies on the flow in a turbomachine are recently on the rise by using CFD (Computational Fluid Dynamics) methods thanks to the development of both computer performance and commercial CFD programs. The results based upon CFD simulations are able to show slight disagreement with those founded on experimental data. However, the CFD method makes it possible to generalize the flow inside labyrinth seals.

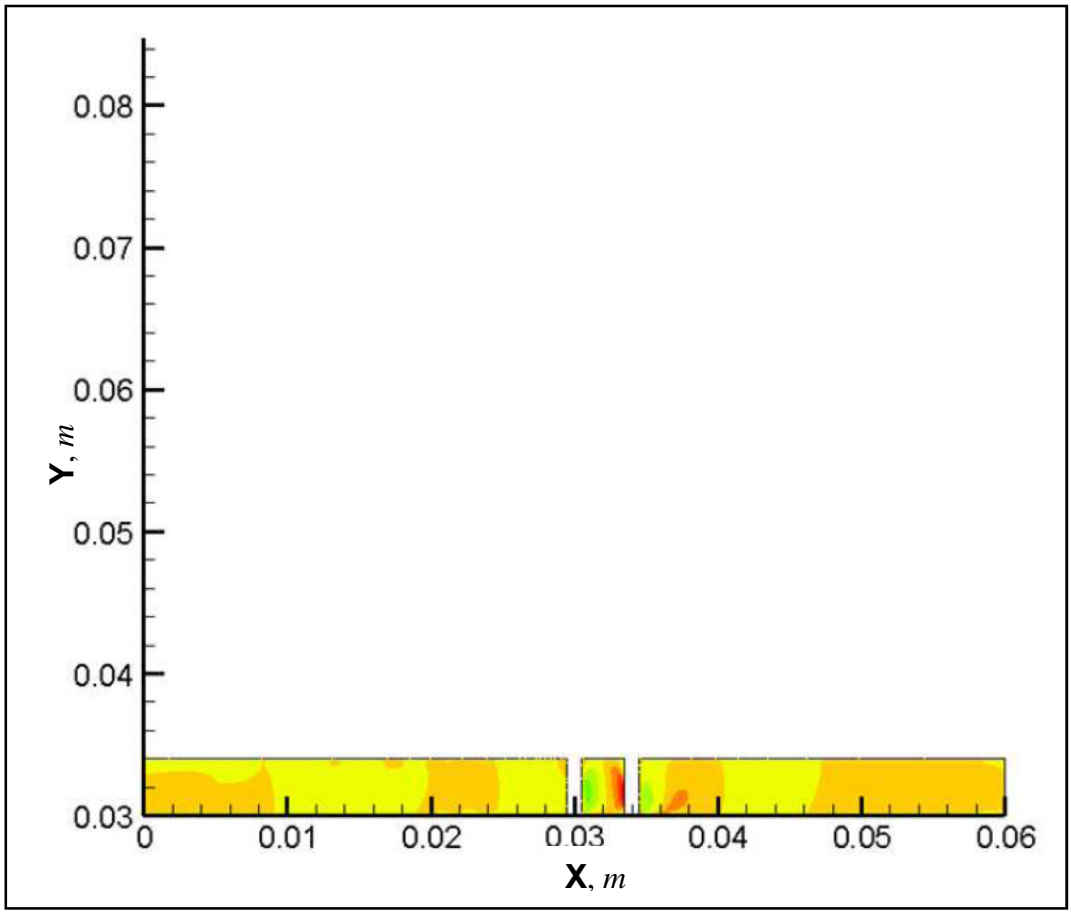

Figure 4.1. Seal geometry and lengths of inlet and outlet

Figure 4.1 shows a tooth configuration and its cavity of a labyrinth seal selected for this study in order to help comprehend the characteristics of the flow through the labyrinth seal. It is also shown that the lengths of the inlet and the outlet are extended for the purpose of guaranteeing the validity of establishing boundary conditions and the accuracy of the outcomes.

The effects of flow and geometric parameters on the carry-over coefficient and the discharge coefficient are investigated for a generic rectangular cavity, tooth on stator labyrinth seal. A single cavity labyrinth seal with two teeth is analyzed for the initial study and then a multiple cavity labyrinth seal with four teeth is considered in order to extend the application to generally employed labyrinth seals.

It is necessary to acquire solutions of the consummate governing equations derived from the Navier-Stokes equations and the turbulence model in order to exam the flow within the labyrinth seal. Since these derived governing equations are so complicated, it is arduous to find the solutions. This study analyzes the flow in see-through labyrinth seals by employing the widely used computer program FLUENT.

FLUENT, which was developed to analyze numerical models of compressible or incompressible, and 2-D or 3-D flows, is composed of the preprocessor, GAMBIT and the equation solver, FLUENT. This research inspects compressible, incompressible, 2-D (axial-radial), and axisymmetric flow by utilizing the FLUENT program.

The computational mesh, as in Figure 4.2, is much finer in the regions near the stator walls, in the seal clearance region, and near the rotor surface. Morrison and Al-Ghasem [13] demonstrated that for seal analyses, the enhanced wall treatment must be

utilized to obtain accurate prediction of leakage mass flow rate. Further, it is also necessary to place nodes closest to the walls at Y^+ values less than 5 in order to resolve the laminar sublayer.

A grid independence study is performed by observing the mass flow rates predicted for a given pressure ratio for various levels of grid refinement. Figure 4.3 presents that the change in mass flow rate is less than 0.5% when more than 20000 nodes are applied.

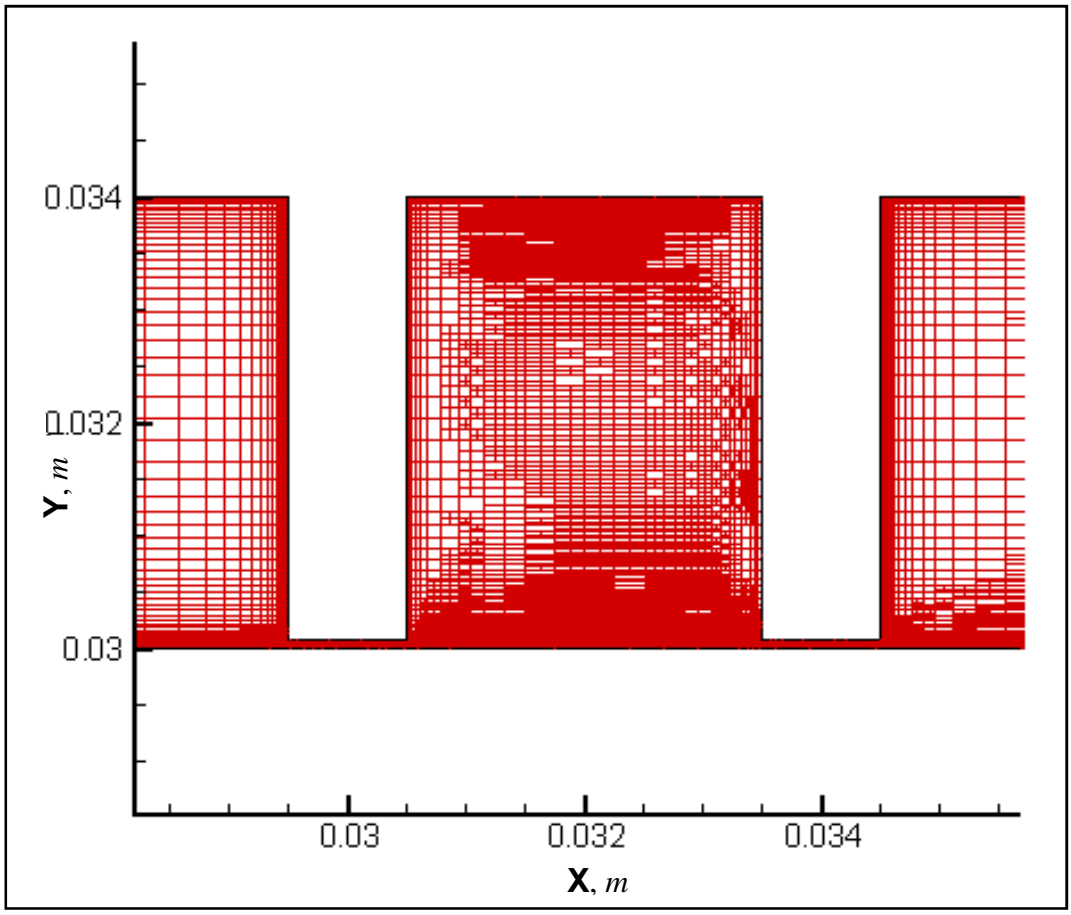

Figure 4.2. Seal geometry and computational mesh

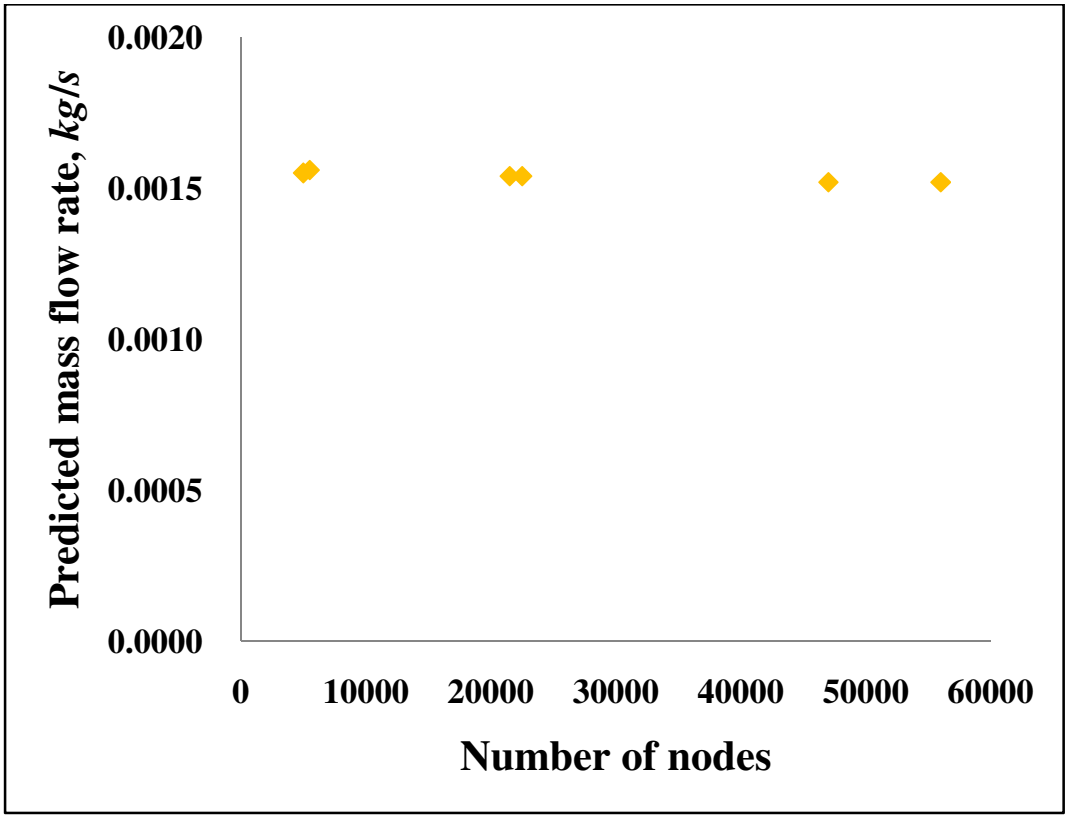

Figure 4.3. Accuracy of mass flow rate prediction with number of nodes (based on Saikishan's studies)

The standard κ-ε turbulence model (see Appendix C) is chosen because it has been proven to accurately simulate the flow through the labyrinth seals compared with experimental data [13]. Another reason for selecting the standard κ-ε turbulence model is that this model has been widely employed for computational analysis of the labyrinth seals in earlier studies [18], [19], [20], [21].

The assessment of convergence tests terminates when residuals have became less than10^{-4}. This research also applies the FVM (Finite Volume Method) (see Appendix D)

utilizing the fully implicit scheme based upon the SIMPLE (Semi-Implicit Method for Pressure Linked Equations) algorithm (see Appendix E).

CHAPTER V

CARRY-OVER COEFFICIENT

DETERMINATION OF CARRY-OVER COEFFICIENT

Hodkinson [2] interpreted the carry-over coefficient, γ, as a function of the divergence angle of the orifice jet, β, which represents the angle of the streamline flowing under the exit of the first tooth parallel to the longitudinal line of the rotor and the streamline re-circulating in the cavity while impinging on the inlet of the second tooth after flowing under the exit of the first tooth. This angle is utilized to calculate the percentage of the kinetic energy carried over, χ, into the next cavity.

$$\gamma^2 = \frac{1}{1-\chi} \tag{5.1}$$

$$tan\,\beta = c\frac{(1-\chi)}{\chi s} \tag{5.2}$$

$$\chi = \frac{c}{c + s\,tan\,\beta} \tag{5.3}$$

In order to determine the divergence angle of the jet, the distance between the exit of the first tooth and the inlet of the second tooth as well as the location where the radial velocity is zero in the collision with the inlet of the second tooth must be measured. Figure 5.1 shows the contour plots of the radial velocity and the method for measuring the divergence angle of the jet. It is necessary to find the position $(x_1,\ y_1)$ at the exit of the first tooth and the position $(x_2,\ y_2)$ at the inlet of the second tooth in order to compute the divergence angle of the jet by employing the definition of the

tangent trigonometric function. Here, the program TECPLOT 360 is used to calculate all the above mentioned parameters.

$$tan\,\beta = \frac{y_2 - y_1}{x_2 - x_1} \tag{5.4}$$

After substituting $tan\,\beta$ from Equation 5.4 into Equation 5.3, the percentage of kinetic energy carried over can be determined. This percentage is then substituted once more into the Equation 5.1 and then the carry-over coefficient is computed.

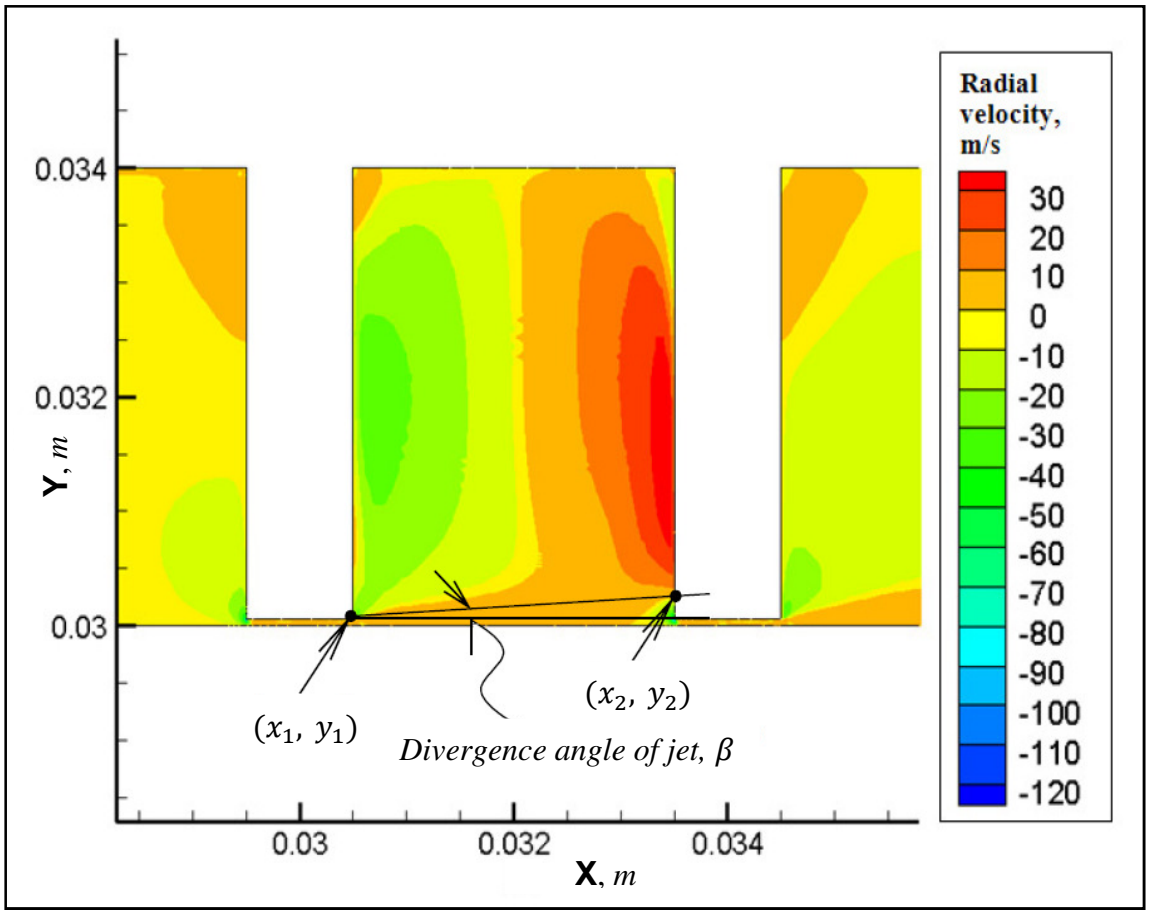

Figure 5.1. Contour plots of radial velocity and measurement of divergence angle of jet

ANALYSIS OF CARRY-OVER COEFFICIENT FOR EACH INSTANCE

In order to isolate the influence of the flow conditions, the labyrinth seal geometry is fixed and then the carry-over coefficients of the compressible and the incompressible flows are calculated. The Reynolds number is utilized as the significant component of the flow parameters, and the following six numbers are selected to analyze the carry-over coefficient for each instance: 100, 200, 500, 1000, 2000, and 5000. For the fixed seal geometry, the mass flow rate is computed for each non-identical Reynolds number by applying the definition of the dimensionless Reynolds number. Next, the carry-over coefficients of the compressible and the incompressible flows corresponding to various geometric configurations in the tooth of the labyrinth seals are compared in order to predict the leakage mass flow rate for the selected instances.

Saikishan [14] found that at low Reynolds numbers, the carry-over coefficient tends to become almost 1.0, which implies that all of the kinetic energy is dissipated in the cavity of the labyrinth seal. According to him, the carry-over coefficient increases with increasing Reynolds number, indicating an ever-increasing amount of kinetic energy which is not dissipated in the cavity but rather convected out of the cavity. This suggests a reduced effectiveness of this seal with increasing Reynolds number.

The definition of the Reynolds number provides the measure of the ratio of the inertial force to the viscous force. Since the section under the tooth can be regarded as a concentric tube annulus, application of this definition to the labyrinth seal reveals that the Reynolds number in the labyrinth seal, which is based on the clearance, is equivalent to the ratio of the inertial force of the jet emerging from under the tooth to the viscous

force under the same tooth. At higher Reynolds numbers, the higher inertial force of the jet and the lower viscous force from under the tooth cause the smaller divergence angle of the jet to generate the larger portion of the jet's kinetic energy traversing the cavity and passing under the downstream tooth without being dissipated by turbulence viscosity interactions in the cavity. Therefore, a relatively smaller portion of the kinetic energy is dissipated in the cavity producing the larger carry-over coefficient. On the other hand, at lower Reynolds numbers, a relatively larger portion of the kinetic energy is dissipated in the cavity yielding the smaller carry-over coefficient (see Figure 5.2).

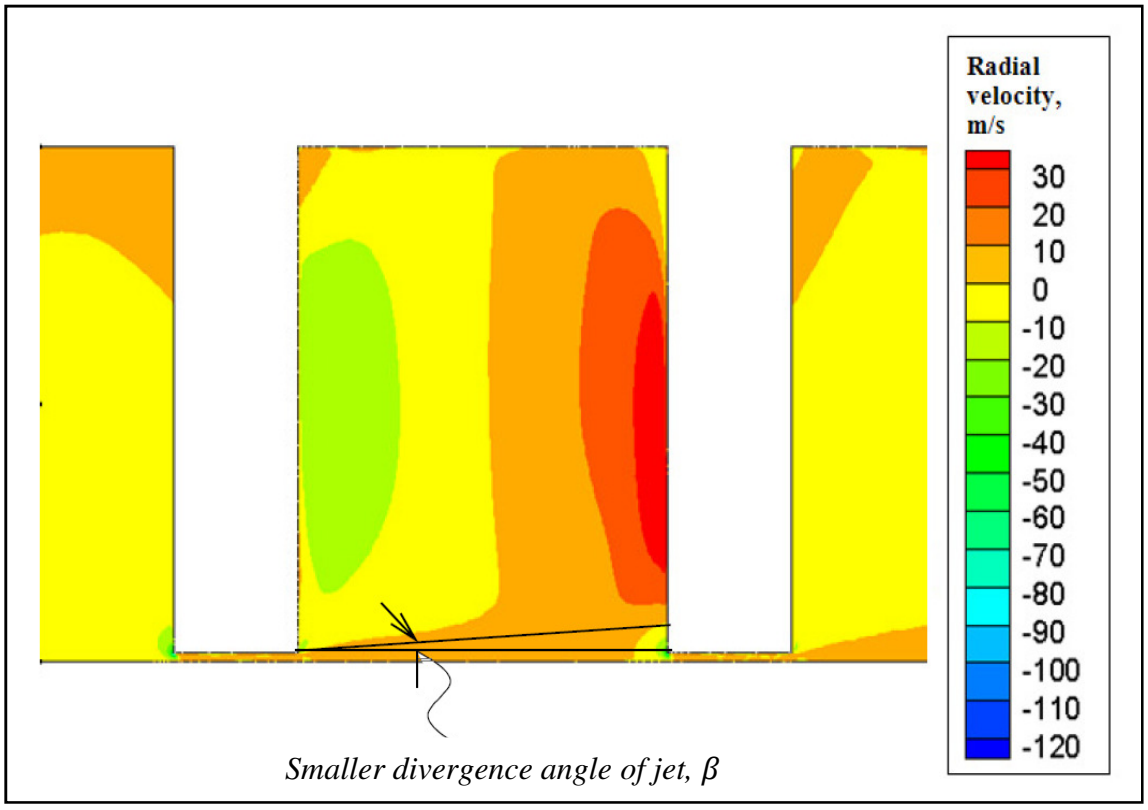

(a) Smaller divergence angle of jet with higher Reynolds number

Figure 5.2. Comparison of divergence angles of jet with Reynolds numbers

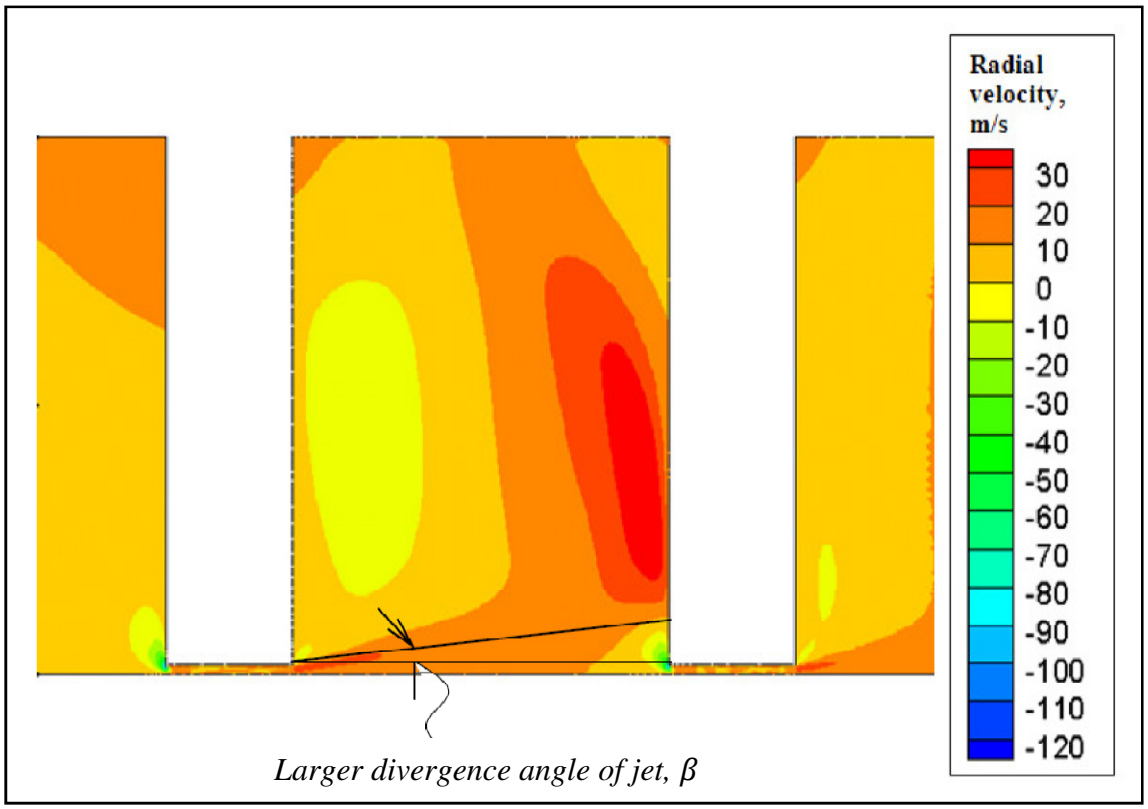

(b) Larger divergence angle of jet with smaller Reynolds number

Figure 5.2. Continued

Table 5.1. Seal geometries applied for simulations of air and water

Case No.	Reynolds No.	No. of Teeth	Clearance (mm)	Pitch (mm)	Tooth Width (mm)	Tooth Height (mm)	Shaft Diameter (mm)
1–6	100 – 5000	2	0.06	4	0.03	3.94	60
7–12	100 – 5000	2	0.06	4	1	3.94	60
13–18	100 – 5000	2	0.09	4	1	3.91	60
19–24	100 – 5000	2	0.15	4	0.4	3.85	60
25–30	100 – 5000	4	0.06	4	1	3.94	60

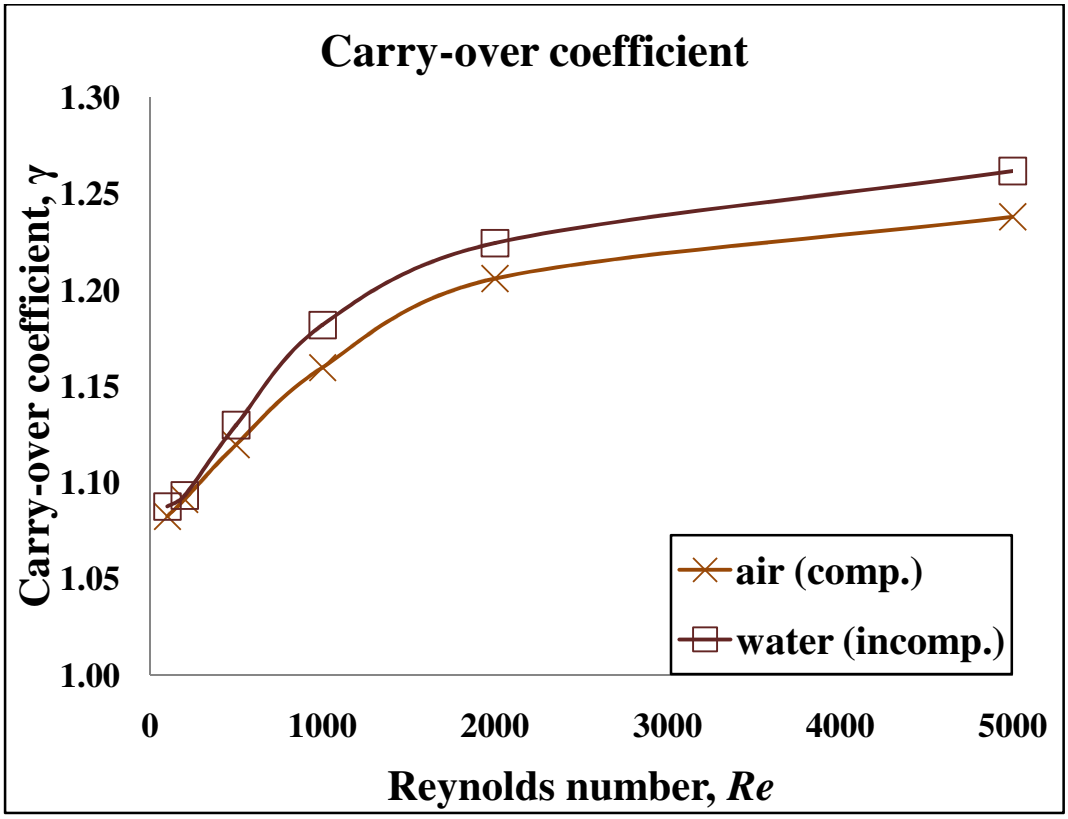

Figure 5.3. Carry-over coefficient vs. Reynolds number for air and water (case #1–6)

The first instance ($n = 2, c = 0.06\ mm, s = 4\ mm, w = 0.03\ mm$) presented in Figure 5.3 suggests that the carry-over coefficients for both air and water increase with increasing Reynolds number. This reveals that since the higher Reynolds number enables the inertial force of the jet from under the tooth to be higher and the viscous force under the same tooth to be lower, a smaller portion of kinetic energy in the cavity is dissipated. It also implies that the carry-over coefficient of water becomes greater than that of air according to the Reynolds number. This is because the undissipated portion of the kinetic energy in the cavity becomes greater when applying water as the working fluid rather than air. Since the larger value of the carry-over coefficient shows that the

labyrinth seal is less effective in dissipating the kinetic energy, it seems better to employ air rather than water as the working fluid under this geometric condition in order to reduce the leakage mass flow rate in the labyrinth seal.

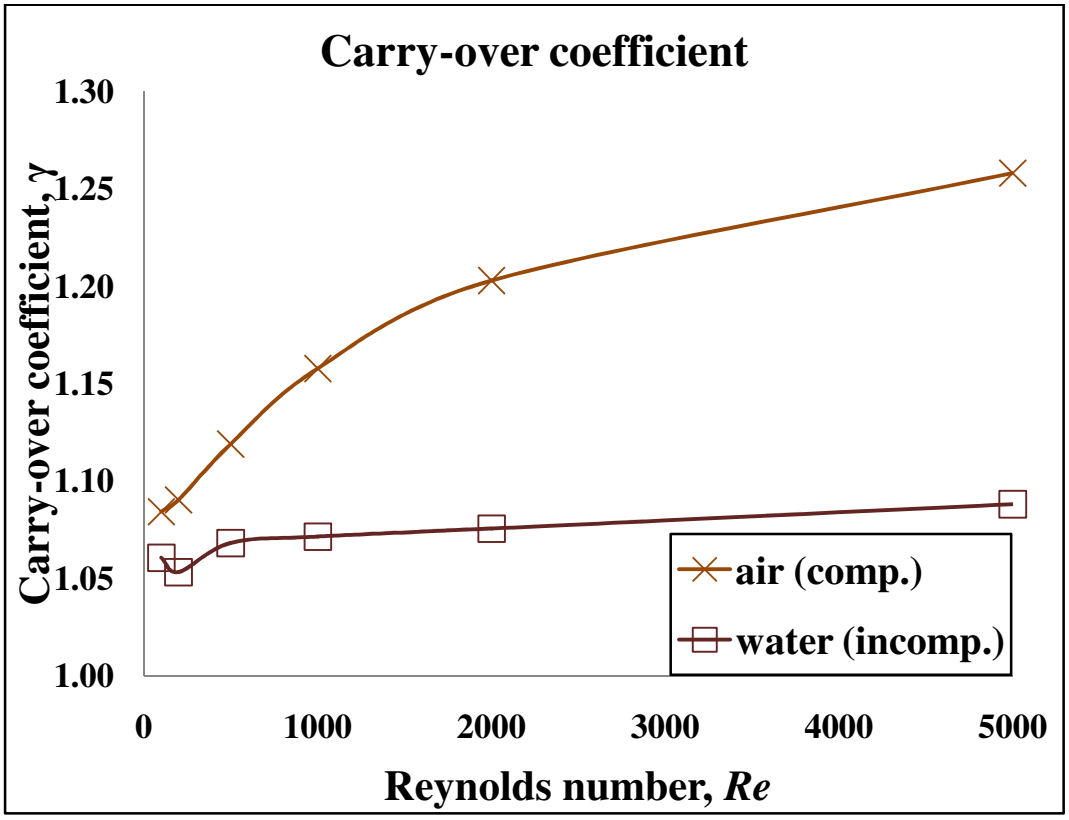

Figure 5.4. Carry-over coefficient vs. Reynolds number for air and water (case #7–12)

The second instance ($n = 2, c = 0.06\ mm, s = 4\ mm, w = 1\ mm$) where the tooth width is increased from $0.03\ mm$ to $1\ mm$ in Figure 5.4 also shows that the carry-over coefficients for both air and water increase with increasing Reynolds number. However, in this instance, the carry-over coefficient of water becomes smaller than that of air, and the variation rate of water's carry-over coefficient appears to be nearly immutable. It is

due to the flow under the tooth or the shorter cavity. To be more specific, since the viscous force under the tooth is more dominant in the labyrinth seal rather than the inertial force of the jet from under the same tooth due to wide tooth width, the kinetic energy in the cavity is dissipated better than that with narrow one. Hence, the carry-over coefficient of water with the wide tooth width does not increase as fast as that with the narrow one and tends to be almost constant despite an increasing Reynolds number. In addition, the fact that the undissipated portion of the kinetic energy in the cavity becomes greater with air rather than water as the working fluid implies that it is more effective to employ water rather than air as the working fluid in order to reduce the leakage mass flow rate in the labyrinth seal.

The third instance ($n = 2, c = 0.09\ mm, s = 4\ mm, w = 1\ mm$)where the clearance is increased from $0.06\ mm$ to $0.09\ mm$ in Figure 5.5 indicates that the carry-over coefficients for both air and water increase with increasing Reynolds number. It also shows that the carry-over coefficient of water becomes greater than that of air according to the Reynolds number. This is because the undissipated portion of the kinetic energy in the cavity becomes greater when using water rather than air as the working fluid. As a result, since a larger carry-over coefficient shows that the labyrinth seal is less useful in dissipating kinetic energy, air should be a better working fluid than water with this particular geometry for a lower leakage mass flow rate through the labyrinth seal.

In order to analyze the effects of flow geometry for the first three instances, simulations are performed for different tooth width and radial clearance for the range of

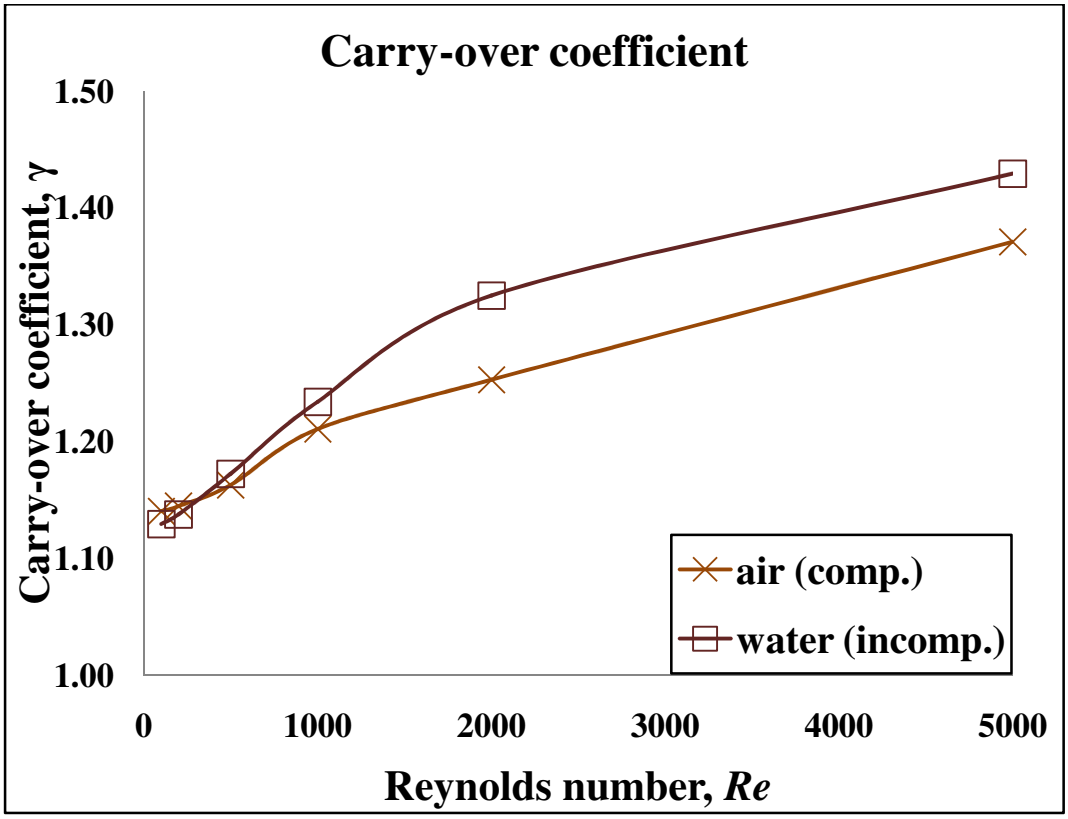

Figure 5.5. Carry-over coefficient vs. Reynolds number for air and water (case #13–18)

Reynolds numbers (cases #1–18 for the three instances in Table 5.1) with fixed tooth pitch. It can be concluded from Figures 5.4, and 5.5 that for a given Reynolds number, the carry-over coefficient of air has been slightly increased if radial clearance to tooth width ratio (c/w) and radial clearance to tooth pitch ratio (c/s) are increased (cases #7–12 and #13–18: c/w: $0.06 \rightarrow 0.09, c/s$: $0.015 \rightarrow 0.0225$) when tooth width and tooth pitch are fixed. However, it can be analyzed from Figures 5.3 and 5.5, the carry-over coefficient of air does not considerably change if only radial clearance to tooth width ratio (c/w) is decreased (cases #1–6 and #7–12: c/w: $2 \rightarrow 0.06, c/s$: 0.015) when radial clearance, tooth width, and tooth pitch are fixed.

Moreover, it can be also concluded from Figures 5.3 and 5.4 that as only radial clearance to tooth width ratio (c/w) is decreased (cases #1–6 and #7–12: c/w: $2 \rightarrow 0.06$, c/s: 0.015) when radial clearance, tooth width and tooth pitch are fixed, the turbulent dissipation of the kinetic energy of water in the cavity relatively increases with an increasing Reynolds number. Hence, the carry-over coefficient of water tends not to significantly increase as shown in Figure 5.4. Furthermore, it has to be noted from Figures 5.3, 5.4 and 5.5 that for a given Reynolds number, the carry-over coefficient of water strongly depends on radial clearance to tooth width ratio (c/w) because not only the carry-over coefficient increases when both radial clearance to tooth width ratio (c/w) and radial clearance to tooth pitch ratio (c/s) are increased (cases #7–12 and #13–18: c/w: $0.06 \rightarrow 0.09, c/s$: $0.015 \rightarrow 0.0225$) but the coefficient also decreases when only radial clearance to tooth width ratio (c/w) is decreased (cases #1–6 and #7–12: c/w: $2 \rightarrow 0.06, c/s$: 0.015) for fixed radial clearance to tooth pitch ratio (c/s). Figures 5.6, 5.7, and 5.8 summarize the results for the first three instances and show streamlines within the cavity for each tooth.

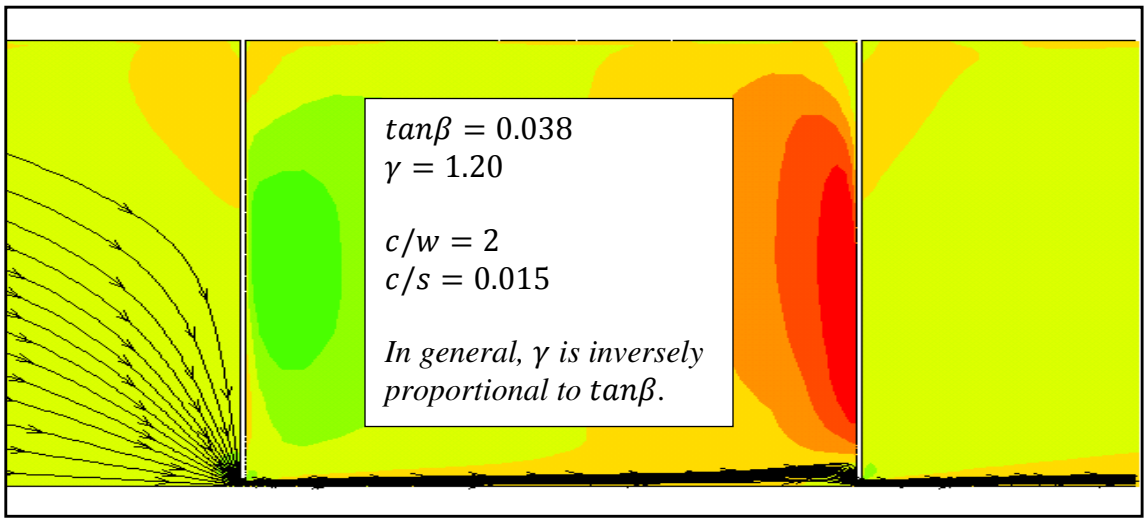

Figure 5.6. Streamlines within cavity for first instance (case #1–6, Re = 1000)

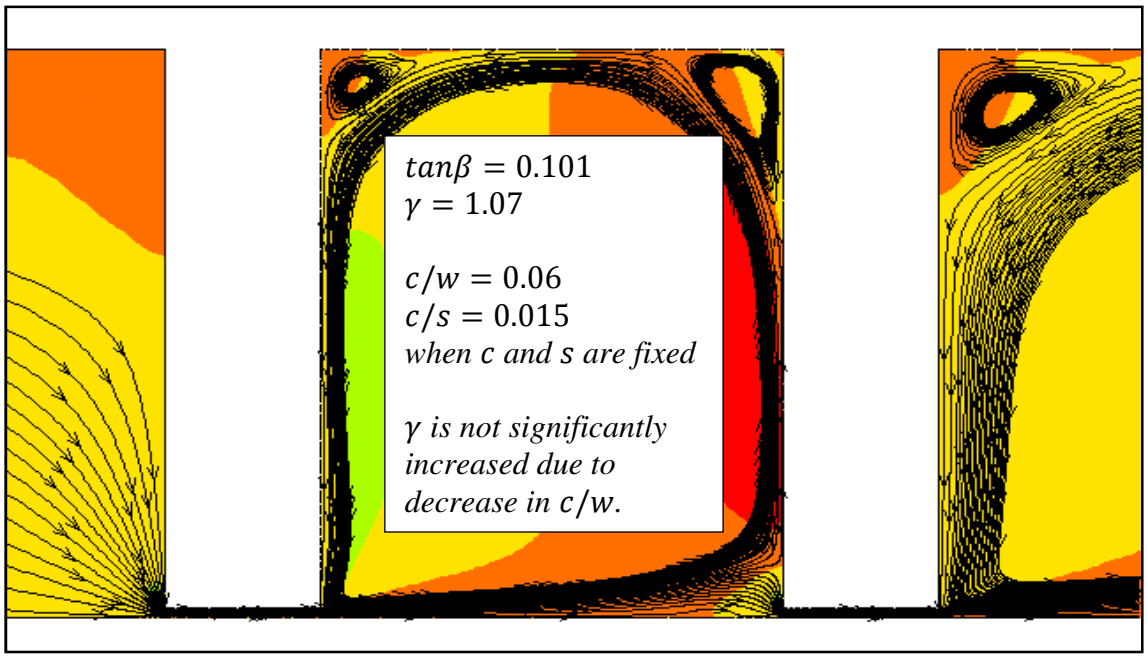

Figure 5.7. Streamlines within cavity for second instance (case #7–12, Re = 1000)

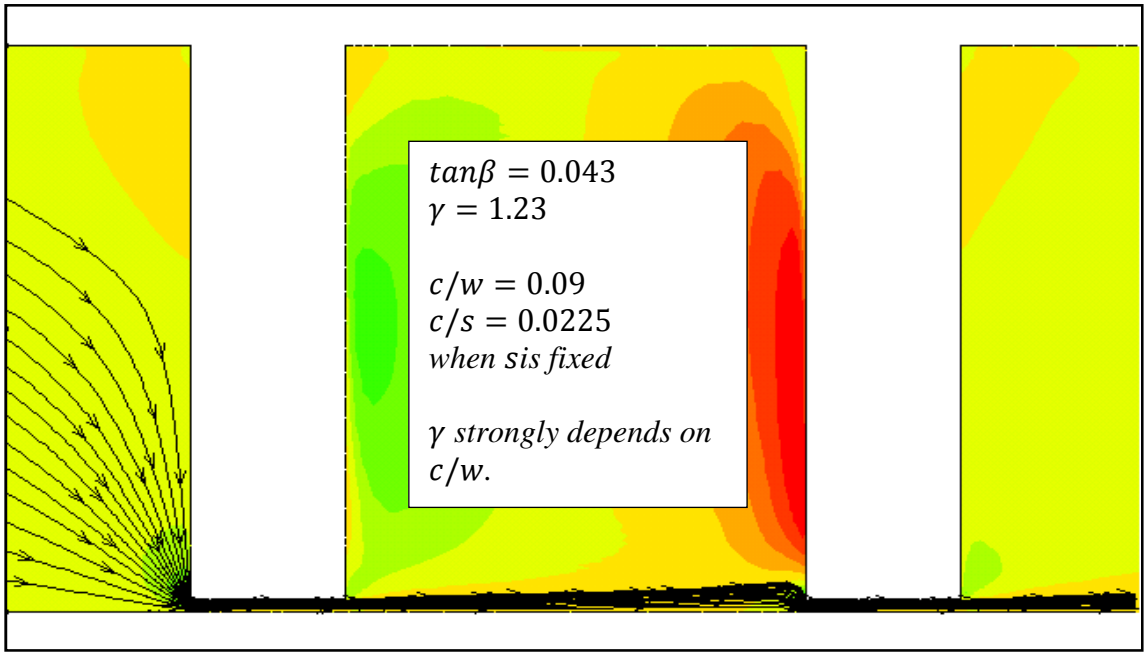

Figure 5.8. Streamlines within cavity for third instance (case #13–18, Re = 1000)

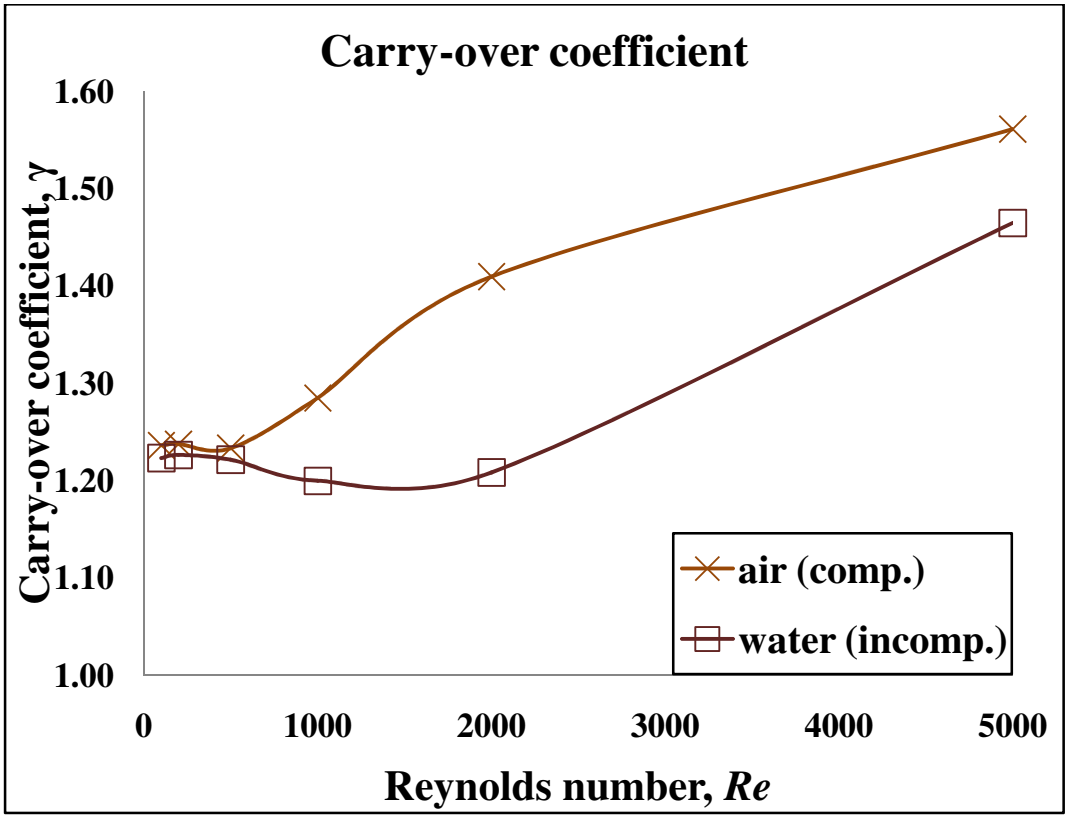

Figure 5.9. Carry-over coefficient vs. Reynolds number for air and water (case #19–24)

In the fourth instance ($n = 2, c = 0.15\ mm, s = 4\ mm, w = 0.4\ mm$) presented in Figure 5.9, the data shows that the carry-over coefficients for both air and water increase with increasing Reynolds number. The data also suggests that the carry-over coefficient of water becomes smaller than that of air since the undissipated portion of the kinetic energy in the cavity increases when air is the working fluid rather than water. Thus, it is more productive to use water as the working fluid rather than air for a lower leakage mass flow rate through the labyrinth seal.

In general, the lower the Reynolds number, the larger is the inertial force of the jet emerging from under the tooth and the smaller is the viscous force under the same

tooth. The divergence angle of the jet becomes larger and this results in a smaller carry-over coefficient at the lower Reynolds numbers. However, in this instance, there are some notable points which are different from other data of water as shown in Figure 5.9. Specifically, despite the fact that the divergence angle of the jet at Reynolds number 1000 should be less than that at 500, the simulation shows an unexpected outcome (see Figures 5.10 and 5.11). The transition process explains why the carry-over coefficient for water near Reynolds number of 1000 tends to slightly decrease and then recover. More specifically, during transition from laminar to turbulent, the carry-over coefficient reduces initially and once the Reynolds number attains a critical value 2000, the carry-over coefficient increases again. This result shows the carry-over coefficient at the Reynolds number 1000 to be less than that at Reynolds number 500.

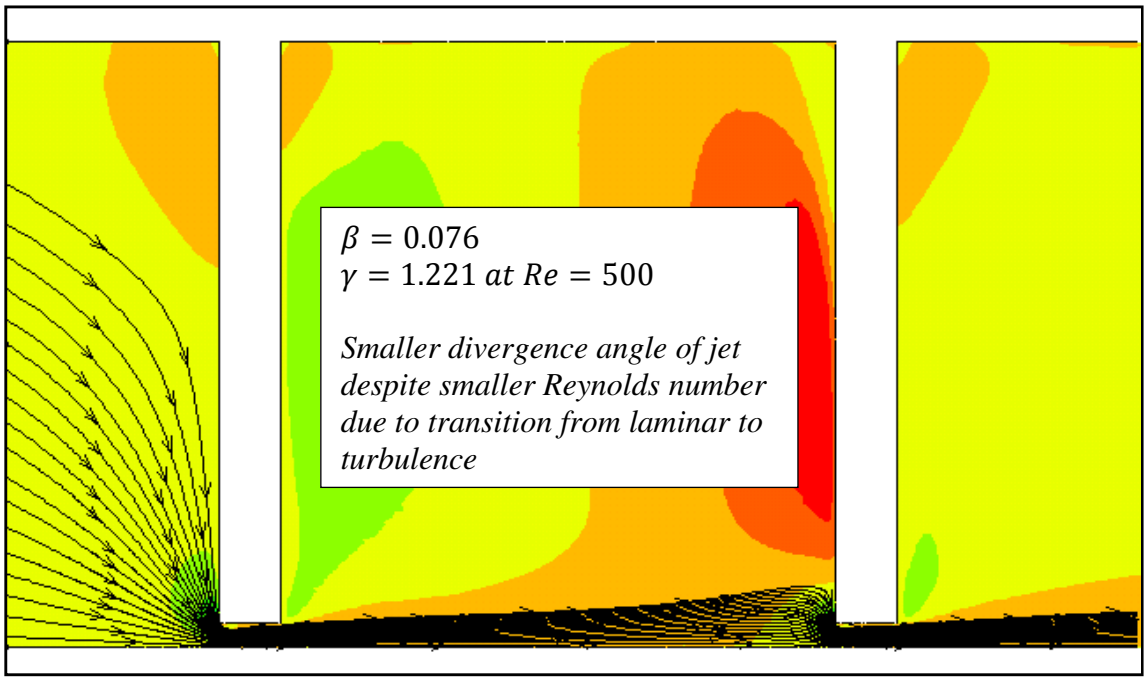

Figure 5.10. Streamlines within cavity at Reynolds number 500 (case #19–24)

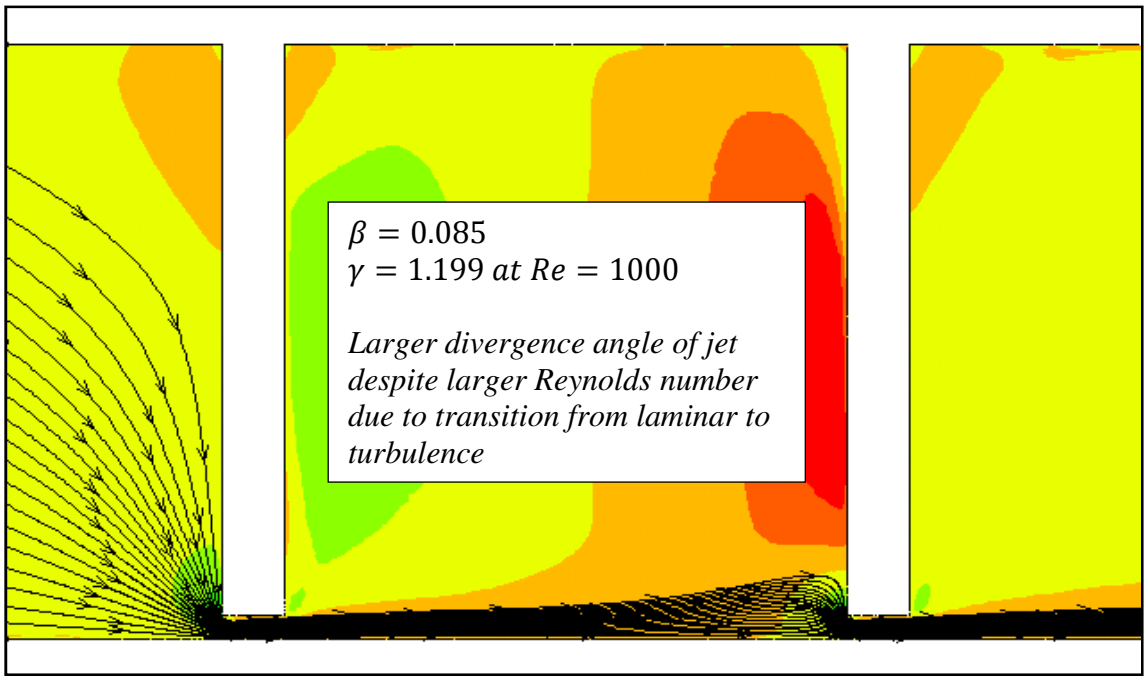

Figure 5.11. Streamlines within cavity at Reynolds number 1000 (case #19–24)

In the last instance ($n = 4, c = 0.06\ mm, s = 4\ mm, w = 1\ mm$) presented in Figures 5.12, 5.13 and 5.14, the data shows that the carry-over coefficients for both air and water increase with increasing Reynolds number. In this final instance, the carry-over coefficient of water becomes smaller than that of air. This is because the undissipated portion of the kinetic energy in the cavity is greater when using air as the working fluid rather than water under the same geometric conditions. Hence, it is more effective to use water than air as the working fluid for lower leakage mass flow rate through the labyrinth seal.

Moreover, the dominant consideration about this instance is that this is the labyrinth seal with multiple cavities and one needs to compute all the carry-over coefficients occurring in each cavity. As shown by the data in Figures 5.12, 5.13, and

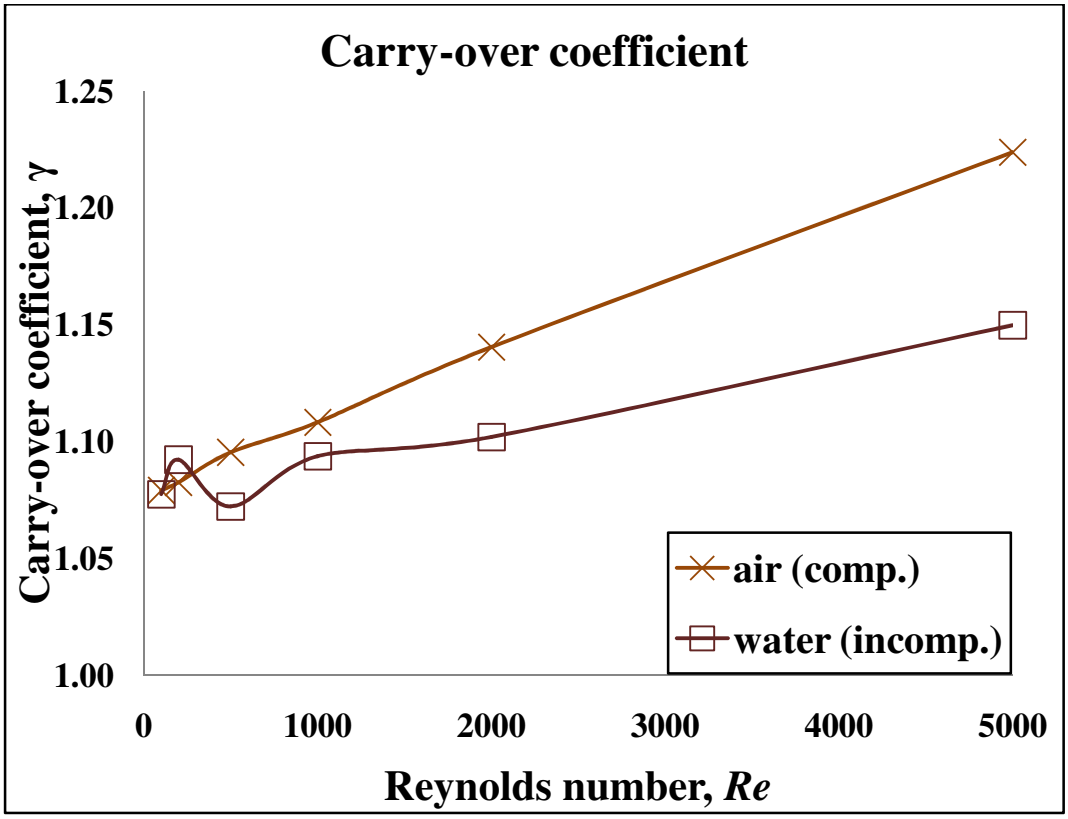

Figure 5.12. Carry-over coefficient vs. Reynolds number for air and water within first cavity (case #25–30)

5.14, (without reference to the number of cavities), air's carry-over coefficient in the cavity has the tendency to increase because with an increase in the Reynolds number, the inertial force of the jet from under the tooth increases faster than the viscous force under the same tooth while making a smaller divergence angle. However, it can be also seen in Figures 5.12, 5.13, and 5.14, that there exists an unusual point at Reynolds number 500 for water, where the carry-over coefficient tends to deviate from other general values. This is probably because of the transition process at the Reynolds numbers between 200 and 500. Even though the divergence angle of the jet at Reynolds number 500 should be

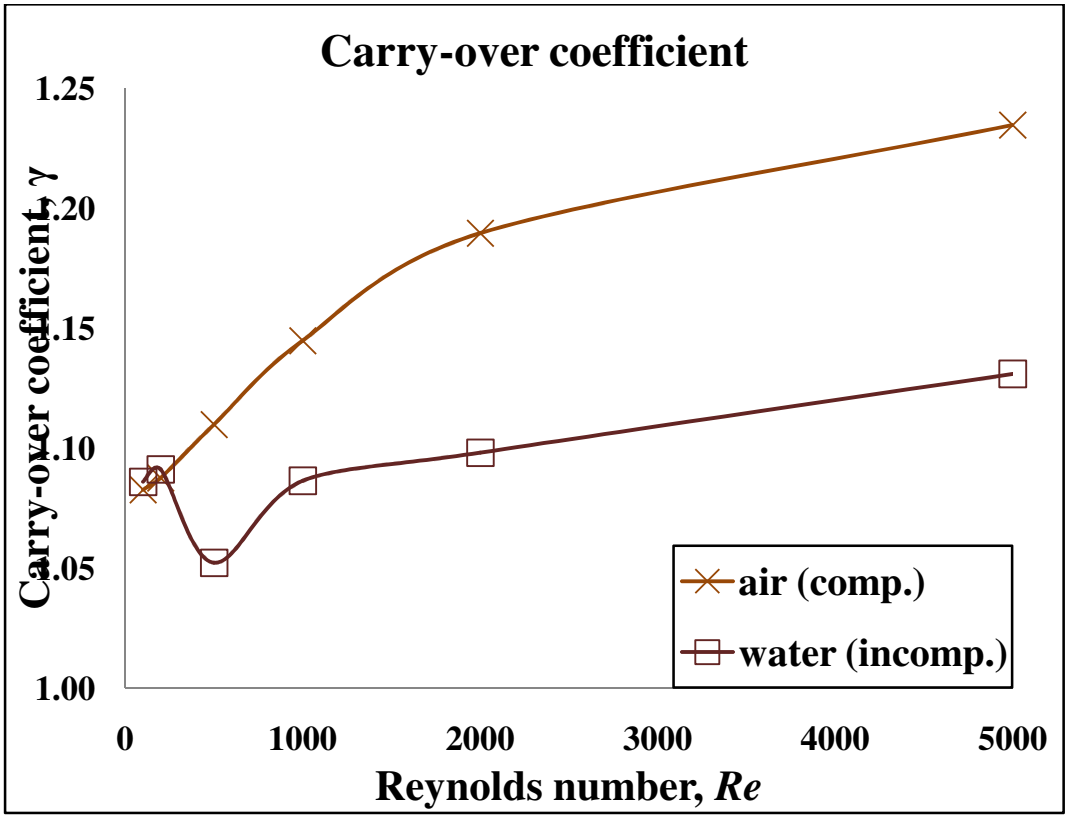

Figure 5.13. Carry-over coefficient vs. Reynolds number for air and water within second cavity (case #25–30)

less than that at Reynolds number 200, the simulation shows the opposite result. This causes the carry-over coefficient at Reynolds number 500 to be less than that at Reynolds number 200. As water undergoes transition from laminar to turbulent flow, the carry-over coefficient reduces; further, after the flow becomes turbulent at the Reynolds numbers greater than 1000, the carry-over coefficient increases again. At the Reynolds number 500, the third cavity possesses a secondary re-circulation zone. This is a departure from all other instances and is responsible for the very low value of the carry-over coefficient at this value (see Figures 5.15, 5.16, and 5.17).

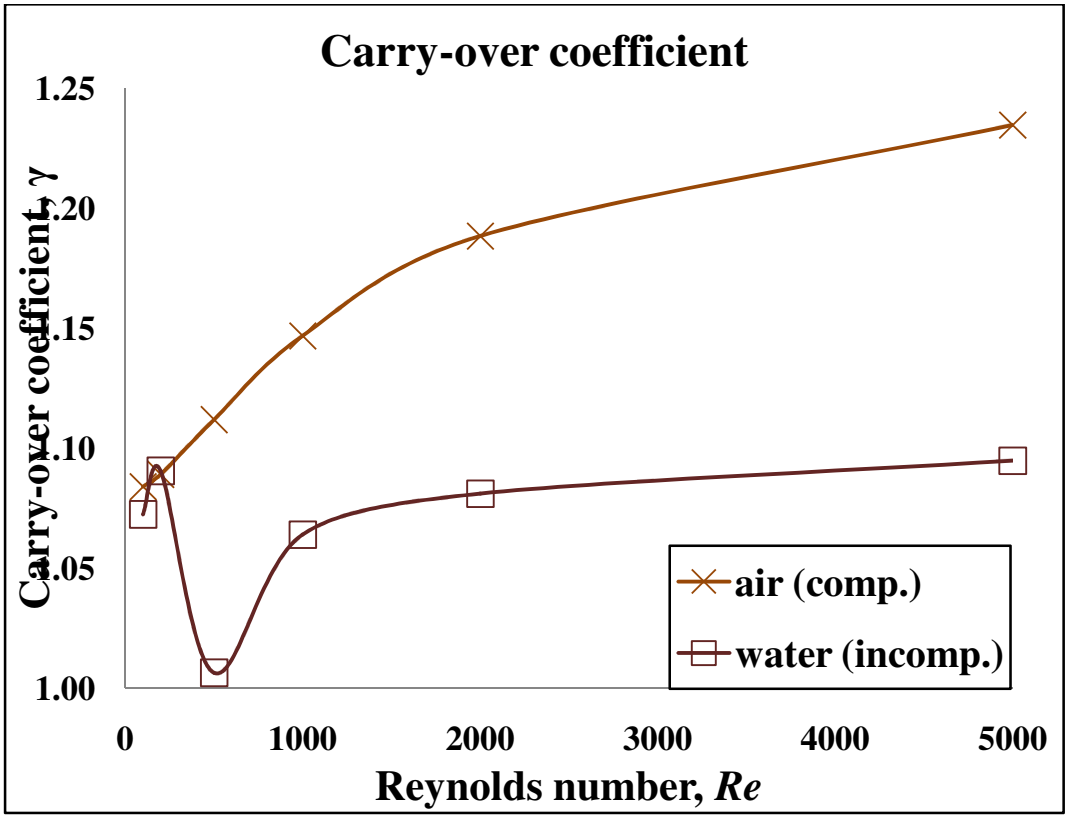

Figure 5.14. Carry-over coefficient vs. Reynolds number for air and water within third cavity (case #25–30)

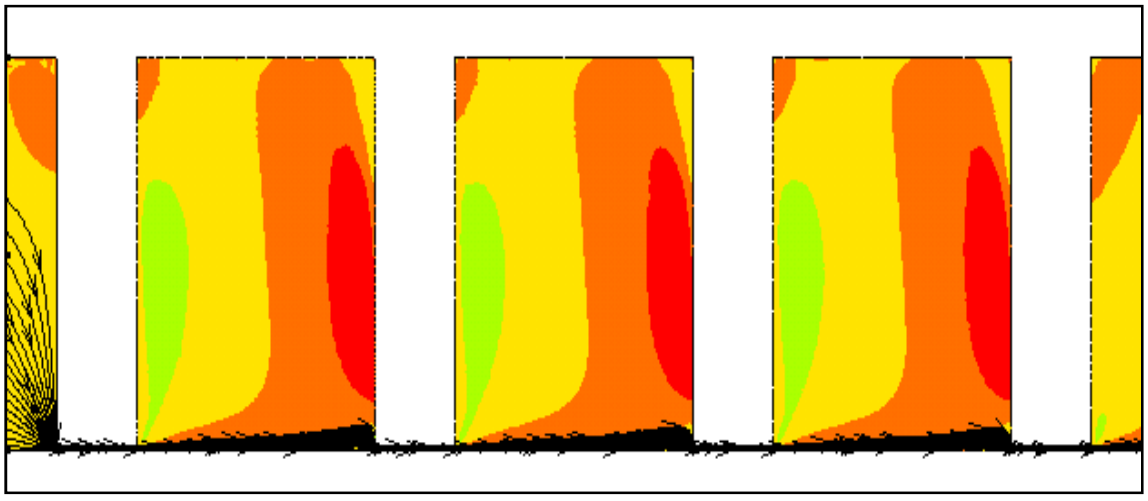

Figure 5.15. Streamlines within cavities at Reynolds number 200 (case #25–30)

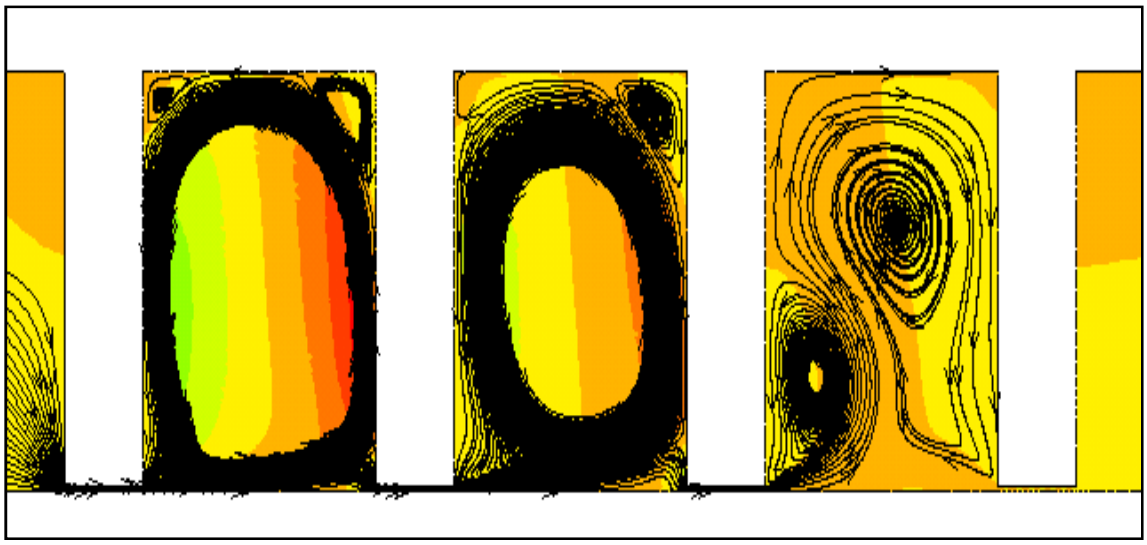

Figure 5.16. Streamlines within cavities at Reynolds number 500 (case #25–30)

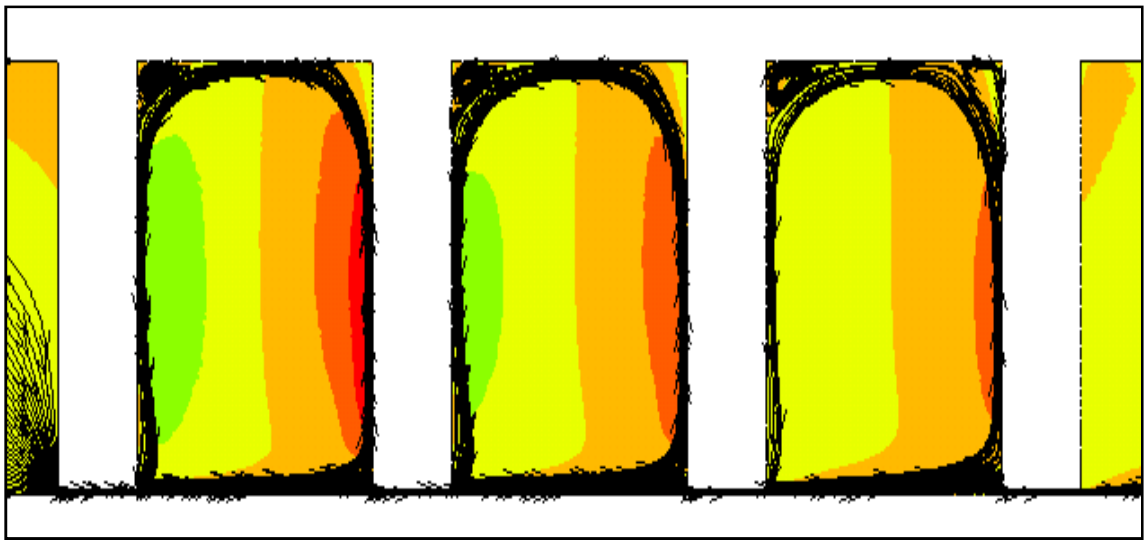

Figure 5.17. Streamlines within cavities at Reynolds number 1000 (case #25–30)

Lastly, the second instance (cases #7–12) and the last instance (cases #25–30) possess the same seal geometry except for the total number of teeth, 2 compared to 4. The presence of subsequent cavities for the last instance (cases #25–30) results in a

larger dip in the carry-over coefficient with Reynolds number for water at low Reynolds numbers. For water, the carry-over coefficient is larger at the higher Reynolds numbers for the first two cavities. Hence, the number of cavities does affect real carry-over coefficients.

CHAPTER VI

DISCHARGE COEFFICIENT

DETERMINATION OF DISCHARGE COEFFICIENT

The rate of seal leakage is dependent upon how much energy is dissipated in each cavity. Therefore, it is necessary to study the discharge coefficient and its relationship to the carry-over coefficient in order to analyze the flow field within a labyrinth seal. The discharge coefficient, C_d, represents both the flow losses occurring when a fluid flows through the labyrinth cavity and the frictional losses arising when the fluid flows under the tooth in the labyrinth seal. Further, the discharge coefficient can be expressed in terms of the mass flow rate, $\dot{m}$, the clearance area, $A(=\pi Dc)$, the fluid density, ρ, and the inlet and the outlet pressures across the tooth, p_i and p_e.

$$C_d = \frac{\dot{m}}{A\sqrt{2\,\rho\,(p_\iota - p_e)}} \tag{6.1}$$

From Equation 6.1, it is found that the leakage mass flow rate can be computed on the basis of the overall pressure difference across the tooth, provided that the discharge coefficients of all the teeth of the labyrinth seal are known.

$$\dot{m} = C_d A\sqrt{2\rho(p_i - p_e)} \tag{6.2}$$

The discharge coefficient under certain flow and geometry conditions must be determined using a method similar to that used to determine the carry-over coefficient. In general, it is expected that the discharge coefficient of the first tooth of the labyrinth seal will be different from the discharge coefficients of the subsequent teeth; however, in

order to draw a fair comparison between the discharge coefficients of the successive teeth, the discharge coefficient of a tooth is determined under the same conditions as those used to determine the discharge coefficient of the preceding tooth.

ANALYSIS OF DISCHARGE COEFFICIENT FOR EACH INSTANCE

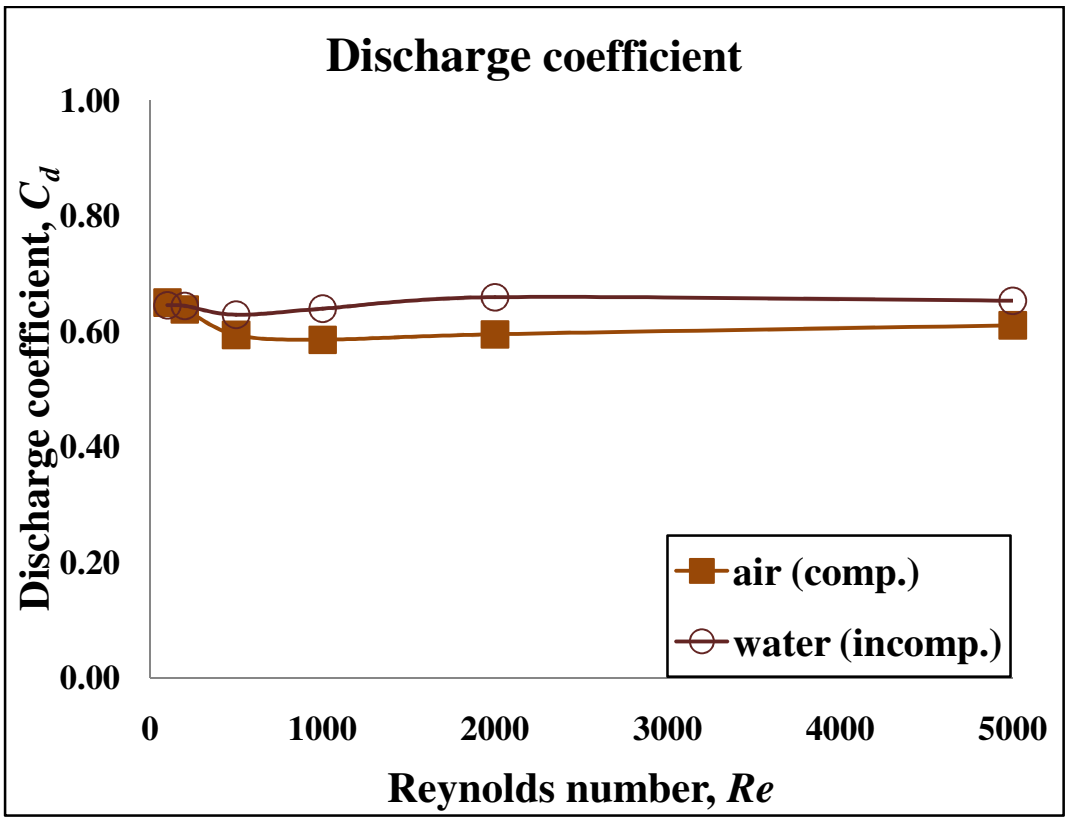

Figure 6.1. Discharge coefficient of first tooth vs. Reynolds number for both air and water (case #1–6 in Appendix A)

In the first instance ($n = 2, c = 0.06\ mm, s = 4\ mm, w = 0.03\ mm$) shown in Figure 6.1, it is found that that the discharge coefficients of the first tooth for both air

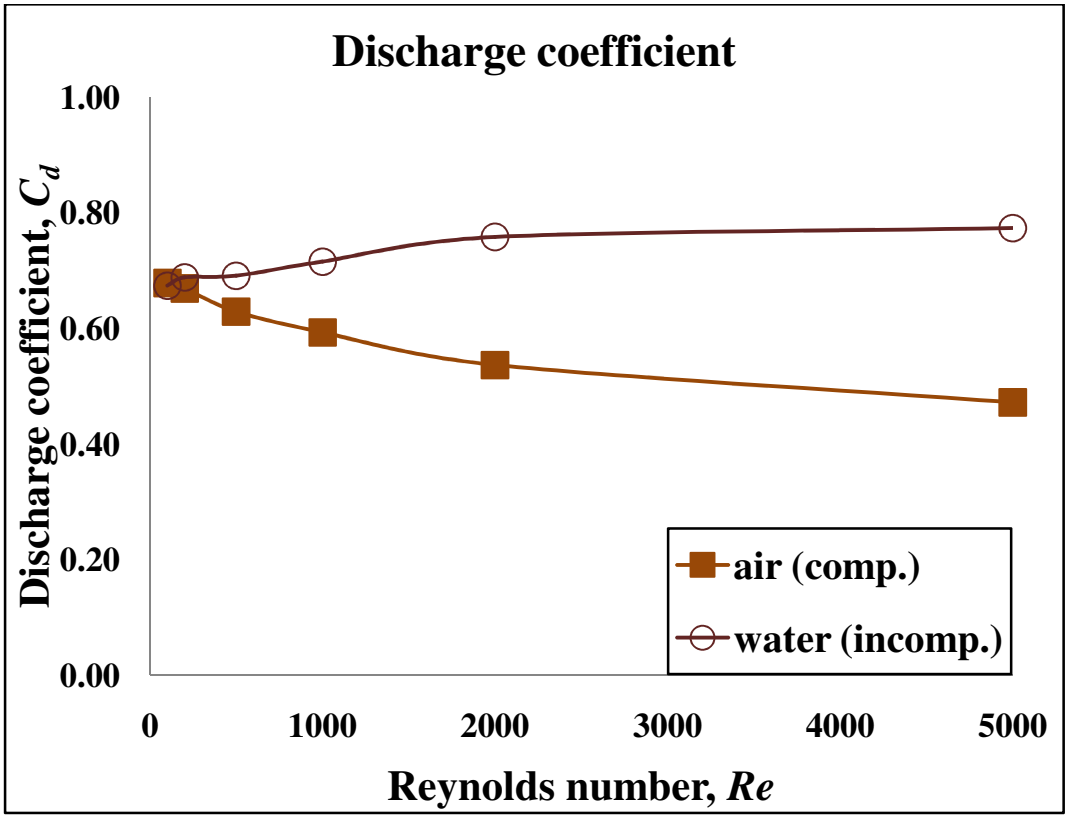

Figure 6.2. Discharge coefficient of second tooth vs. Reynolds number for both air and water (case #1–6 in Appendix A)

and water remain almost constant with an increase in the Reynolds number. This finding suggests that for a given geometry, the discharge coefficients of the first tooth for both air and water are independent of the Reynolds number and that their values remain constant under high and low fluid velocities. To be more specific, this finding indicates that regardless of the fluid velocity, the total losses occurring as the fluid flows through the cavity and under the first tooth approach a nearly constant value and that these losses do not increase further with an increase in the Reynolds number. Because the discharge

coefficient of air is less than that of water, it can be safely said that the total losses caused by air are more than those caused by water.

In the case of the second tooth, as in Figure 6.2, the discharge coefficient for water increases with an increase in the Reynolds number while that for air decreases with an increase in the Reynolds number. The total losses occurring as water flows under the first tooth and through the cavity remain virtually constant with an increase in the Reynolds number; however, the total losses occurring when water flows through the cavity and under the second tooth decrease gradually with an increase in the Reynolds number. The total losses occurring as air passes under the first tooth and through the cavity remain practically steady with an increase in the Reynolds number; this observation is almost similar to that when water flows under the first tooth. However, the total losses occurring as air passes through the cavity and under the second tooth increase with an increase in the Reynolds number.

There are two reasons why the discharge coefficient of air does not increase with an increase in the Reynolds number. One reason is related to the pressure ratio, Pr, which is defined as the ratio of the inlet pressure, p_i to the outlet pressure, p_e of a tooth expressed in absolute values. It is considered that the discharge coefficients of successive teeth depend on both their respective pressure ratio and the Reynolds number as formulated in Equation 6.3. The discharge coefficient is found to have a greater dependence on the pressure ratio than the Reynolds number. Thus, it can be concluded that since the pressure ratio of the fluid decreases gradually as the fluid flows across each tooth of the labyrinth

seal, the discharge coefficient of air tends to decrease in spite of an increase in the Reynolds number.

$$C_d = f(Pr, Re) \tag{6.3}$$

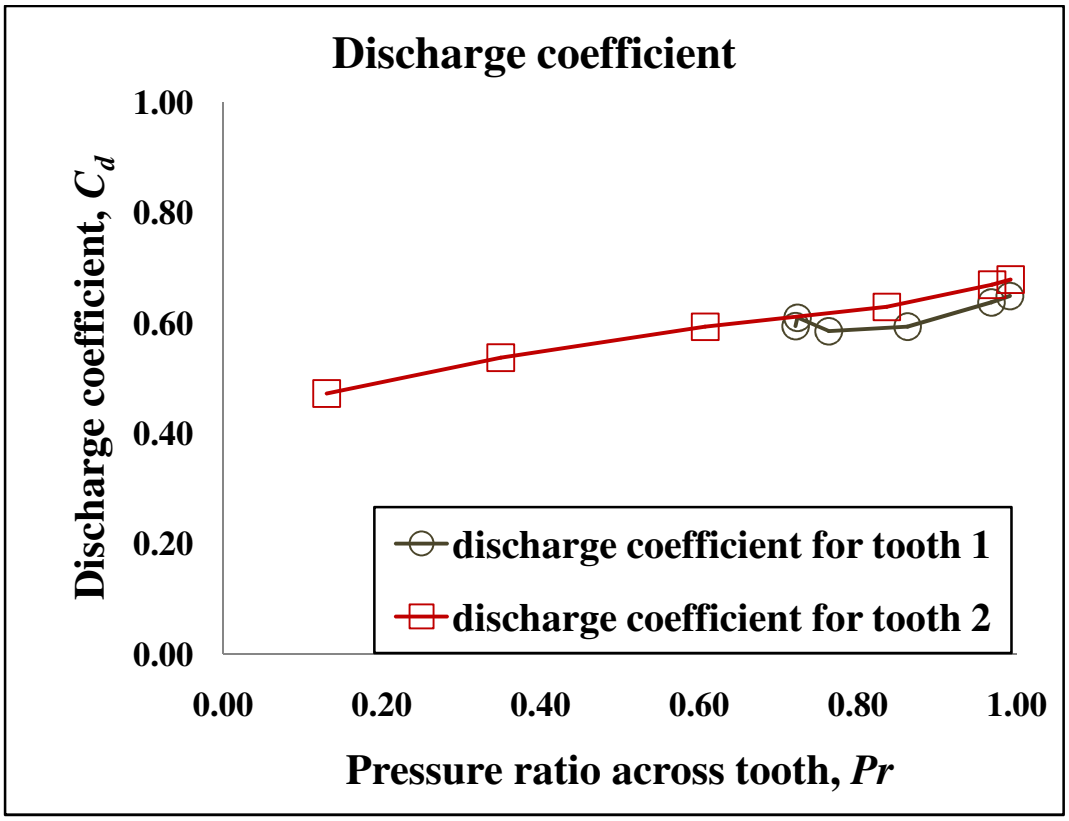

Figure 6.3. Discharge coefficient of each tooth vs. Pressure ratio across tooth for air (single cavity labyrinth seal for only air: case #1–6 in Appendix A)

To examine the effect of the pressure ratio on the discharge coefficient of air, one needs to compare the relationship between the discharge coefficient and the pressure ratio of air for each tooth. Figure 6.3 shows that as the pressure ratio across the tooth decreases, the variation rate of the discharge coefficient occurring through the first tooth

is insignificant for the entire range of Reynolds numbers; however, the discharge coefficient occurring through the second tooth only decreases. Thus, it can be observed that from Figure 6.1, the discharge coefficient of the first tooth remains almost invariant with an increasing Reynolds number and that from Figure 6.2, only the discharge coefficient of the second tooth decreases.

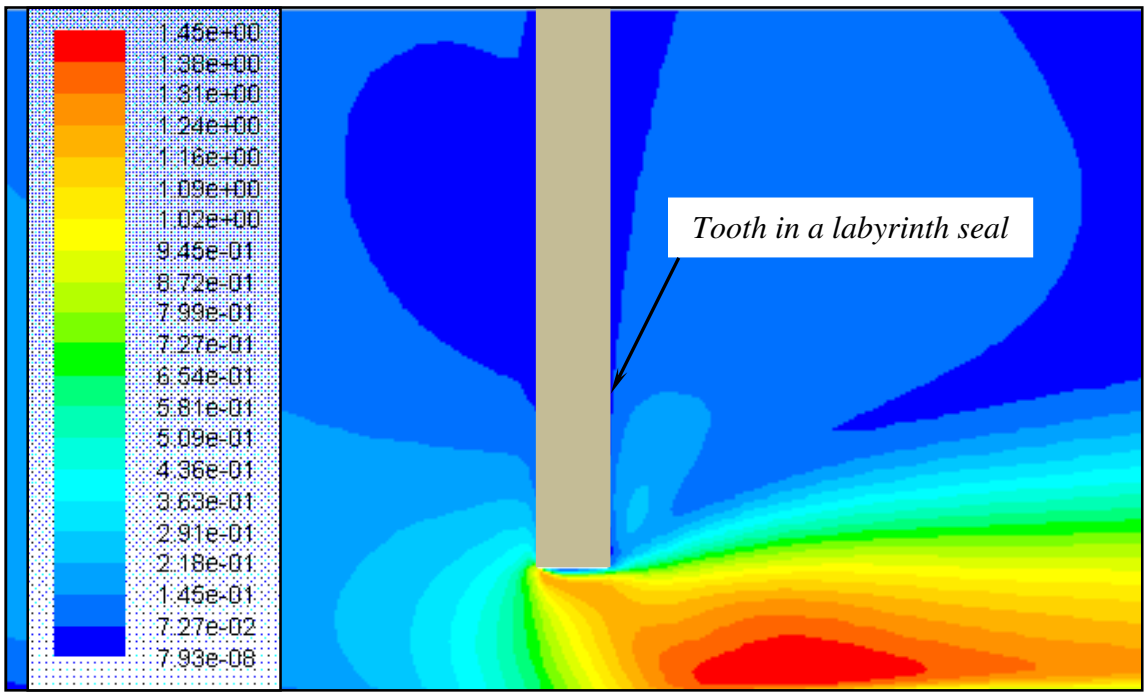

Figure 6.4. Contours for Mach number through constriction of second tooth for air (choked due to $Ma > 1$: case #1–6 in Appendix A)

As seen in Figure 6.4, the second reason is that the flow of the fluid through the constriction becomes compressible and the flow eventually is choked; this condition is known as the fluid dynamic condition, which is correlated with the Venturi effect. That

is, when a fluid at a given pressure and temperature flows through the constriction, the velocity of the fluid increases according to Bernoulli's equation for the initially subsonic upstream conditions as it flows through the smaller cross-sectional area of the labyrinth seal. As the pressure ratio becomes larger, the flow becomes compressible and Bernoulli's equation is no longer valid. For a $Pr < 0.5283$, the fluid Mach number reaches 1 [1]. Choked flow is a restricted condition that occurs when the mass flow rate does not increase with a further decrease in the downstream pressure while the upstream pressure is fixed.

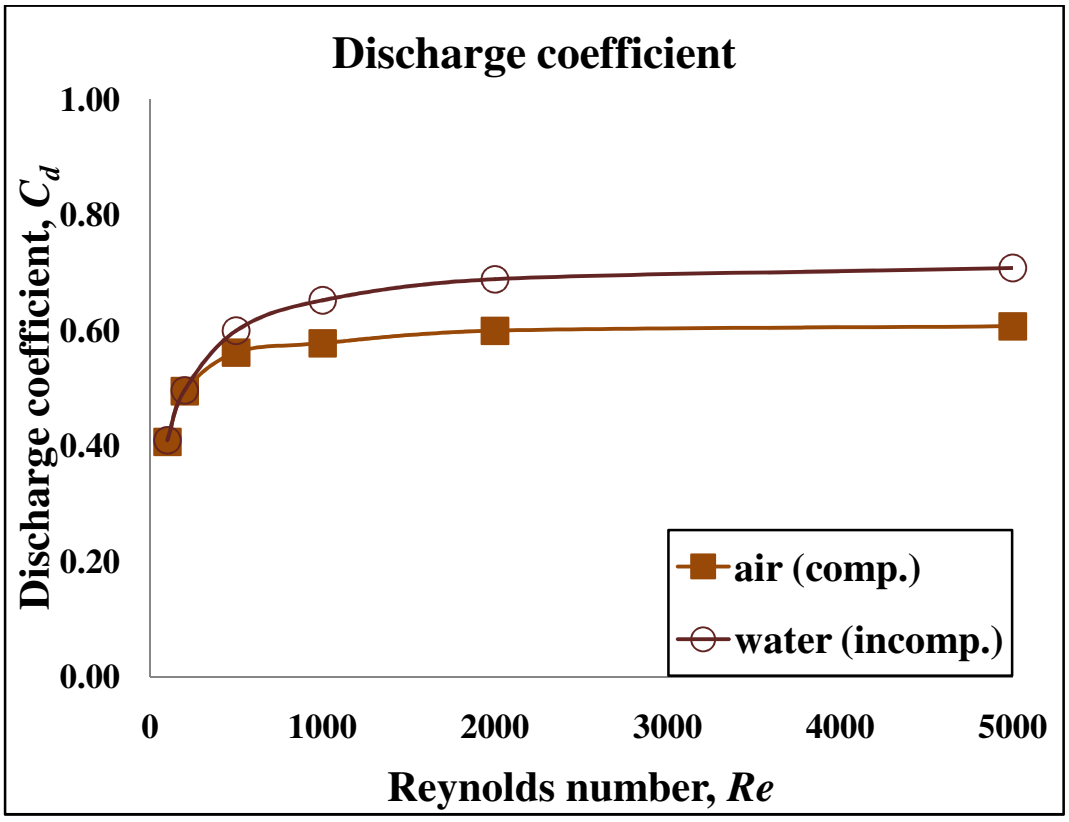

Figure 6.5. Discharge coefficient of first tooth vs. Reynolds number for both air and water (case #7–12 in Appendix A)

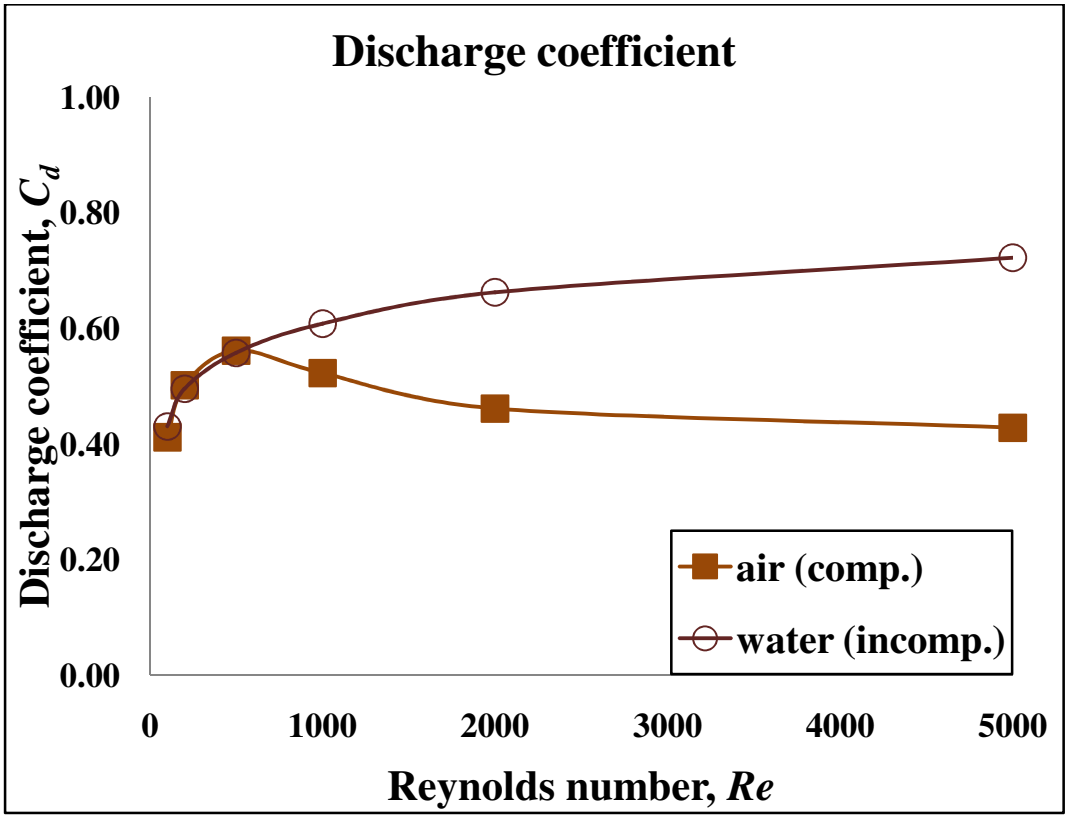

Figure 6.6. Discharge coefficient of second tooth vs. Reynolds number for both air and water (case #7–12 in Appendix A)

In the second instance ($n = 2, c = 0.06\ mm, s = 4\ mm, w = 1\ mm$) shown in Figure 6.5, it is found that the discharge coefficients of the first tooth for both air and water increase with the Reynolds number as if they are logarithmical curves with each base > 0. This finding suggests that because a high Reynolds number increases the inertial force of the jet of the fluid emerging from under the tooth and decreases the viscous force under the same tooth, a small fraction of the kinetic energy of the fluid in the cavity is dissipated; in other words, because of the low kinetic energy of the jet caused by its large divergence angle of the jet, the fluid in the cavity is not dissipated, decreasing the

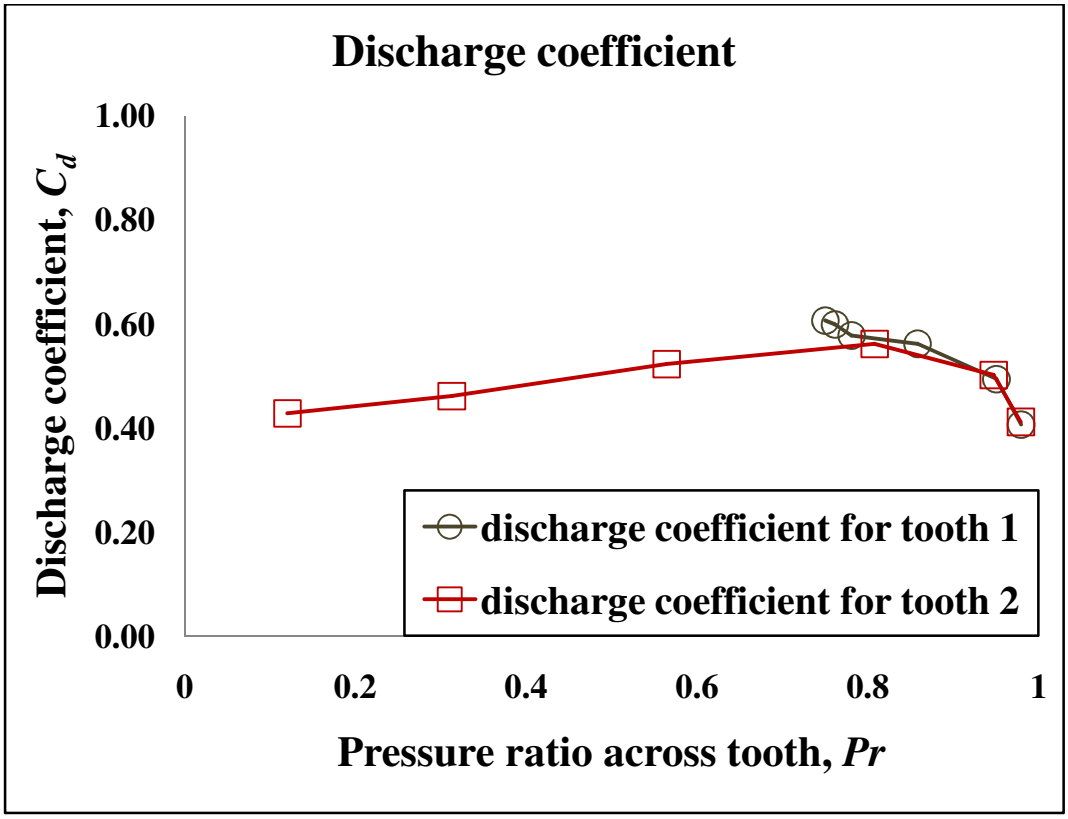

Figure 6.7. Discharge coefficient of each tooth vs. Pressure ratio across tooth for air (single cavity labyrinth seal for only air: case #7–12 in Appendix A)

losses in the cavity; therefore, the total losses occurring as the fluid flows through the cavity and under the tooth cause the discharge coefficient of the first tooth to increase. This finding also indicates that the discharge coefficient of the first tooth for water becomes greater than that of the first tooth for air on the basis of the Reynolds number. This is, previously stated on the carry-over coefficient, also true for the discharge coefficient because the amount of undissipated kinetic energy in the cavity is greater when water is used as the working fluid than air is applied. A high discharge coefficient indicates that the labyrinth seal is less effective in dissipating kinetic energy. Therefore, in order to reduce

the leakage mass flow rate in the labyrinth seal, it is better to employ air as the working fluid than water under the given geometric condition.

When water is used as the working fluid, the discharge coefficient of the second tooth also increases with an increase in the Reynolds number as shown in Figure 6.6 and is almost identical to the values for the first tooth. However, in the case of air, the discharge coefficient of the second tooth decreases with an increase in the Reynolds number after the value of 500.

Figure 6.7 shows that the relationship between the discharge coefficient and the pressure ratio of air for each tooth. It can be seen that as the pressure ratio across the tooth decreases, the discharge coefficient occurring through the first tooth only increases for the entire range of Reynolds numbers; however, until the pressure ratio decreases to 0.8075, the discharge coefficient occurring through the second tooth increases and after the value, the coefficient decreases. Therefore, it can be observed that from Figure 6.5, the discharge coefficient of the first tooth increases with an increasing Reynolds number and that from Figure 6.6, the discharge coefficient of the second tooth increases until Reynolds number 500 ($Pr = 0.8075$) and then decreases after the Reynolds number.

In addition, as explained previously for the discharge coefficient of the second tooth for air (case #1–6), it is obvious that the total losses occurring when air passes through the cavity and under the second tooth increase with an increase in the Reynolds number after the value of 500; that is to say, the pressure ratio across each tooth of the labyrinth seal decreases and the flow of the fluid through the constriction is choked as seen in Figure 6.8. The discharge coefficient of the first tooth is greater than that of the

second tooth because of the effect of the kinetic energy carry-over and a lower value of the pressure ratio across the tooth.

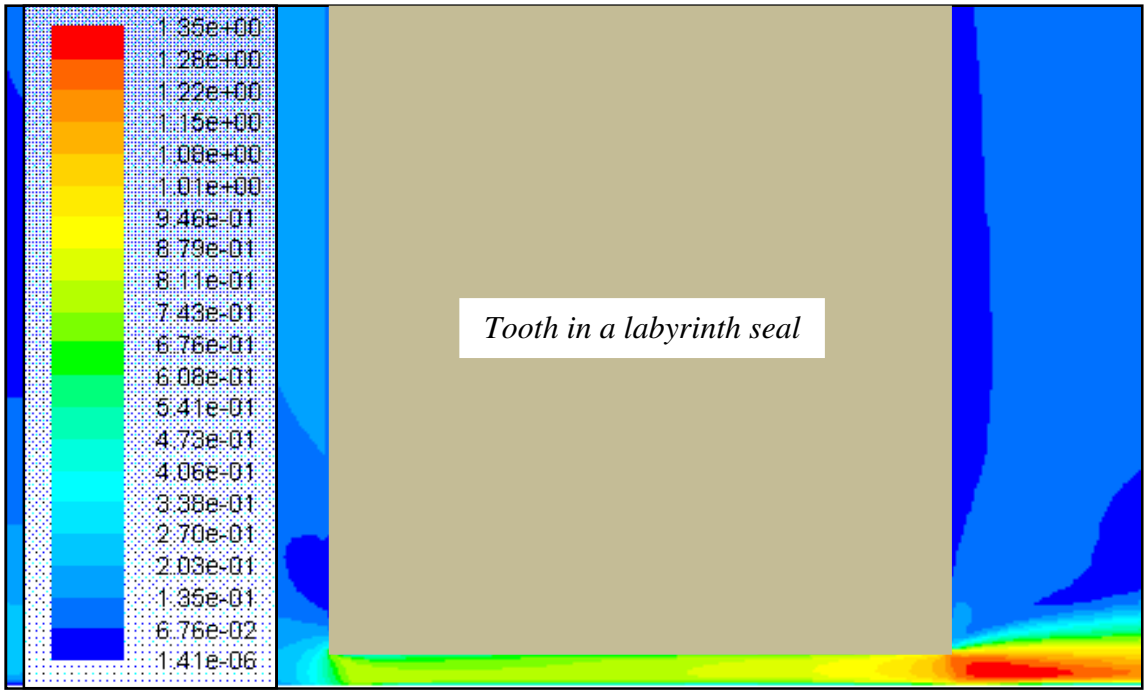

Figure 6.8. Contours for Mach number through constriction of second tooth for air (choked due to $Ma > 1$: case #7–12 in Appendix A)

In the third instance ($n = 2, c = 0.09\,mm, s = 4\,mm, w = 1\,mm$) shown in Figure 6.9, it is observed that the discharge coefficients of the first tooth for both air and water increase with an increase in the Reynolds numbers. The analysis used for the second instance can also be used to elucidate the fact that because of the low kinetic energy caused by its large divergence angle of the jet, the fluid in the cavity is not dissipated, decreasing the losses in the cavity; therefore, the total losses occurring as the

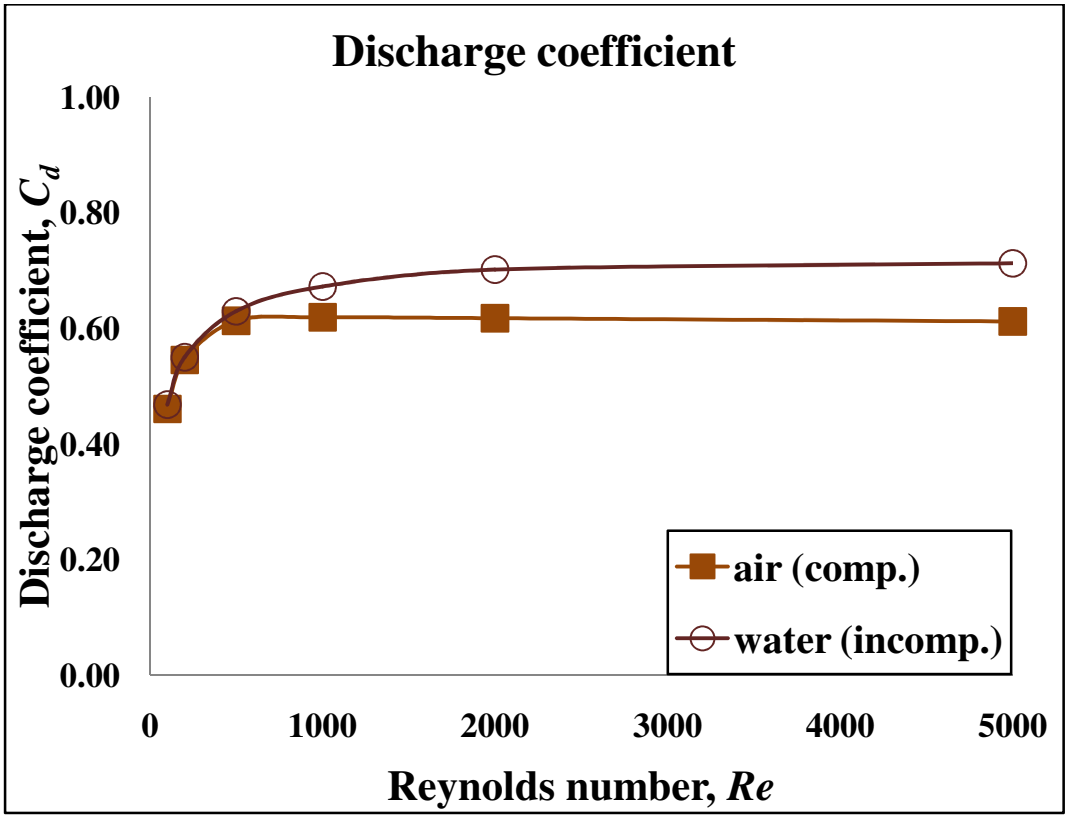

Figure 6.9. Discharge coefficient of first tooth vs. Reynolds number for both air and water (case #13–18 in Appendix)

fluid flows through the cavity and under the tooth cause the discharge coefficient of the first tooth to increase. This analysis also shows that the discharge coefficient of the first tooth for water becomes greater than that of the first tooth for air on the basis of the Reynolds number. To be more specific, the reason for this difference in the discharge coefficients is that the undissipated portion of the kinetic energy in the cavity increases when water is utilized as the working fluid, and not air. Because a high discharge coefficient indicates that the labyrinth seal is less effective in dissipating the kinetic

energy, in order to reduce the leakage mass flow rate in the labyrinth seal, it is more effective to use air as the working fluid than water for the given geometric condition.

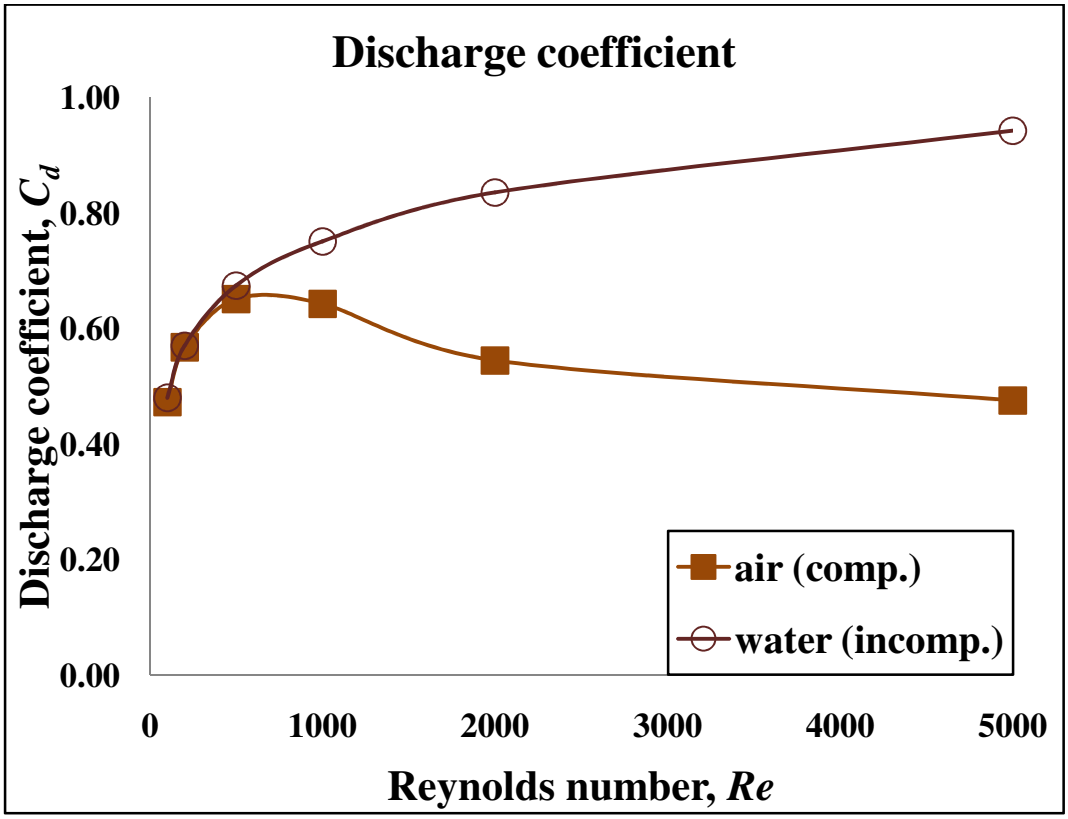

Figure 6.10. Discharge coefficient of second tooth vs. Reynolds number for both air and water (case #13–18 in Appendix A)

As shown in Figure 6.10, the discharge coefficient of the second tooth for water increases with the Reynolds number as if it is a logarithmical curve with a base > 0; however, the discharge coefficient of the second tooth for air decreases with the Reynolds number after the value of 500.

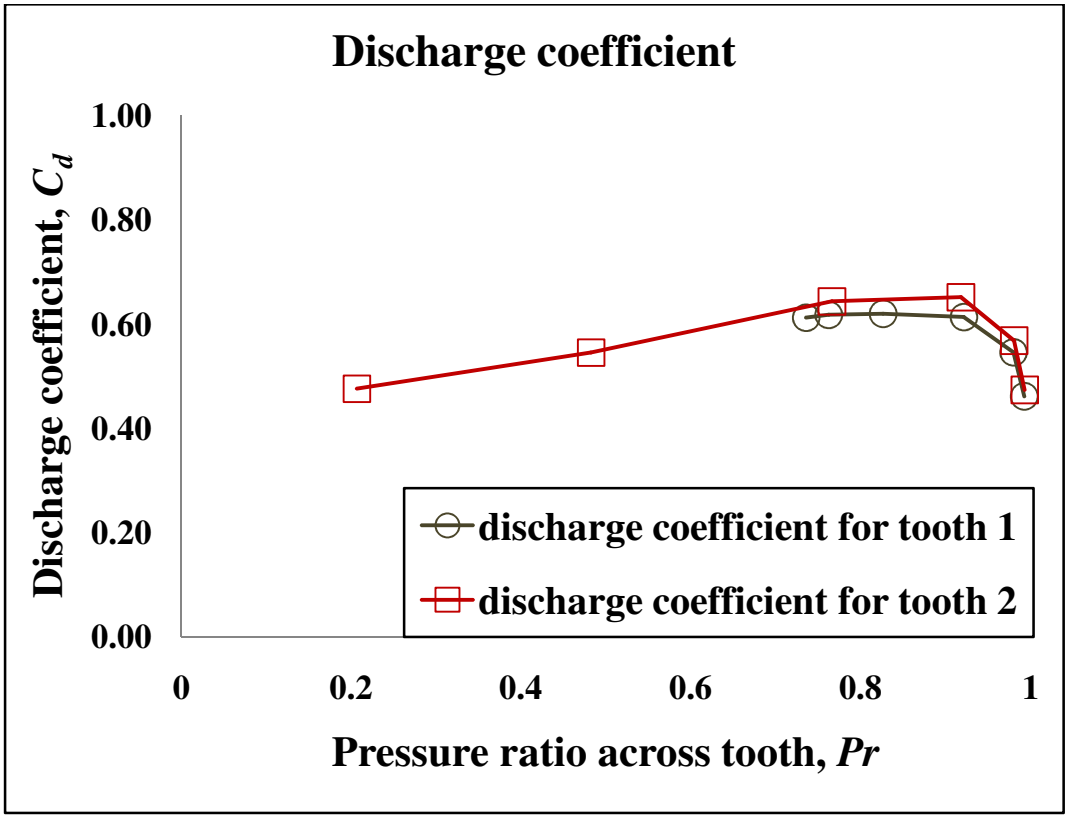

Figure 6.11. Discharge coefficient of each tooth vs. Pressure ratio across tooth for air (single cavity labyrinth seal for only air: case #13–18 in Appendix A)

In order to analyze why the discharge coefficient of air through the second tooth decreases with an increase in the Reynolds number, it is also necessary to compare the relationship between the discharge coefficient and the pressure ratio of air for each tooth. It can be seen in Figure 6.11 that as the pressure ratio across the tooth decreases, the discharge coefficient occurring through the first tooth only increases for the entire range of Reynolds numbers; however, until the pressure ratio decreases to 0.9179, the discharge coefficient occurring through the second tooth increases and after the value, the coefficient decreases. Therefore, it can be also observed that from Figure 6.9, the discharge coefficient

of the first tooth increases with an increasing Reynolds number and that from Figure 6.10, the discharge coefficient of the second tooth increases until Reynolds number 500 ($Pr = 0.9179$) and then decreases after the Reynolds number.

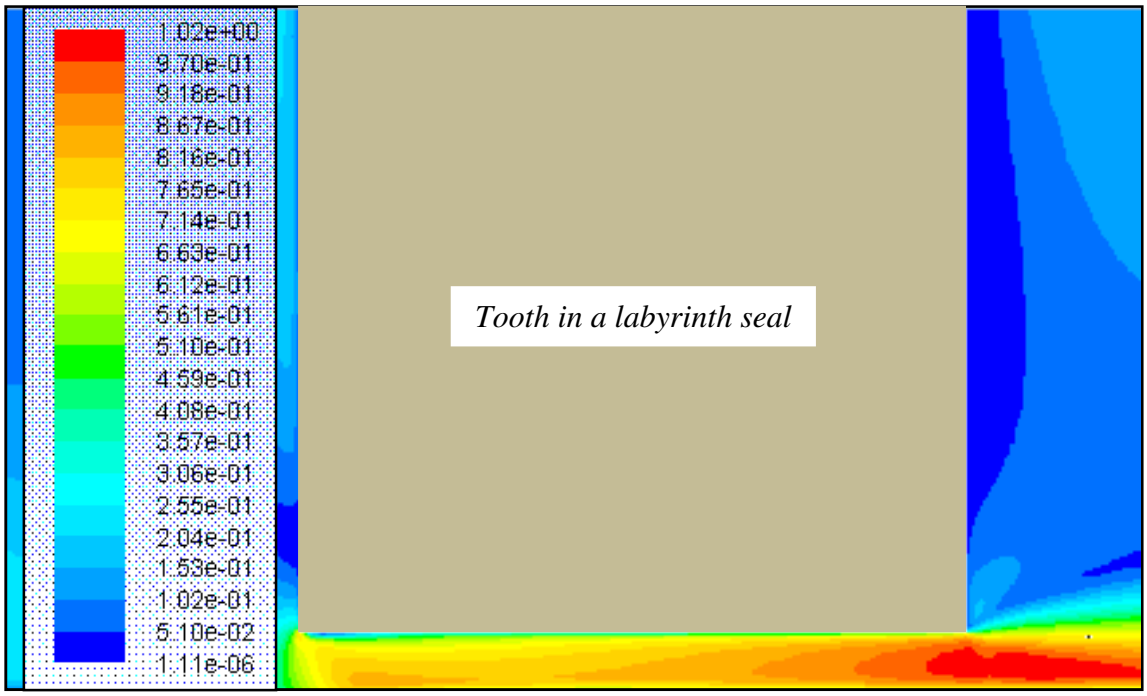

Figure 6.12. Contours for Mach number through constriction of second tooth for air (choked due to $Ma > 1$: case #13–18 in Appendix A)

As previously explained for the discharge coefficient of the second tooth for air (case #7–12), it is evident that the total losses occurring when air passes through the cavity and under the second tooth increase with an increase in the Reynolds number after the value of 500; that is, the pressure ratio across each tooth of the labyrinth seal decreases and the flow of the fluid through the constriction is choked as seen in Figure 6.12. The

difference in the discharge coefficients is attributed to the effect of the kinetic energy carry-over and compressible flow effects.

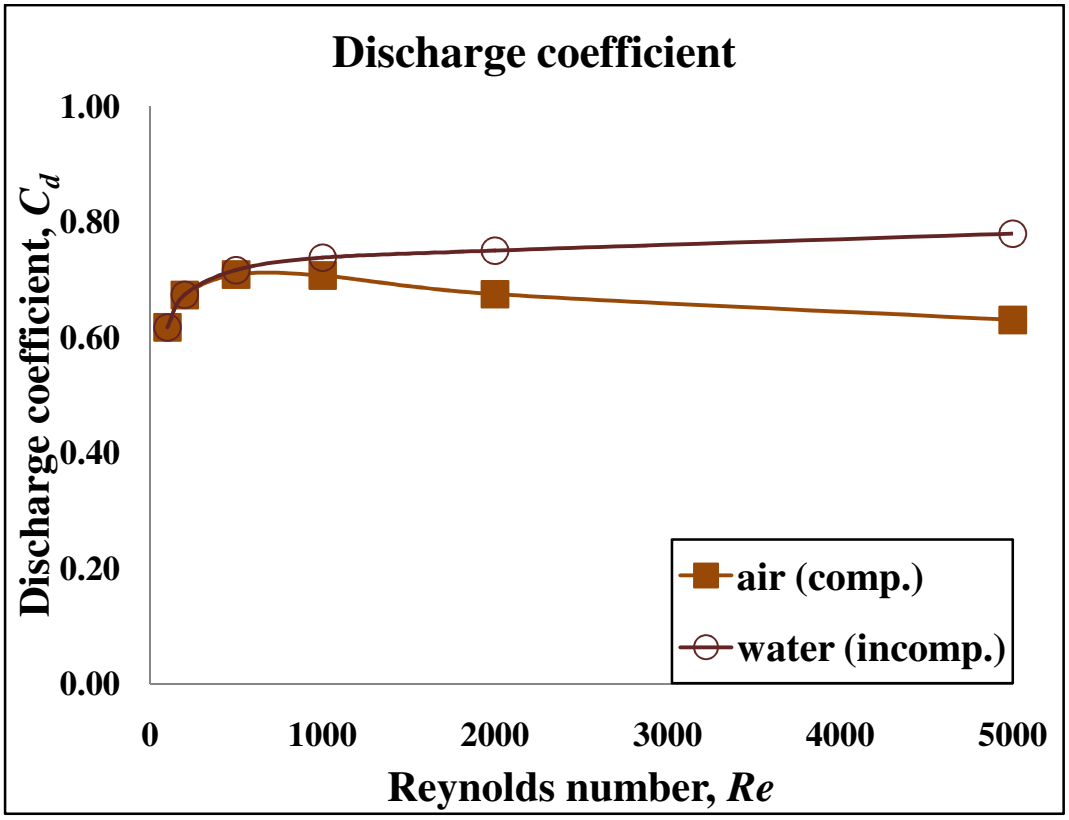

Figure 6.13. Discharge coefficient of first tooth vs. Reynolds number for both air and water (case #19–24 in Appendix A)

In the fourth instance ($n = 2, c = 0.15\ mm, s = 4\ mm, w = 0.4\ mm$) shown in Figures 6.13 and 6.14, it is observed that the discharge coefficients of the first and second teeth for water increase with an increase in the Reynolds number; however, the discharge coefficients of the first and second teeth for air decrease with an increase in the Reynolds number after the value of 500. This result suggests that because of the low

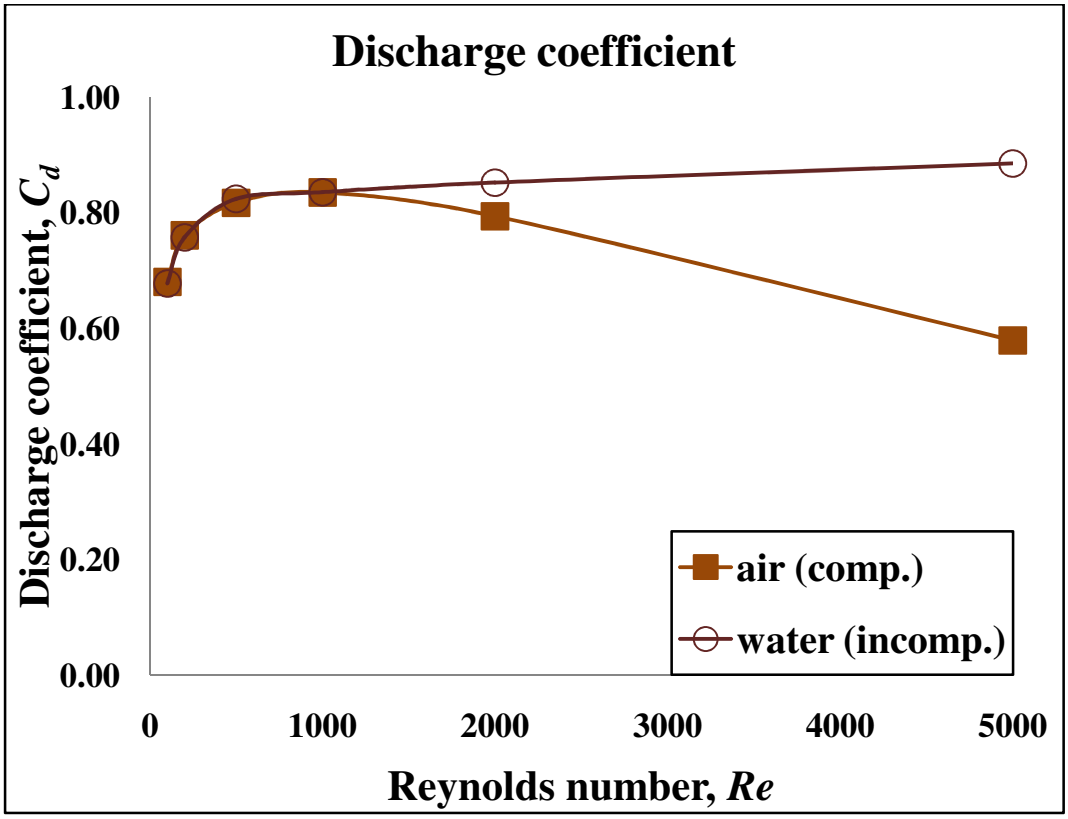

Figure 6.14. Discharge coefficient of second tooth vs. Reynolds number for both air and water (case #19–24 in Appendix A)

kinetic energy caused by its large divergence angle of the jet owing to a small Reynolds number, the water in the cavity is not dissipated, decreasing the losses in the cavity; therefore, the total losses occurring as water flows through the cavity and under the first and the second teeth cause the discharge coefficients to increase. Besides, it is apparent from Figures 6.13, and 6.14 that the total losses occurring as air flows through the cavity and under the first and the second teeth increase with an increase in the Reynolds numbers after the values of 500 and 1000, respectively and that the pressure ratio through each tooth in the labyrinth seal decreases. Further, as seen in Figures 6.15, and 6.16,

even though the flow of the fluid through the constriction is not choked, the decrease in the discharge coefficient for air is attributed to the pressure ratio.

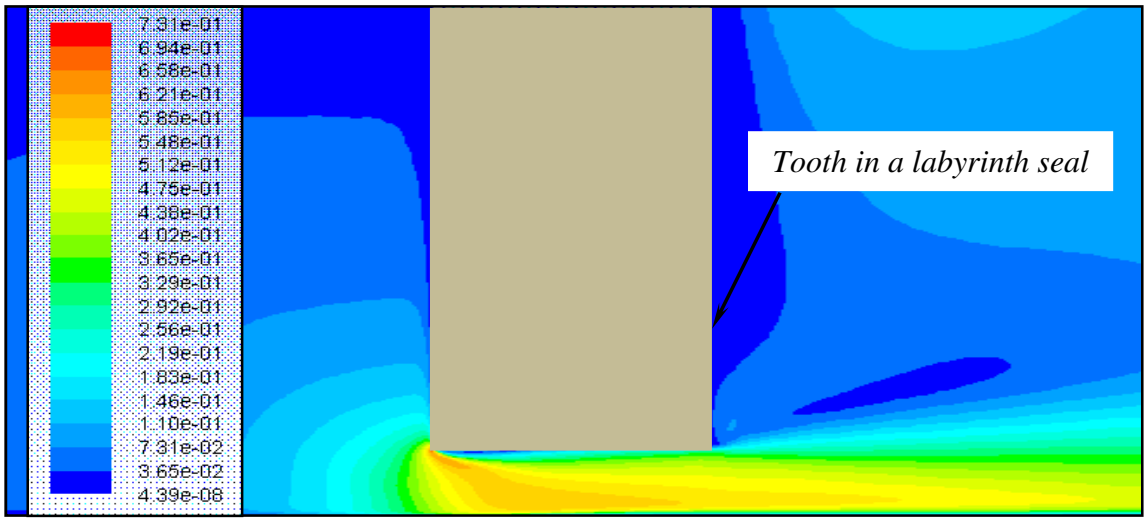

Figure 6.15. Contours for Mach number through constriction of first tooth for air (unchoked due to $Ma < 1$: case #19–24 in Appendix A)

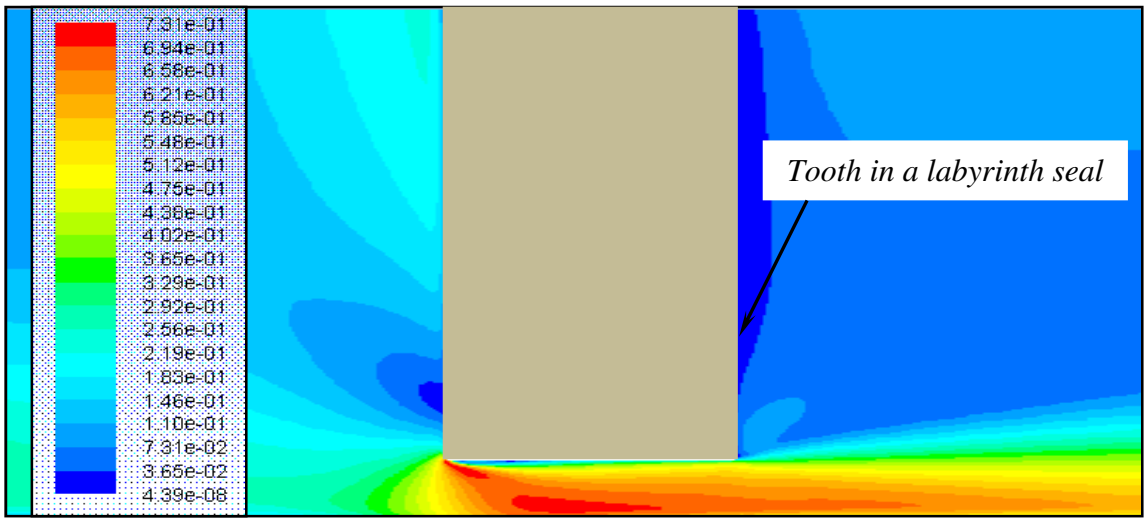

Figure 6.16. Contours for Mach number through constriction of second tooth for air (unchoked due to $Ma < 1$: case #19–24 in Appendix A)

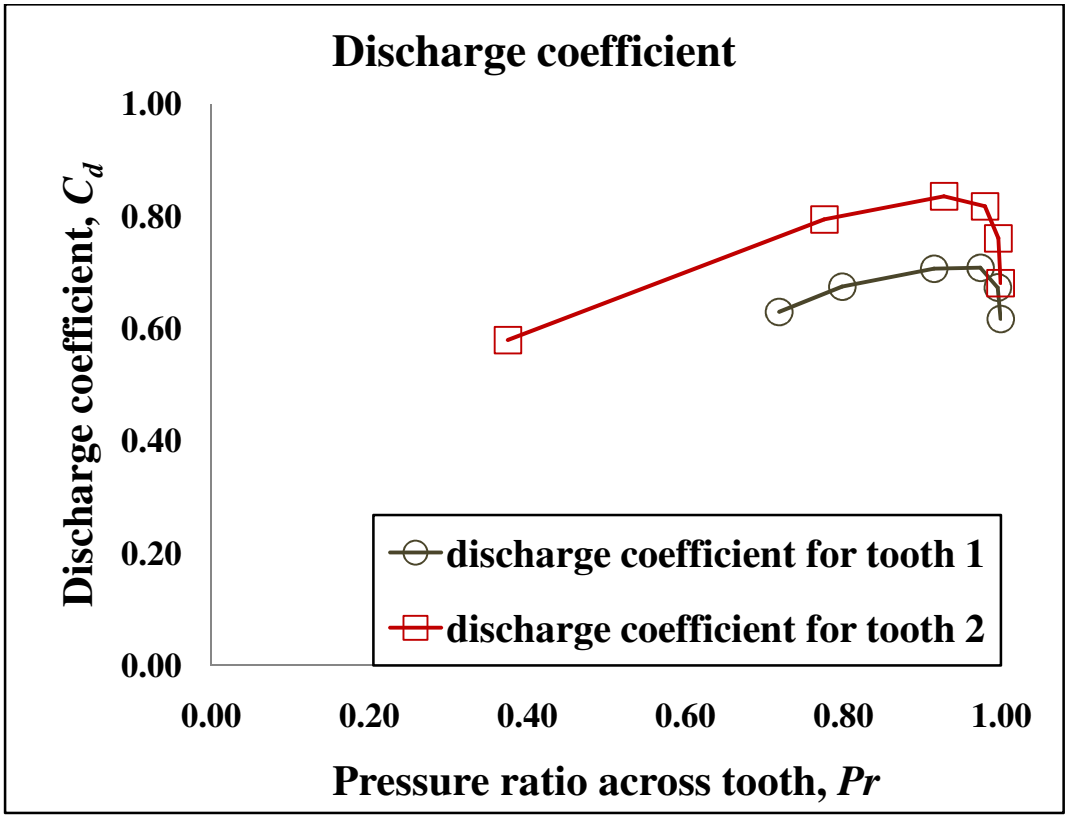

Figure 6.17. Discharge coefficient of each tooth vs. Pressure ratio across tooth for air (single cavity labyrinth seal for only air: case #19–24 in Appendix A)

Figure 6.17 shows that the relationship between the discharge coefficient and the pressure ratio of air for each tooth. It can be seen that until the pressure ratio across the tooth decreases to 0.9730, the discharge coefficient occurring through the first tooth increases and after the value, the coefficient decreases. Similarly, it can also be seen that until the pressure ratio across the tooth decrease to 0.9269, the discharge coefficient occurring through the second tooth increases and after the value, the coefficient decreases. Hence, it can be observed that from Figures 6.13 and 6.14, the discharge coefficients of the first and the second teeth increase until Reynolds numbers 500 and 1000, respectively

($Pr = 0.9730$ and $Pr = 0.9730$) and then decrease after the Reynolds numbers. This seal behaves significantly different from the first three instances, and this difference can be attributed to its large clearance and small tooth width.

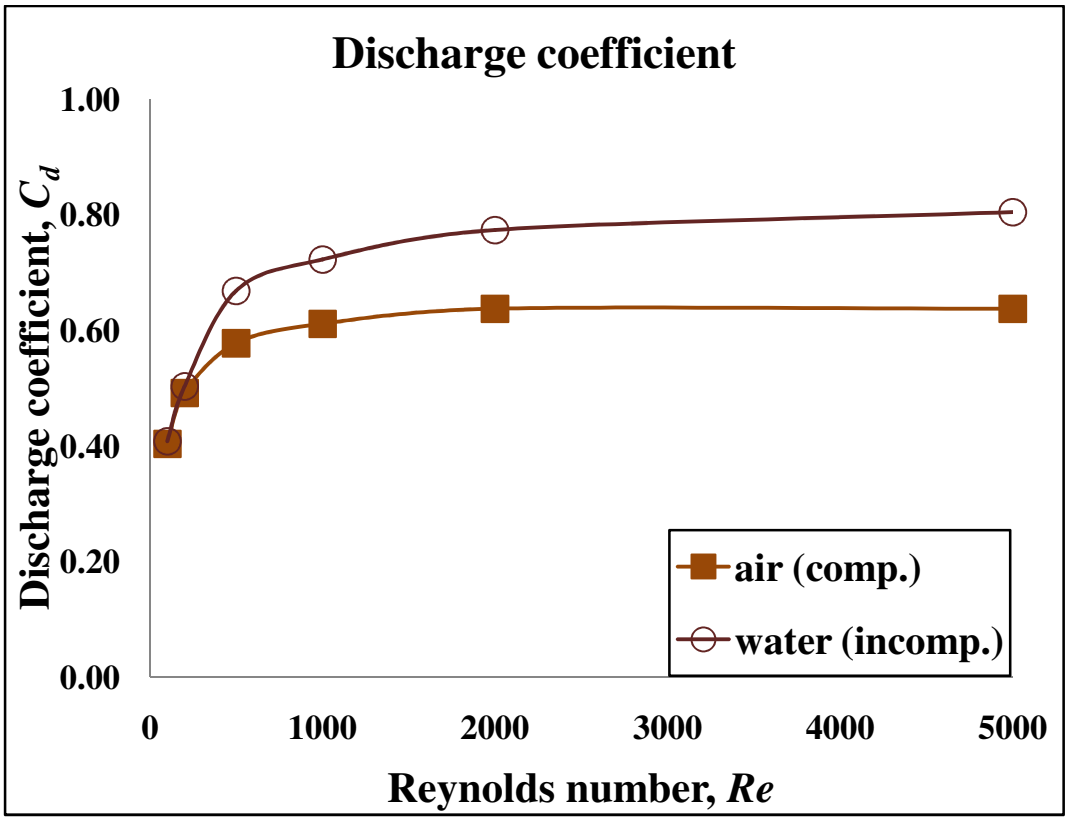

Figure 6.18. Discharge coefficient of first tooth vs. Reynolds number for both air and water (case #25–30 in Appendix A)

In the last instance ($n = 4, c = 0.06\,mm, s = 4\,mm, w = 1\,mm$) shown in Figures 6.18, 6.19, and 6.20, it is found that the discharge coefficients of the first, the second, and the third teeth for both air and water increase with the Reynolds number as if they are logarithmical curves with each base > 0. The discharge coefficient is essentially

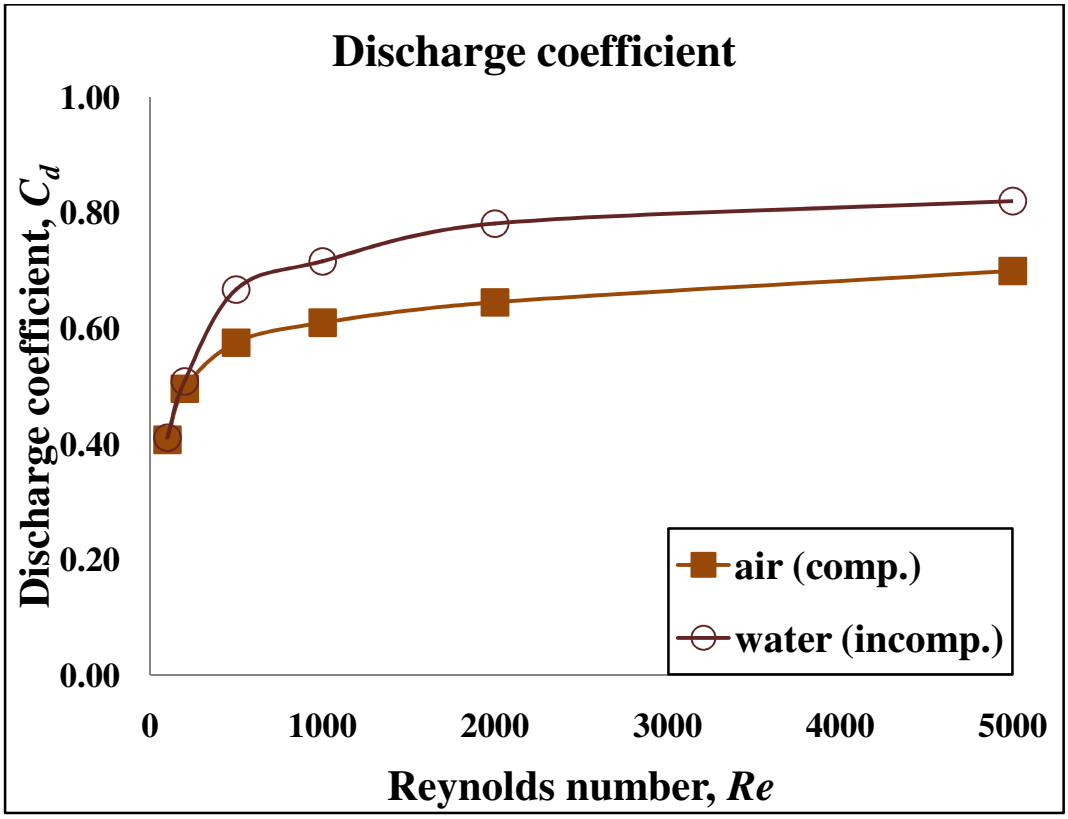

Figure 6.19. Discharge coefficient of second tooth vs. Reynolds number for both air and water (case #25–30 in Appendix A)

the same for all three teeth for the water flow and varies slightly at high Reynolds number for the air flow. These figures also show that because a large Reynolds number increases the inertial force of the jet of fluid emerging from under the tooth and decreases the viscous force under the same tooth, a small fraction of the kinetic energy of the fluid in the cavity is dissipated. In other words, due to the low kinetic energy caused by its large divergence angle of the jet, the fluid in the cavity is not dissipated, decreasing the losses in the cavity; therefore, the total losses occurring when the fluid flows through the two cavities and under the teeth cause the discharge coefficients of the first, the second,

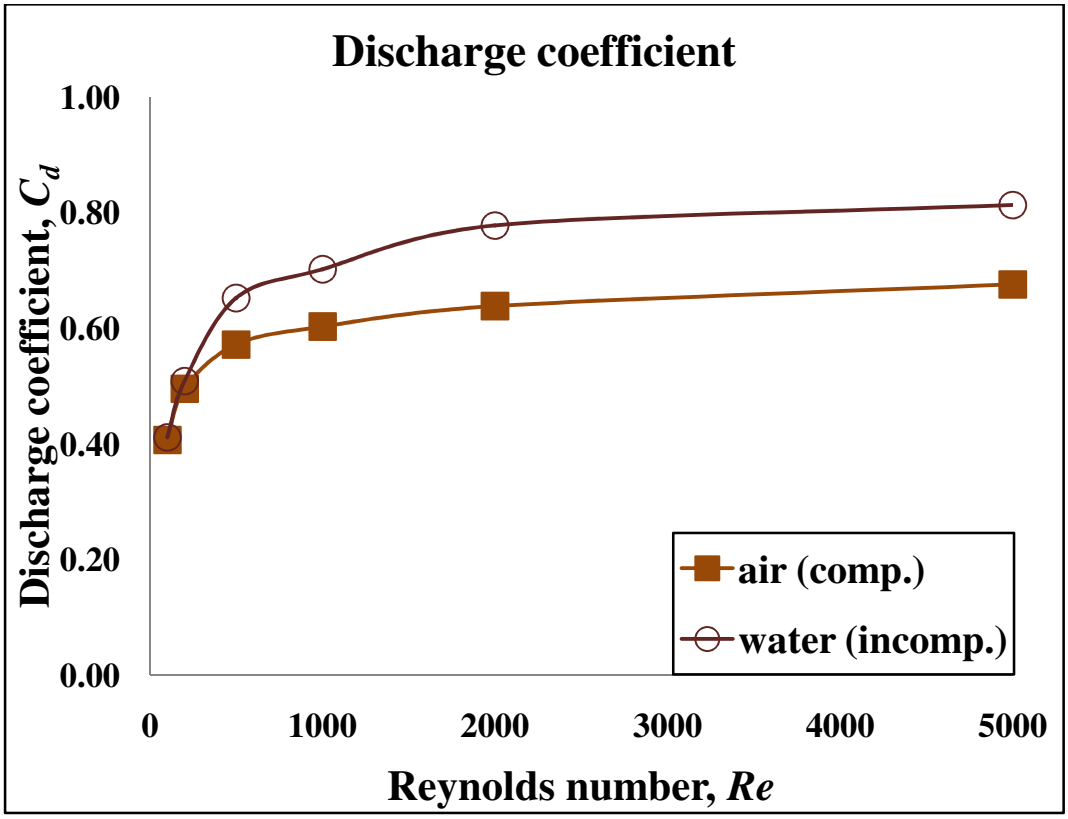

Figure 6.20. Discharge coefficient of third tooth vs. Reynolds number for both air and water (case #25–30 in Appendix A)

and the third teeth to increase. These Figures also show that the discharge coefficients of the first, the second, and the third teeth for water become greater than those for air on the basis of the Reynolds number. These results also hold for the carry-over coefficient. In other words, the difference in the discharge coefficients is attributed to the fact that the amount of the undissipated portion of the kinetic energy in the cavity increases when water is considered to be the working fluid, and not air. Because a high value of the discharge coefficient indicates that the labyrinth seal is less effective in dissipating the

kinetic energy, in order to reduce the leakage mass flow rate in the labyrinth seal, it is better to utilize air as the working fluid than water for the given geometric condition.

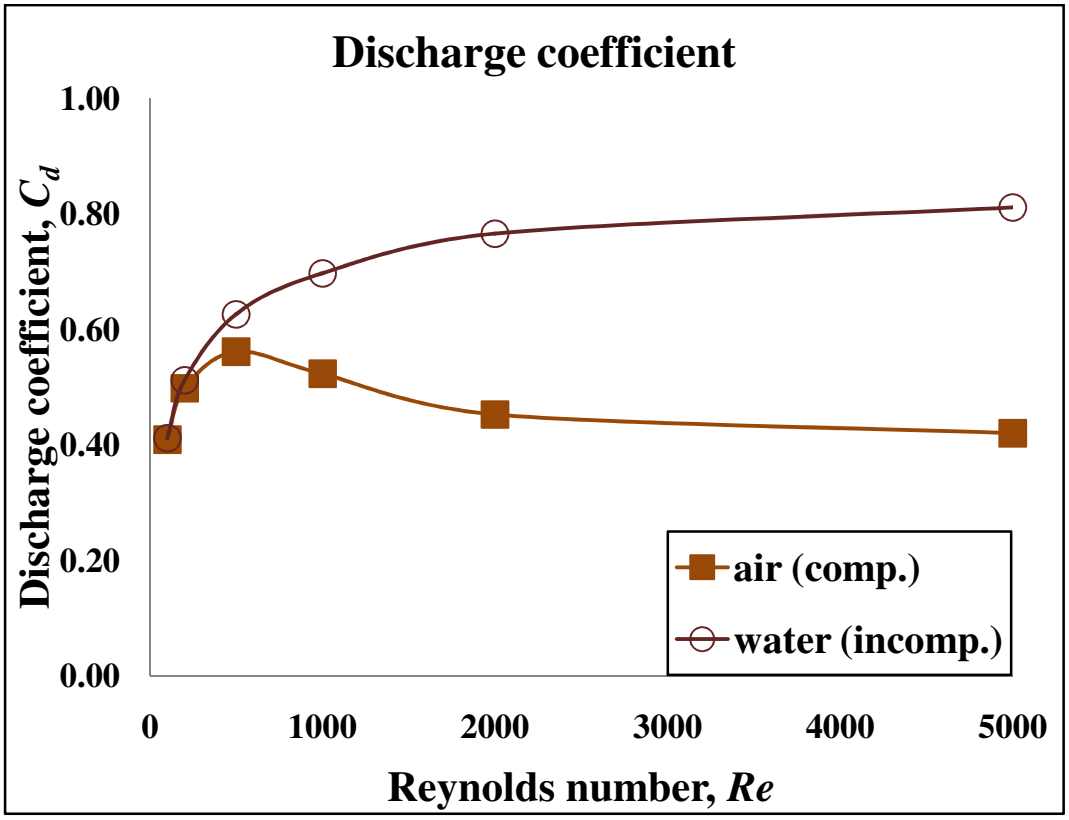

Figure 6.21. Discharge coefficient of fourth tooth vs. Reynolds number for both air and water (case #25–30 in Appendix A)

Figure 6.21 shows that the discharge coefficient of the fourth tooth for water has the same tendency as the first three teeth and increases with the Reynolds number as if it is a logarithmical curve with a base > 0; however, the discharge coefficient of the fourth tooth for air is very different from the first three teeth because it decreases with the Reynolds number after the value of 500. It is also found that because of the low kinetic

energy caused by its large divergence angle of the jet owing to a small Reynolds number, the fluid in the cavity does not dissipate, decreasing the losses in the cavity; therefore, the total losses occurring as the fluid flows through the last cavity and under the fourth tooth cause the discharge coefficient of the fourth tooth to increase.

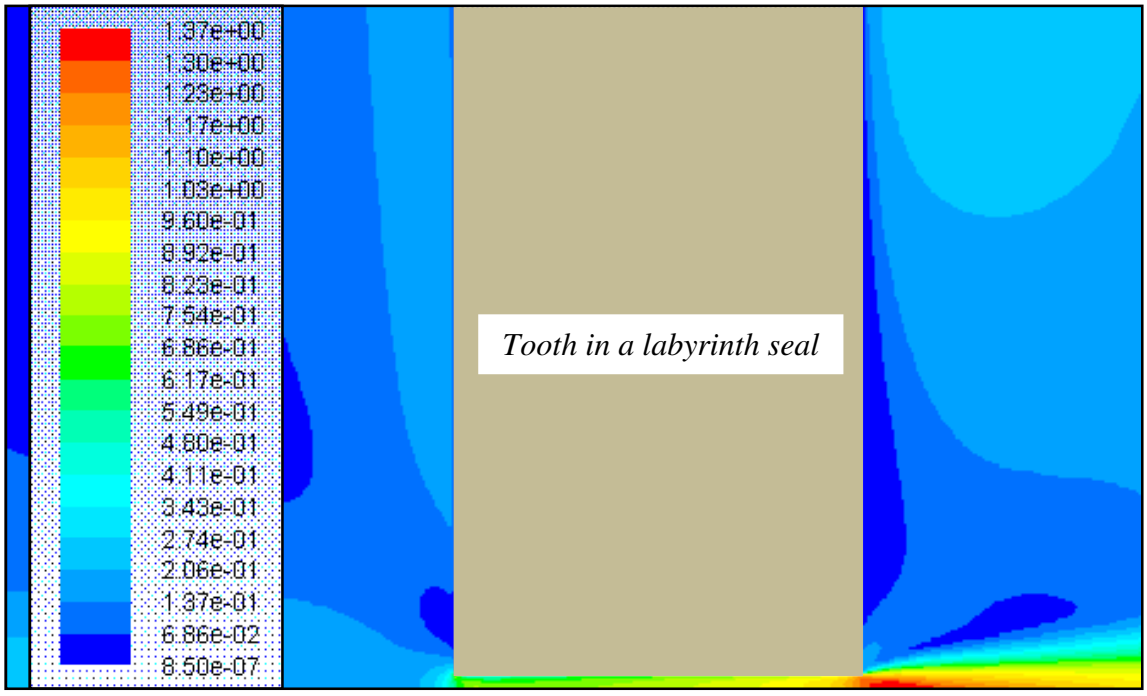

Figure 6.22. Contours for Mach number through constriction of fourth tooth for air (choked due to $Ma > 1$: case #25–30 in Appendix A)

Further, as previously explained for the discharge coefficient of the second tooth for air (case #19–24), it is found from Figure 6.21 that the total losses occurring when air passes through the last cavity and under the fourth tooth increase with an increase in the Reynolds number after the value of 500; in other words, the pressure ratio across each

tooth in the labyrinth seal decreases and the flow of the fluid through the constriction becomes compressible and the flow eventually choked as seen in Figure 6.22. The effect of the kinetic energy carry-over and compressible flow effects are responsible for the fact that the discharge coefficients of the first, the second, and the third teeth are greater than that of the fourth tooth.

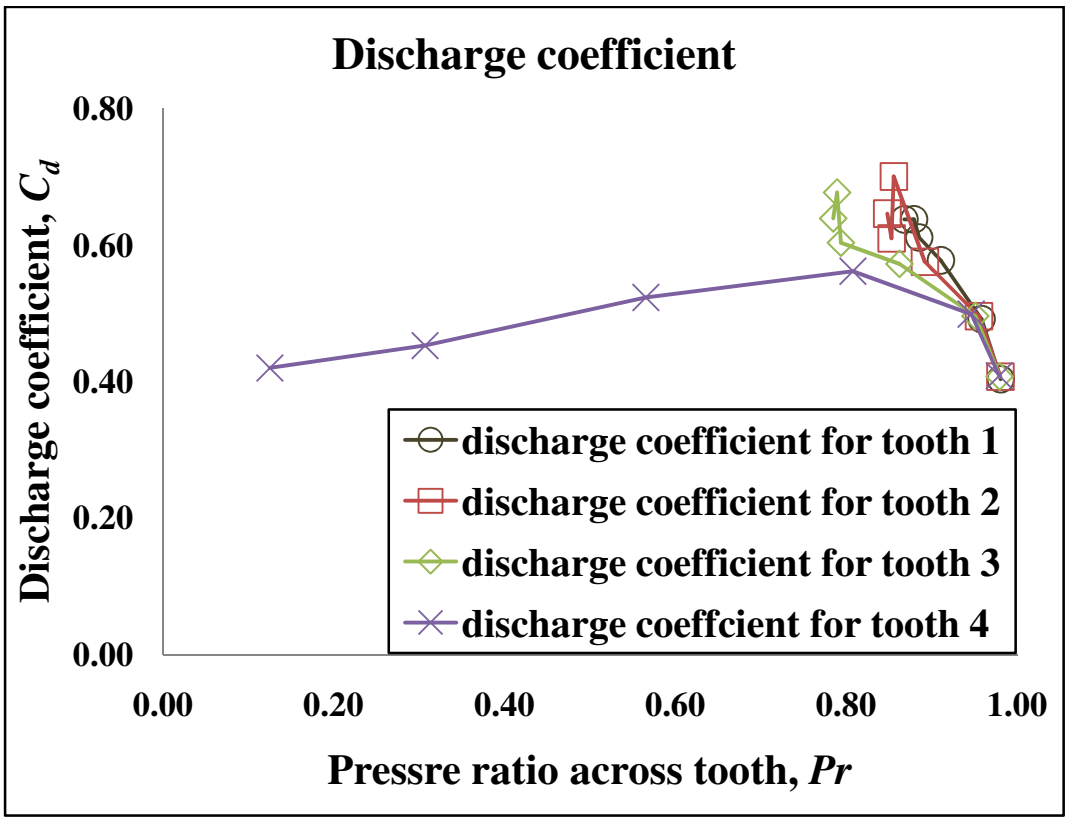

Figure 6.23. Discharge coefficient of each tooth vs. Pressure ratio across tooth for air (multiple cavity labyrinth seal for only air: case #25–30 in Appendix A)

In order to examine why the discharge coefficient of air through the fourth tooth does not increase with an increase in the Reynolds number, it also needs to collate the

relationship between the discharge coefficient and the pressure ratio of air for each tooth. It can be seen in Figure 6.23 that as the pressure ratio across the tooth decreases, the discharge coefficients occurring through the first, the second, and the third teeth increase for the entire range of Reynolds numbers; however, until the pressure ratio decreases to 0.8074, the discharge coefficient occurring through the fourth tooth increases and after the value, the coefficient decreases. Hence, it can be observed that from Figures 6.18, 6.19, and 6.20, the discharge coefficients of the first, the second, and the third teeth increase with an increasing Reynolds number and that from Figure 6.21, the discharge coefficient of the fourth tooth increases until Reynolds number 500 ($Pr = 0.8074$) and then decreases after the Reynolds number.

CHAPTER VII

EFFECT OF COMPRESSIBILITY

DEFINITION OF CARRY-OVER COEFFICIENT COMPRESSIBILITY FACTOR

Both compressible and incompressible fluids can be used as a working fluid in a turbomachine equipped with a labyrinth seal in order to reduce the internal leakage mass flow rate. Hence, it is necessary to analyze both compressible and incompressible flows as a working fluid.

This thesis defines the carry-over coefficient compressibility factor, φ, as the ratio of the carry-over coefficient of a cavity that includes effect of kinetic energy carry-over for compressible flow to that for incompressible flow through a labyrinth seal with the same geometry and at the same Reynolds number.

$$\varphi = \frac{\gamma_{compressible}}{\gamma_{incompressible}} \tag{7.1}$$

Therefore, it has to be noted that this carry-over coefficient compressibility factor accounts for the effects of compressibility on the kinetic energy carry-over, the carry-over coefficient and on the relationship between the carry-over coefficient and the discharge coefficient. Thus, in order to develop a model that provides accurate leakage mass flow rate prediction for compressible fluids, it needs to investigate whether the effect of the carry-over coefficient compressibility factor can influence the leakage mass flow rate through labyrinth seals. Moreover, in order to compensate for the effects of compressibility in the leakage model, it also needs to analyze the carry-over coefficient

compressibility factor and incorporate the factor into the leakage model to obtain more precise leakage mass flow rate through labyrinth seals.

EFFECT OF FLOW PARAMETERS ON CARRY-OVER COEFFICIENT COMPRESSIBILITY FACTOR

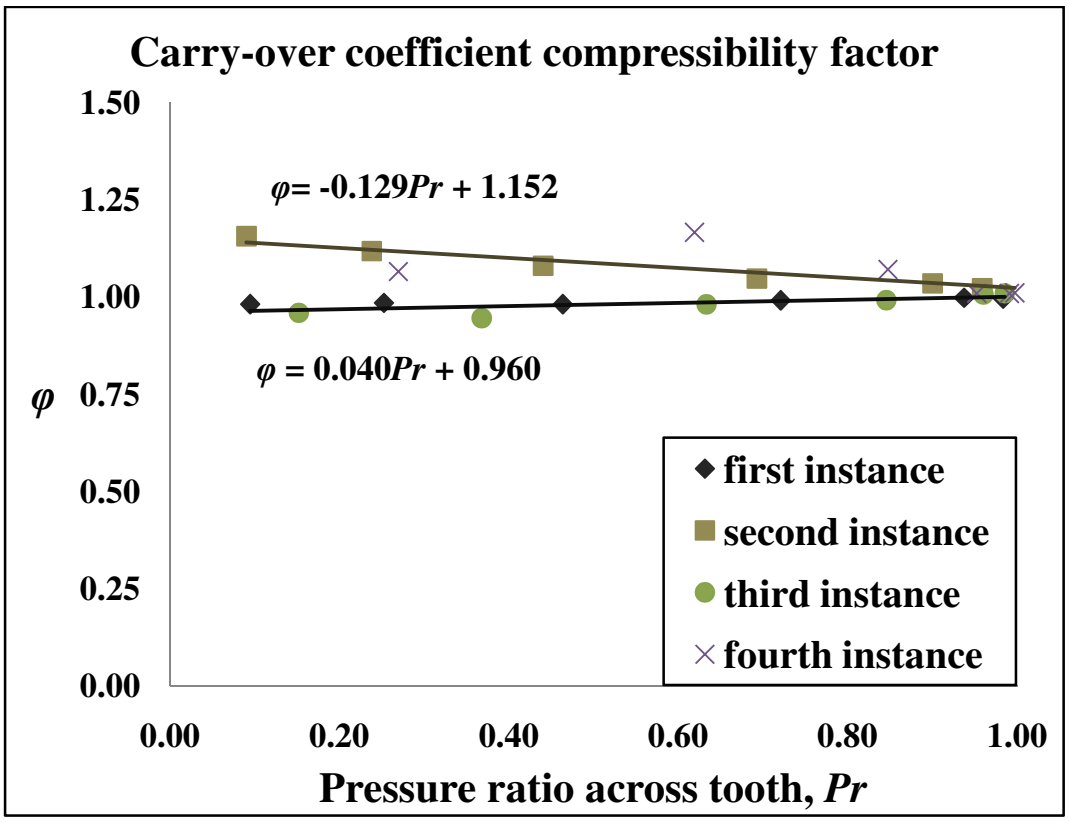

Figure 7.1. Comparison of carry-over coefficient compressibility factor for cavity between two teeth of single cavity labyrinth seal (cases #1–24 in Appendix A)

The effects of compressibility are generally quantified by pressure ratios. The carry-over coefficient compressibility factor is evaluated for the cavity between two

teeth in each instance and is plotted against the respective tooth pressure ratios. It can be observed from Figure 7.1 that regardless of the outlet pressure or Reynolds number, the carry-over coefficient compressibility factors of a single cavity labyrinth seal for the individual instances (cases #1–24 in Appendix A) possess two linear relationships with positive and negative slopes. More specifically, the first and the third instances create a positive slope while the second and the fourth instances produce a negative one with an increasing Reynolds number.

In order to analyze the effects of flow geometry for this result, it needs to observe Table 5.1 to find reasons on the seal geometry. It can be observed from Table 5.1 that this result is not associated with the seal geometry in that radial clearance to tooth width ratio (c/w) and radial clearance to tooth pitch ratio (c/s) for the four successive instances of a single cavity labyrinth seal are located within the nearly same ranges ($0.09 < c/w < 2$, $0.015 < c/s < 0.025$ for the first and the third, $0.06 < c/w < 0.375$, $0.015 < c/s < 0.0375$ for the second and the fourth). However, it is recommended to study more c/w simulations for future work to define c/w dependence.

Nonetheless, there seems to be other reasons beyond the seal geometry to account for the result. Since the variation rate of the carry-over coefficient of a cavity for the compressible flow is smaller than that of the incompressible flow as the pressure ratio is decreased, the carry-over coefficient compressibility factors for the first and the third instances decrease.

$$\varphi = 0.040\, Pr + 0.960 \tag{7.2}$$

Further, for the second and the fourth instances, because the variation rate of the carry-over coefficient of a cavity for the compressible flow is larger than that of the

incompressible flow as the pressure ratio is also decreased, the carry-over coefficient compressibility factors increase.

$$\varphi = -0.129\ Pr + 1.152 \tag{7.3}$$

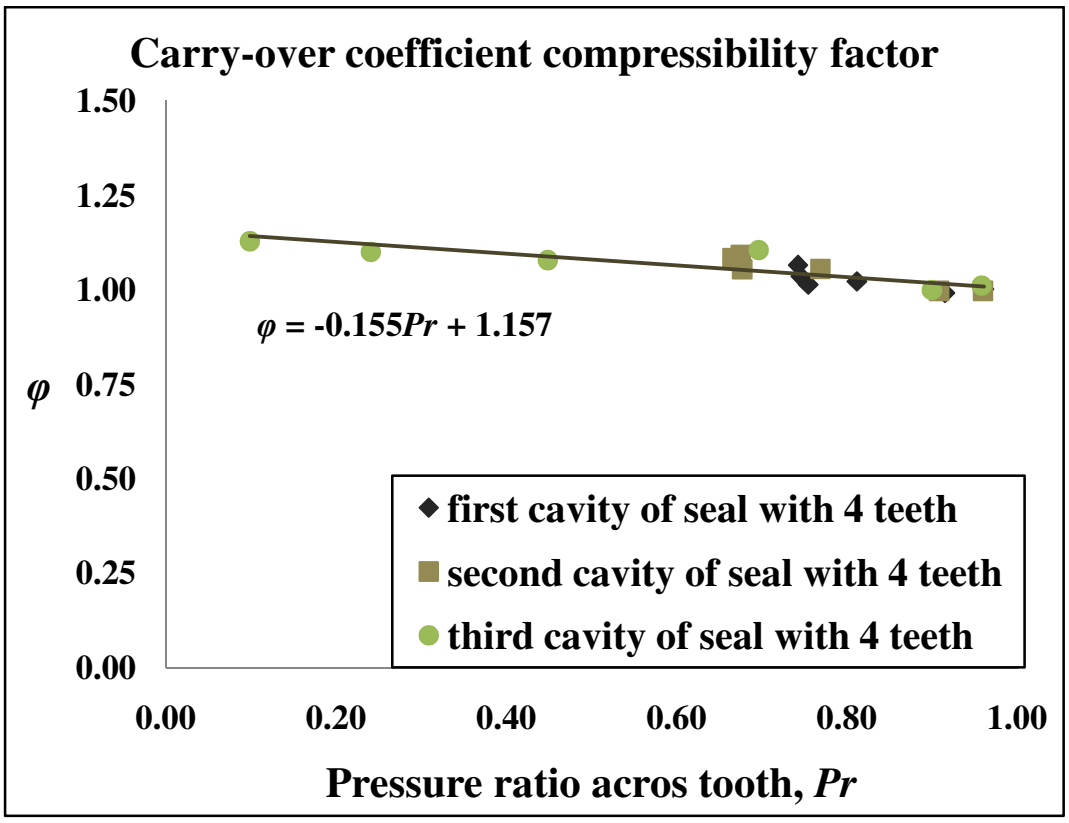

Figure 7.2. Comparison of carry-over coefficient compressibility factor for cavity between two teeth of multiple cavity labyrinth seal with four teeth (cases #25–30 in Appendix A)

The conclusions drawn from the above Figure 7.1 were based on compressible flow simulations performed on a labyrinth seal with a single cavity. In order to extend the application to generally used labyrinth seals which have multiple cavities, simulations

are performed on a four teeth seal as shown in Figure 7.2. For a multiple cavity labyrinth seal with four teeth, it can be seen that regardless of the number of teeth, the carry-over coefficient compressibility factors have a linear relationship possessing a negative slope with the pressure ratios.

$$\varphi = -0.155\ Pr + 1.157 \tag{7.4}$$

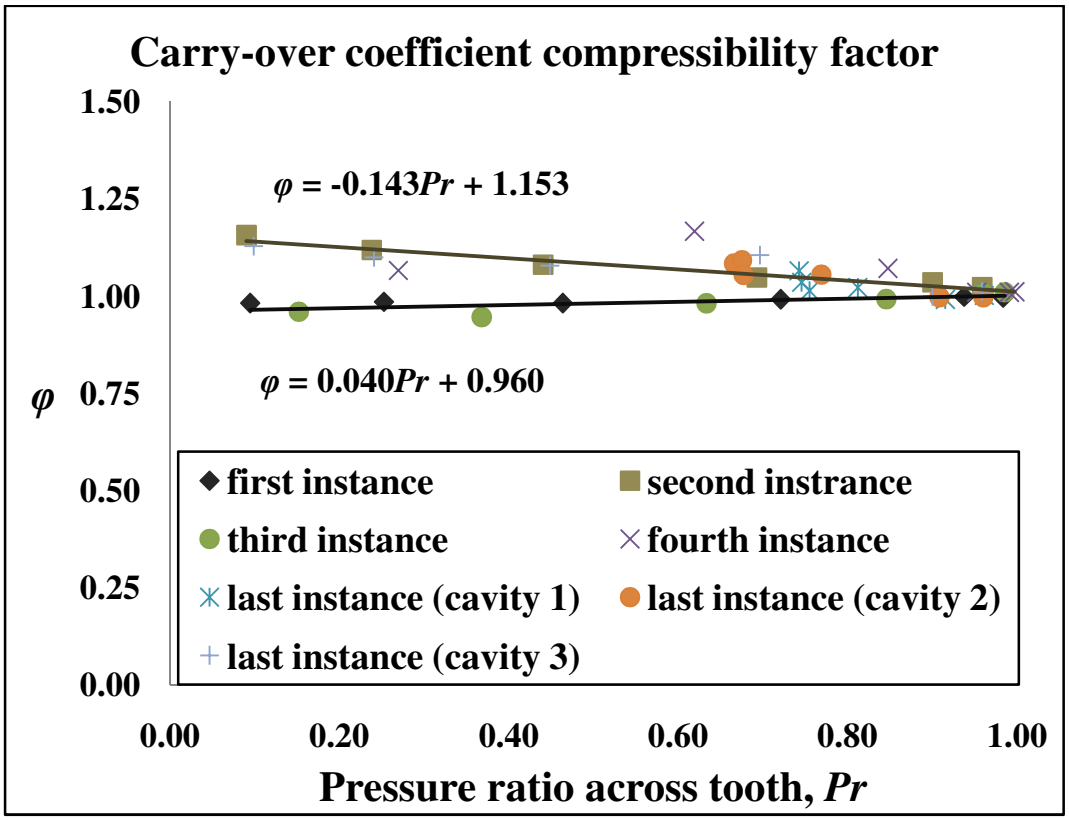

Figure 7.3. Comparison of carry-over coefficient compressibility factor for cavity between two teeth of both single and multiple cavity labyrinth seals (including all the cases #1–30 in Appendix A)

Figure 7.3 collates the carry-over coefficient compressibility factor through each cavity of a multiple cavity labyrinth seal with that through the cavity of a single cavity

labyrinth seal. It can be also observed that the φ-Pr relationship, when using the line of best fit, turns out to be two linear curves with positive and negative slopes. Further, it can be seen that the φ-Pr relationship is independent of the position of the tooth. Thus, it can be concluded that the carry-over coefficient compressibility factors are independent of the number of teeth through a given cavity. Therefore, it is worth mentioning that the φ-Pr relationship, which has considered both single and multiple cavity labyrinth seals for the compressible flow, can be modeled as not only positive linear relationship but also negative linear relationship, and the effect of the carry-over coefficient compressibility factor can be included into the leakage model.

$$\varphi = 0.040\ Pr + 0.960 \qquad for\ positive\ slope \tag{7.5}$$

$$\varphi = -0.143\ Pr + 1.153 \qquad for\ negative\ slope \tag{7.6}$$

DEFINITION OF DISCHARGE COEFFICIENT COMPRESSIBILITY FACTOR

Saikishan [14] discovered that at low pressure ratios (less than 0.7), his incompressible model deviated from CFD (Computational Fluid Dynamics) simulation results. Hence, the effects of compressibility become significant and the discharge coefficient compressibility factor, ψ, needs to be included into the leakage model.

The definition of the discharge coefficient compressibility factor for a labyrinth seal is the ratio of the discharge coefficient of a tooth (that includes the effect of energy carry-over) for compressible flow to that for incompressible flow through a labyrinth seal with the same geometry and at the same Reynolds number.

$$\psi = \frac{C_{d,compressible}}{C_{d,incompressible}} \tag{7.7}$$

Further, his thesis compares compressible discharge coefficients calculated from CFD simulations with the incompressible discharge coefficient predicted by his model.

$$\dot{m} = \psi C_{d\,n} A\sqrt{2\rho_n(p_n - p_{n+1})} \qquad (1 \le n \le N) \tag{7.8}$$

for $0.0075 < c/s < 0.0375$, $0.0075 < w/s < 0.5$, $2.67 < w/c < 66.67$,

$0.75 < h/s < 4$, *and* $250 < Re < 15000$

$$C_{d\,n} = C_d^{1\,tooth} \qquad for\ first\ constriction \qquad (n = 1) \tag{7.9}$$

$$C_{d\,n} = C_d^{1\,tooth}(0.925\,\gamma^{0.861}) \qquad for\ subsequent\ teeth \qquad (n > 1) \tag{7.10}$$

$$C_d{}^{1\,tooth} = \frac{0.7757 - 0.002051(w/c)}{(1 + 44.86(w/c)/Re)^{0.2157}} \tag{7.11}$$

$$\gamma = \left(1 - 6.5\,(c/s) - 8.638(c/s)(w/s)\right)(Re + R_0)^{\left(2.454(c/s)+2.268(c/s)(w/s)^{1.673}\right)} \tag{7.12}$$

$$R_0 = \left(1 - 6.5\,(c/s) - 8.638(c/s)(w/s)\right)^{\left(-\frac{1}{2.454(c/s)+2.268(c/s)(w/s)^{1.673}}\right)} \tag{7.13}$$

$$Re = \frac{\dot{m}}{\mu\pi D} \tag{7.14}$$

$$\psi = 0.558\left(\frac{p_{n+1}}{p_n}\right) + 0.442 \tag{7.15}$$

Therefore, it is necessary to know that the discharge coefficient compressibility factor explains the effects of compressibility on the kinetic energy carry-over, the discharge coefficient and also on the relationship between the carry-over coefficient and the discharge coefficient. In addition, in his study, the discharge coefficient compressibility factor is determined by dividing the discharge coefficient obtained from FLUENT CFD simulations with air as a working fluid (the ideal gas assumption) and by the discharge coefficient of incompressible flow predicted by Equations 7.11 and 7.16.

$$z = 0.925\gamma^{0.861} \tag{7.16}$$

Where, by defining z as the ratio of the discharge coefficient of the second tooth to that of the first tooth (or the discharge coefficient of the equivalent seal with a single tooth), Saikishan obtained that z should be a function of only the carry-over coefficient.

$$z = \frac{C_d}{C_d^{1\ tooth}} = f(\gamma) \tag{7.17}$$

EFFECT OF FLOW PARAMETERS ON DISCHARGE COEFFICIENT COMPRESSIBILITY FACTOR

Saikishan [14] showed that his model developed for water can be utilized to accurately estimate the leakage mass flow rate and the pressure distribution for air as long as the individual tooth pressure ratios are greater than 0.7. Thus, this is expected that at low pressure ratios, the effects of compressibility become remarkable and hence the discharge coefficient compressibility factor needs to be incorporated into the leakage model. Here, what one should know is that the effects of compressibility are generally quantified by the pressure ratio. Hence, the term $\sqrt{\frac{1-(p_e/p_i)^2}{N-ln(p_e/p_i)}}$ of Martin's model [4] is necessary to compensate for compressibility effects.

In Figure 7.4, the discharge coefficient compressibility factor through each tooth of a single cavity labyrinth seal is presented. It can be observed that irrespective of the outlet pressure or Reynolds number, the ψ-Pr follows a common linear curve. Also, remarkable is the fact that the ψ-Pr of all the four instances can collapse into a single linear relationship if the discharge coefficient compressibility factor through the second

tooth of the third instance is deleted. This is likely because the flow is choked and for the given seal geometry, the flow is strongly dependent on the choke phenomenon. While it is possible that this relationship can depend on geometric parameters, it is also obvious from Figure 7.4 that the pressure ratio across the tooth (not the overall pressure ratio) is the primary flow parameter which determines the discharge coefficient compressibility factor.

$$\psi = 0.463\, Pr + 0.542 \tag{7.18}$$

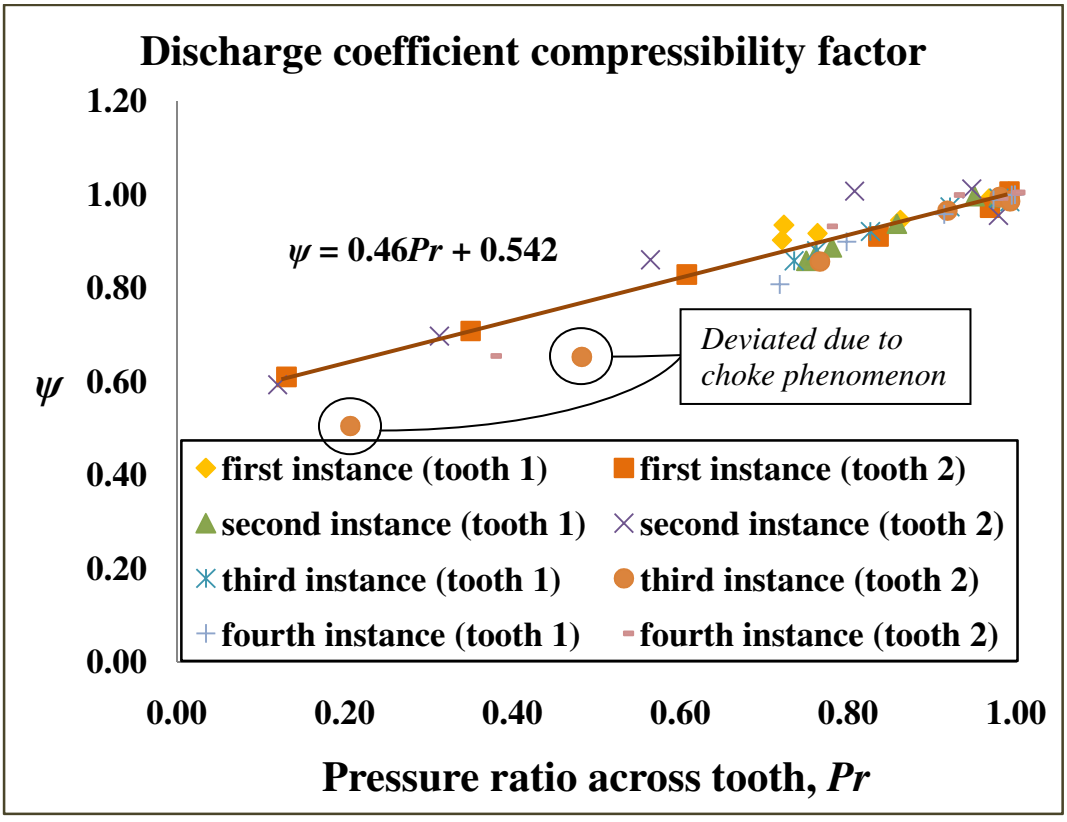

Figure 7.4. Comparison of discharge coefficient compressibility factor through each tooth of single cavity labyrinth seal (cases #1–24 in Appendix A)

Figure 7.5 presents that the discharge coefficient compressibility factor is obviously independent of seal geometry under some limits considered. It seems that clearance may have a small effect on the discharge coefficient compressibility factor. As there is an increase in clearance, there is a slight increase in the discharge coefficient compressibility factor. However, since the variation rate of the discharge coefficient compressibility factor is about 5% even though clearance is increased by 50%, it can be considered negligible.

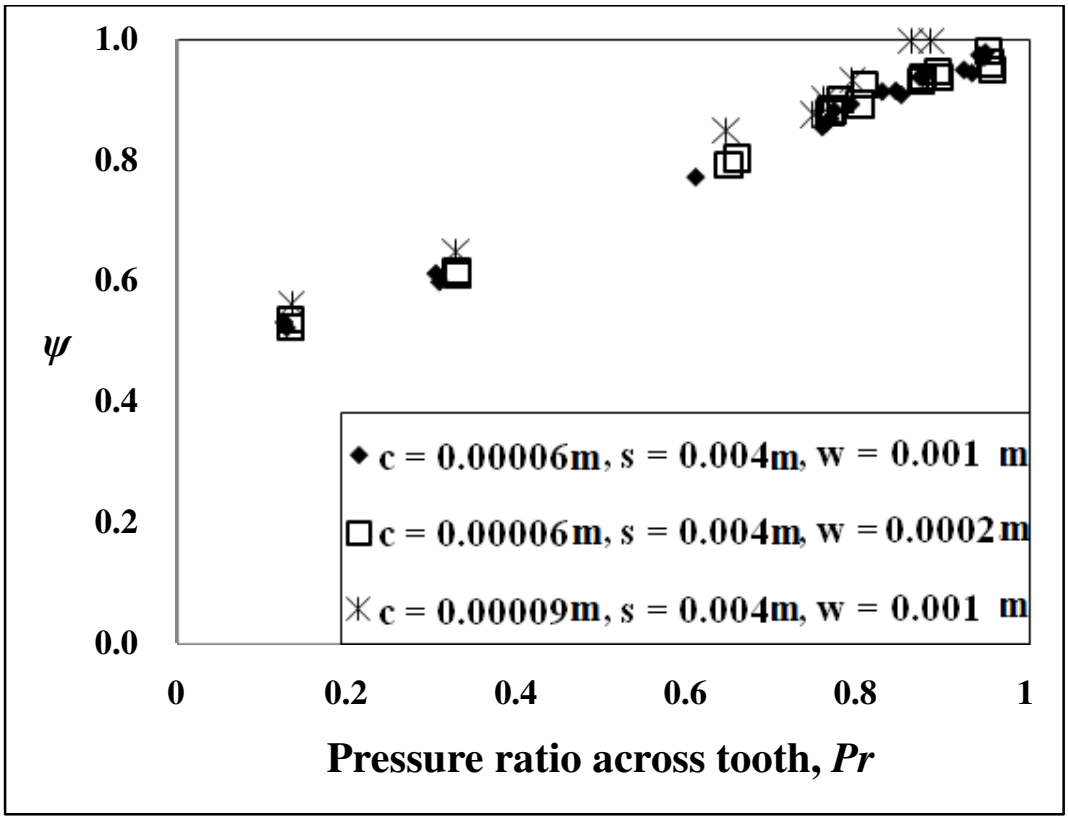

Figure 7.5. Effect of seal geometry on discharge coefficient compressibility factor (cases #10, 13, and 16 in Appendix B based on Saikishan's studies)

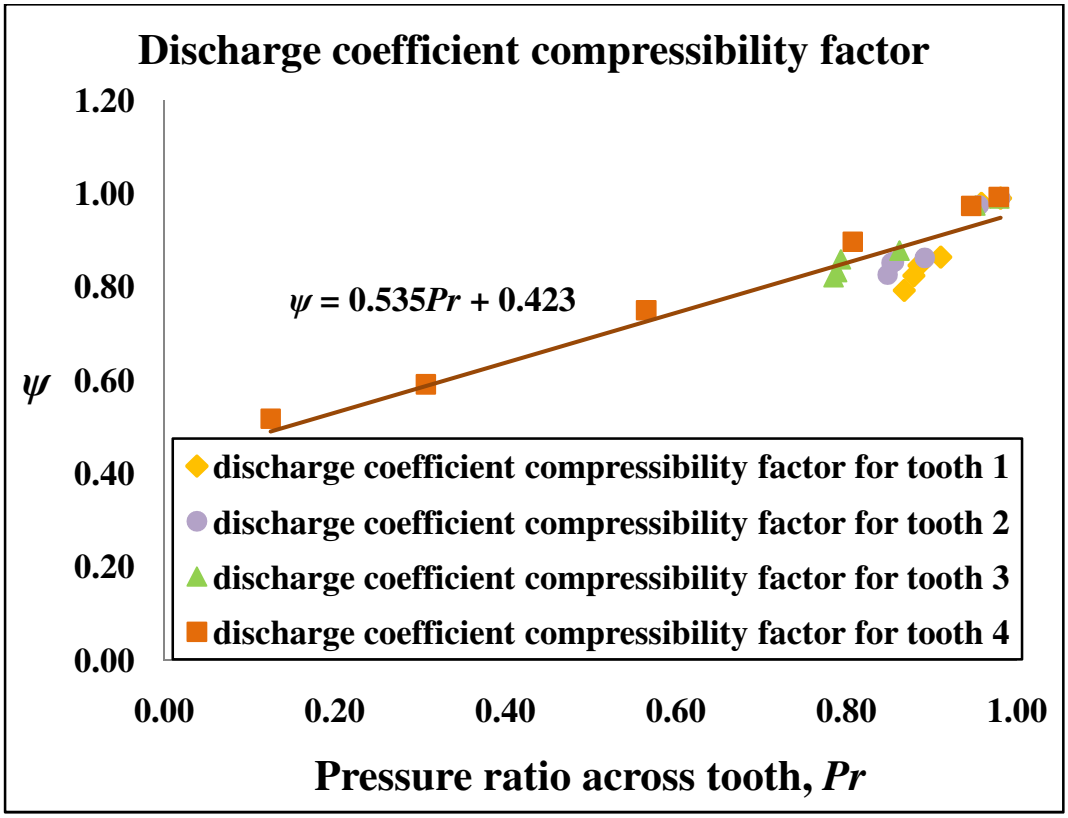

Figure 7.6. Comparison of discharge coefficient compressibility factor through each tooth of multiple cavity labyrinth seal with four teeth (cases #25–30 in Appendix A)

In order to extend the understanding to really use labyrinth seals which have multiple cavities, simulations are also performed on a four teeth seal and then the discharge coefficient compressibility factor is computed for each flow under each tooth through the labyrinth seal. Figure 7.6 compares the discharge coefficient compressibility factor across different teeth of the multiple cavity labyrinth seal (cases #25–30 in Appendix A). The ψ-Pr relationship is also shown to be independent of the number of the teeth and is only dependent on the pressure ratios across the teeth. Thus, the discharge coefficient

compressibility factor across a tooth, based on the tooth pressure ratio, can be modeled by applying the linear relationship as earlier models.

$$\psi = 0.535\, Pr + 0.423 \tag{7.19}$$

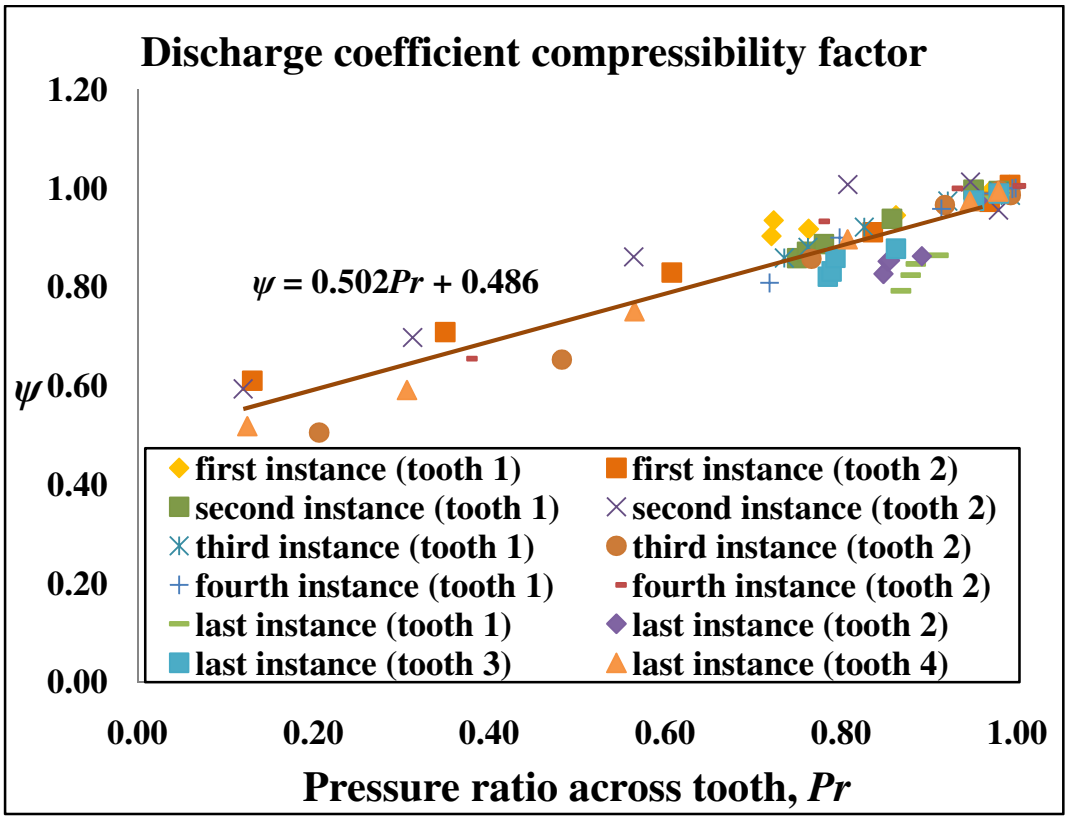

Figure 7.7. Comparison of discharge coefficient compressibility factor through each tooth of both single and multiple cavity labyrinth seals (including all the cases #1–30 in Appendix A)

In order to analyze the entire effect of the discharge coefficient compressibility factor, it needs to consider both single and multiple cavity labyrinth seals. Figure 7.7 represents the discharge coefficient compressibility factors of both single and multiple

cavity labyrinth seals. It can be also observed from Figure 7.7 that the ψ-Pr relationship for the compressible flow can be modeled as a linear relationship and the effect of the discharge coefficient compressibility factor can be included into the leakage model. Further, it is found that the standard deviation of the curve fit is $\pm$ 0.046 showing how much dispersion is from the line of best fit.

$$\psi = 0.502\ Pr + 0.486\ [\pm\ 0.046\ (Standard\ Deviation)] \tag{7.20}$$

The ψ-Pr relationship is marginally different from that estimated by Saikishan presented in Equation 7.15. However, the significant points are that the relationship is only a function of pressure ratio and that as the pressure ratio is decreased by flowing through each tooth within labyrinth seals, the discharge coefficient compressibility factor also decreases.

CHAPTER VIII

VALIDATION AND CONCLUSIONS

In this chapter, the simulations performed in this thesis are evaluated compared with an earlier model. That is to say, the results of this thesis will be validated by being collated with the model derived by Saikishan [14]. Then, conclusions will be described for each parameter: the carry-over coefficient, γ, the discharge coefficient, C_d, and the discharge coefficient compressibility factor, ψ.

Even though the results of this thesis have been developed from CFD (Computational Fluid Dynamics) simulations which apply turbulence models and numerical schemes, it is necessary to perform a direct comparison of the results against the previous models. This work will verify not only the accuracy of the results conducted in this thesis but also the accuracy of the earlier model deduced by Saikishan and also indicate the range of flow and geometric conditions for which the results provides accurate prediction.

VALIDATION OF CARRY-OVER COEFFICIENT AGAINST SIMULATION DATA PERFORMED BY EARLIER MODEL

Table 8.1. Comparison of simulations and Saikishan's flow and geometric conditions

	Reynolds No.	c/w	c/s	w/s	h/s
Simulations	100 – 5000	0.06 – 5	0.015 – 0.0375	0.0075 – 0.25	0.9625 – 0.985
Saikishan's	250 – 15000	0.015 – 0.3745	0.0075 – 0.0375	0.0075 – 0.5	0.75 – 4

Table 8.2. Seal geometry ratios applied for simulations of compressible and incompressible flows

Case No.	Reynolds No.	No. of Teeth	c/w	c/s	w/s	h/s
1–6	100 – 5000	2	**2***	0.015	0.0075	0.985
7–12	100 – 5000	2	0.06	0.015	0.25	0.985
13–18	100 – 5000	2	0.09	0.0225	0.25	0.9775
19–24	100 – 5000	2	**0.375***	**0.0375***	0.1	0.9625
25–30	100 – 5000	4	0.06	0.015	0.25	0.985

Note: * indicates that this value is out of the range of Saikishan's model.

The first instance ($n = 2, c = 0.06\ mm, s = 4\ mm, w = 0.03\ mm$) provided in Figure 8.1 suggests that at low Reynolds numbers ($Re < 500$), the carry-over coefficient of incompressible fluid is approximately equivalent to that of Saikishan's model. However, as the Reynolds number increases ($Re > 500$), the carry-over coefficient of the incompressible fluid continuously deviates from that of Saikishan's model. Since Saikishan's model was deduced under the flow and geometric conditions which are different from those selected in these studies as shown in Table 8.1, it can be safely said that his model can be applied to his limited conditions only. It means that the deviation is due to the difference (mainly $c/w = 2$ out of the range of Saikishan's model) between the simulations and Saikishan's limited conditions presented in Table 8.2. Hence, it is necessary to compensate for the differences between the simulations and Saikishan's model with respect to higher Reynolds

numbers ($Re > 500$) in order to predict more perfect leakage mass flow rate through labyrinth seals.

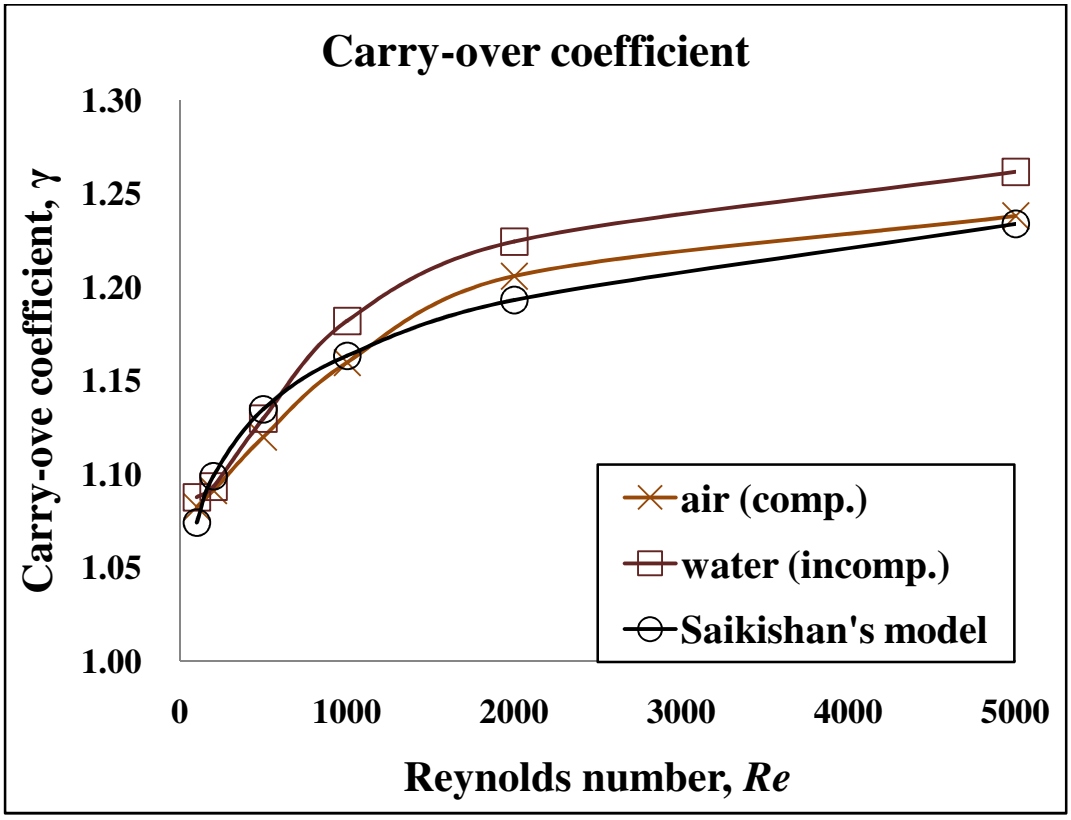

Figure 8.1. Comparison of carry-over coefficient of predicted compressible and incompressible flows of single cavity labyrinth seal with Saikishan's model (case #1–6 in Appendix A)

The second instance ($n = 2, c = 0.06$ mm, $s = 4$ mm, $w = 1$ mm) provided in Figure 8.2 shows that since the carry-over coefficient of incompressible flow performed by simulations appears to be nearly invariant with an increasing Reynolds number, it considerably differs from that of Saikishan's model. Even though the seal geometry

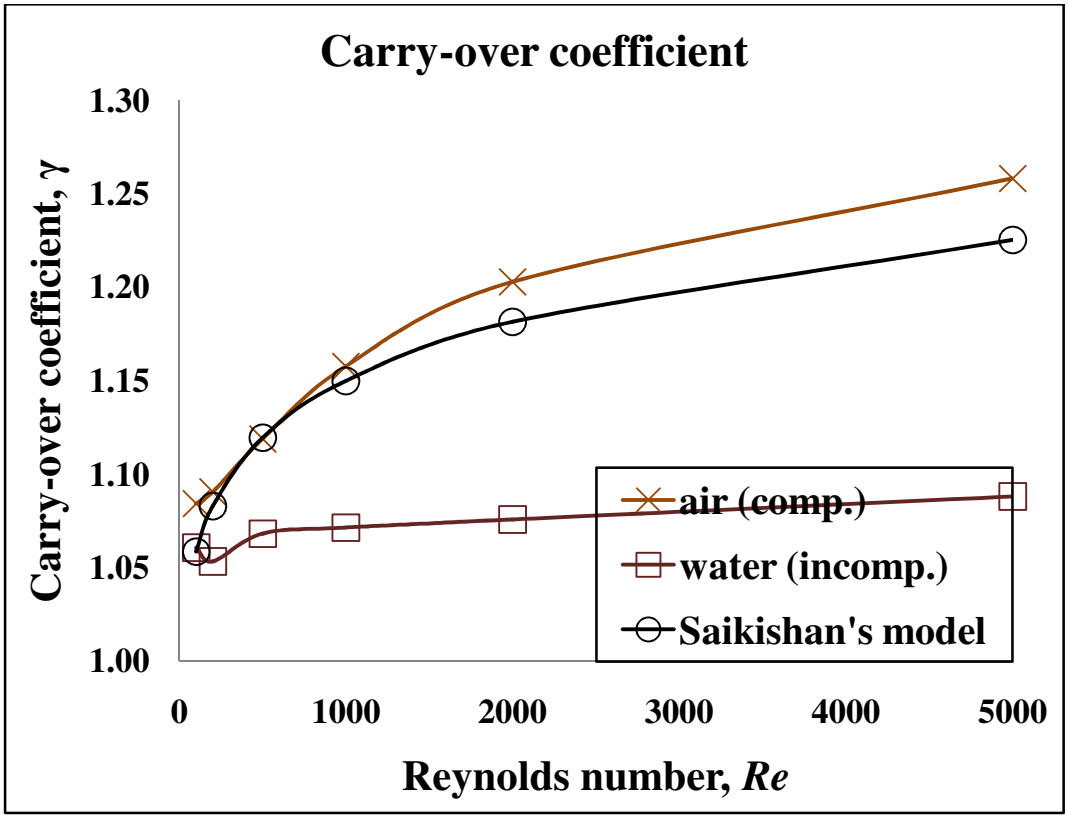

Figure 8.2. Comparison of carry-over coefficient of predicted compressible and incompressible flows of single cavity labyrinth seal with Saikishan's model (case #7–12 in Appendix A)

ratios performed for the simulations presented in Table 8.2 are within the range of Saikishan's model, the outcomes show that there are differences between the simulations and Saikishan's model. The obvious fact is that due to the relatively wide tooth width ($w = 1\ mm$), the viscous force under the tooth is more dominant than the inertial force of the jet from under the same tooth. As a result, the kinetic energy in the cavity is dissipated better than that of the narrow tooth width. It causes the carry-over coefficient of the incompressible flow with the wide tooth width not to increase as fast as that with

the narrow one. Therefore, in order to make sure of the effect of the wide tooth width, it is considered to study more simulations for future work to develop more accurate leakage mass flow rate through labyrinth seals.

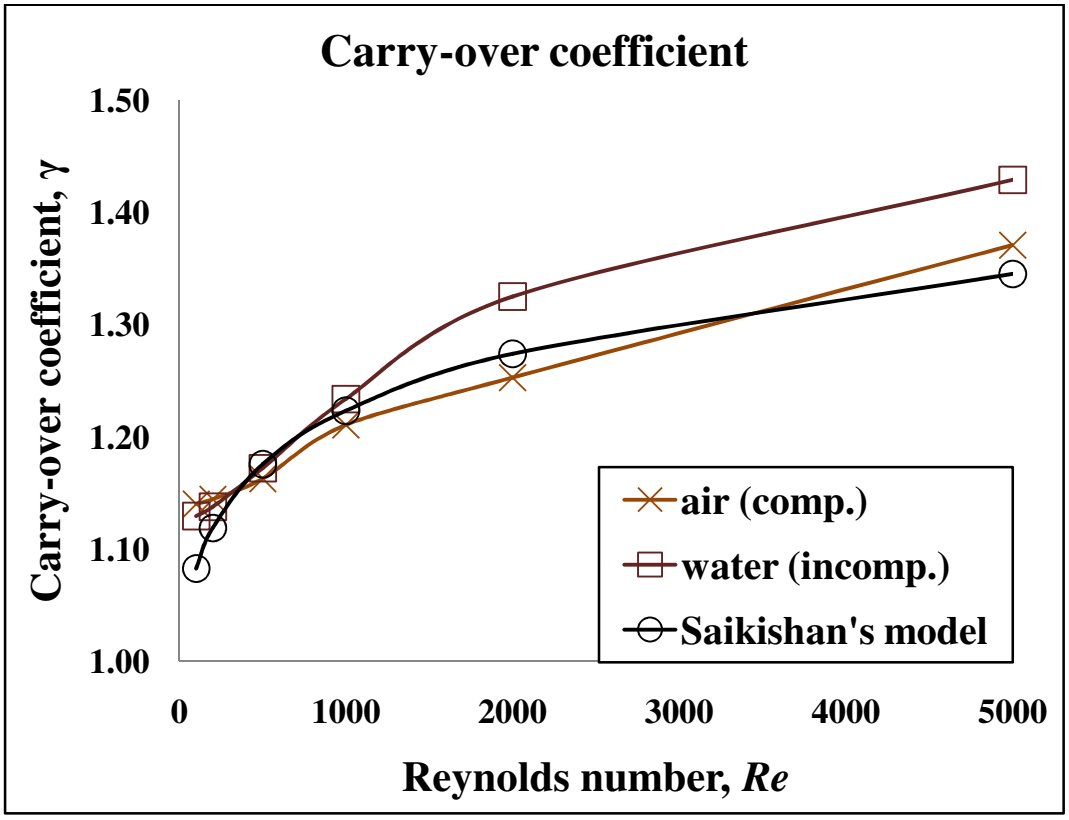

Figure 8.3. Comparison of carry-over coefficient of predicted compressible and incompressible flows of single cavity labyrinth seal with Saikishan's model (case #13–18 in Appendix A)

The third instance ($n = 2, c = 0.09\ mm, s = 4\ mm, w = 1\ mm$) provided in Figure 8.3 indicates that at low Reynolds numbers ($Re < 1000$), the carry-over coefficient of incompressible fluid is almost correspondent with that of Saikishan's model. However,

as the Reynolds number increases ($Re > 1000$), the carry-over coefficient of the incompressible fluid shows gradual deviation with Reynolds number. Table 8.2 shows that the seal geometry ratios performed for this instance are within the range of Saikishan's model; however, the carry-over coefficient conducted by the simulations is different from that predicted by Saikishan's model. Since this instance also deals with the relatively wide tooth width ($w = 1\ mm$), the viscous force under the tooth is more dominant than the inertial force of the jet from under the same tooth and hence the kinetic energy in the cavity is dissipated better than that of the narrow tooth width. Consequently, the carry-over coefficient of the incompressible flow with the wide tooth width more slowly increase than that with the narrow one. Hence, it also needs to investigate the effect of the wide tooth width for developing more exact leakage prediction through labyrinth seals with respect to higher Reynolds numbers ($Re > 1000$).

The fourth instance ($n = 2, c = 0.15\ mm, s = 4\ mm, w = 0.4\ mm$) provided in Figure 8.4 denotes that the carry-over coefficient of incompressible fluid is significantly different from that of Saikishan's model. This is associated with the differences ($c/w = 0.375$, $c/s = 0.0375$ out of the range of Saikishan's model) between the simulations and Saikishan's limited conditions presented in Table 8.2.

Moreover, because of the transition process, the carry-over coefficient of the incompressible fluid near Reynolds number of 1000 tends to slightly decrease and then increase. Thus, it has to be noted that not only should the differences between the simulations and Saikishan's model for the entire range of Reynolds numbers be

compensated for, but the effect of the transition process in the model should also be considered in order to estimate more precise leakage mass flow rate through labyrinth seals.

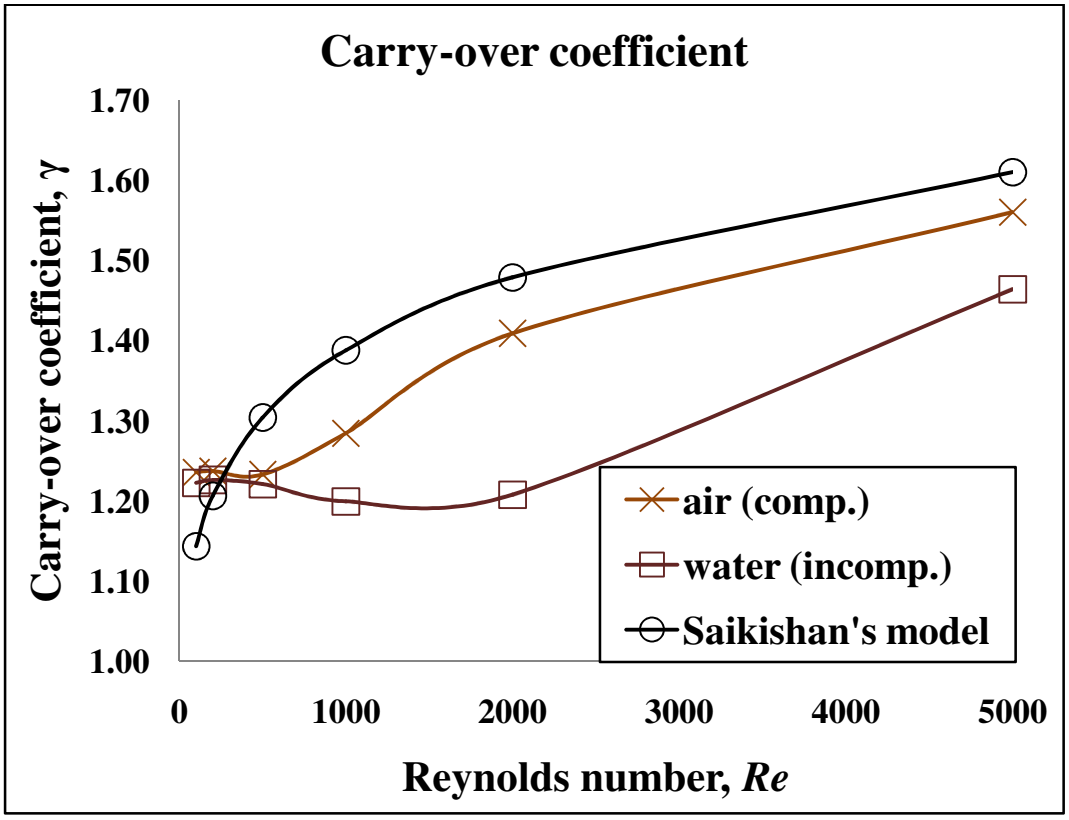

Figure 8.4. Comparison of carry-over coefficient of predicted compressible and incompressible flows of single cavity labyrinth seal with Saikishan's model (case #19–24 in Appendix A)

The last instance ($n = 4, c = 0.06\,mm, s = 4\,mm, w = 1\,mm$) provided in Figures 8.5, 8.6, and 8.7 suggests that this is a multiple cavity labyrinth seal with four teeth. It can be seen in Figures 8.5, 8.6, and 8.7 that the carry-over coefficients of

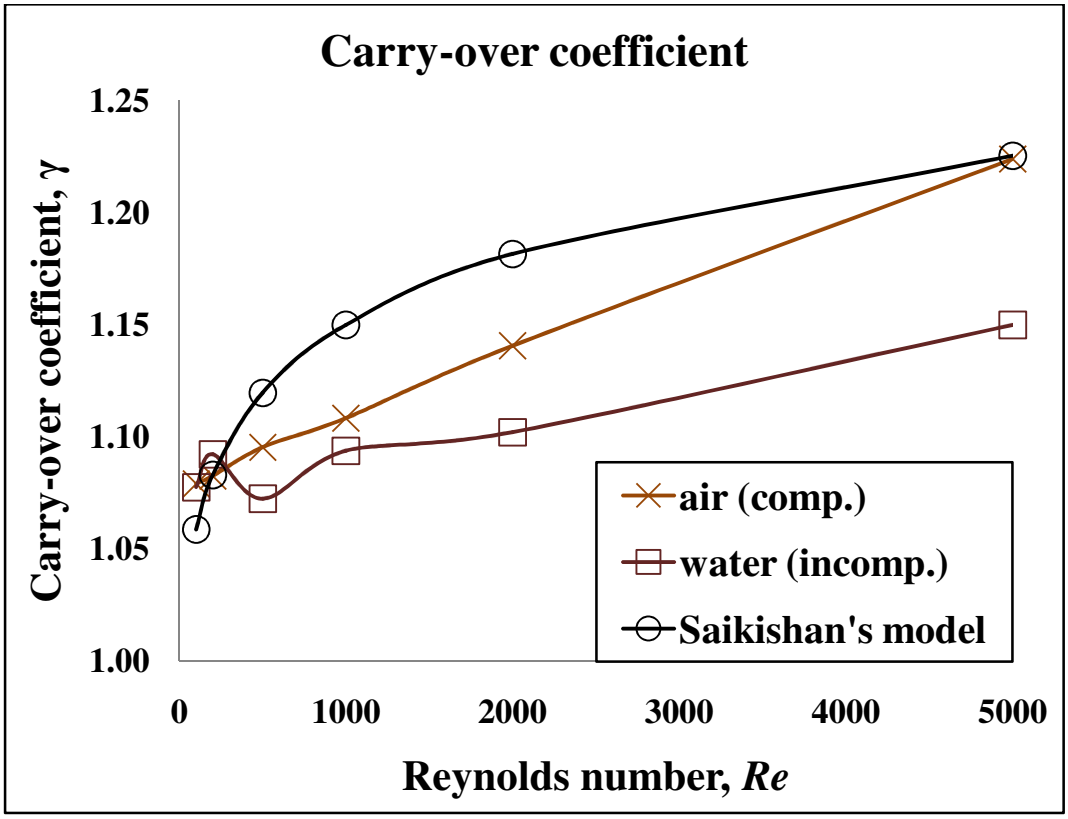

Figure 8.5. Comparison of carry-over coefficient of predicted compressible and incompressible flows within first cavity of multiple cavity labyrinth seal with Saikishan's model (case #25–30 in Appendix A)

incompressible fluid flowing through each cavity are entirely different compared with those of Saikishan's model. Although the seal geometry ratios performed for these simulations presented in Table 8.2 are within the range of Saikishan's model, there are differences between the carry-over coefficient performed by the simulations and that predicted by Saikishan's model. For the relatively wide tooth width ($w = 1\,mm$), similar to the second and the third instances, the viscous force under the tooth is more dominant than the inertial force of the jet from under the same tooth. This means that the

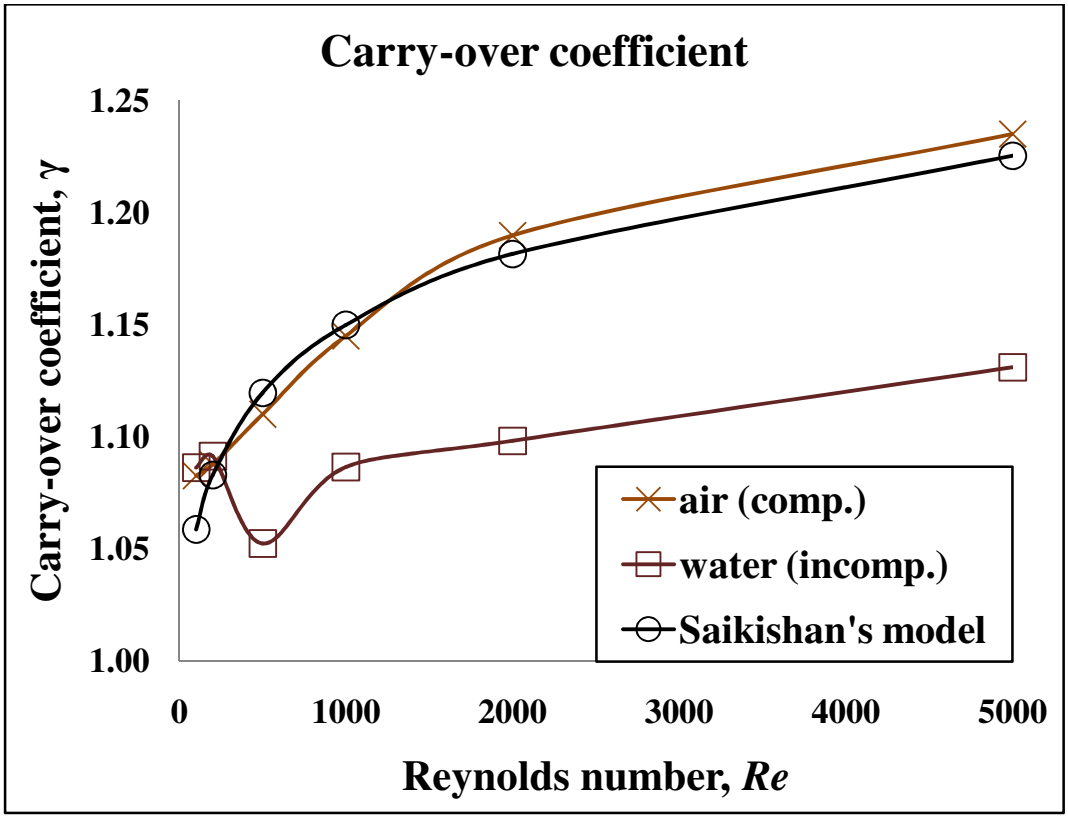

Figure 8.6. Comparison of carry-over coefficient of predicted compressible and incompressible flows within second cavity of multiple cavity labyrinth seal with Saikishan's model (case #25–30 in Appendix A)

kinetic energy in the cavity is dissipated better than that of the narrow tooth width and that the carry-over coefficient of the incompressible flow with the wide tooth width does not increase as fast as that with the narrow one. Therefore, it is also considered to study more simulations for future work in order to make sure whether there is the effect of the wide tooth width through labyrinth seals.

Furthermore, because of the transition process, the carry-over coefficients of the incompressible fluid near Reynolds number of 500 tend to slightly decrease and then

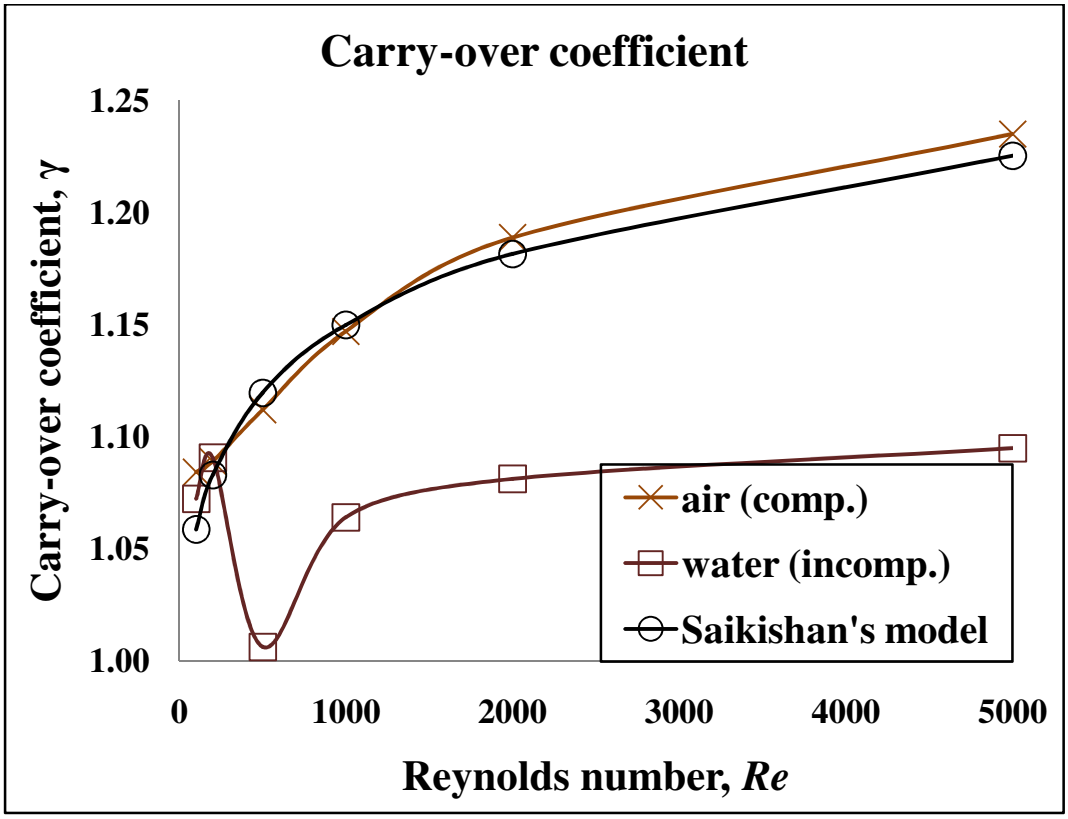

Figure 8.7. Comparison of carry-over coefficient of predicted compressible and incompressible flows within third cavity of multiple cavity labyrinth seal with Saikishan's model (case #25–30 in Appendix A)

recover. Thus, it is necessary to know that the differences between the simulations and Saikishan's model for the entire range of Reynolds numbers should be compensated for. Further, the effect of the transition process in the model should also be considered in order to develop the prediction of more accurate leakage mass flow rate through labyrinth seals.

To sum up the validation of the carry-over coefficient, Saikishan's model can be applied to his limited conditions only. As the tooth width in a labyrinth seal relatively

increases (w: $0.03/0.4\ mm \rightarrow 1\ mm$), even if seal geometry of simulations exists within the range of Saikishan's model (cases #7–12, 13–18, and 25–30), it can be observed that the results predicted by Saikishan's model present a great contrast to those performed by the simulations. Therefore, it is recommended to study more simulations for future work to verify not only the dependence on the wide tooth width within labyrinth seals in more detail but also the accuracy of Saikishan's model for the relatively wide tooth width.

VALIDATION OF DISCHARGE COEFFICIENT AGAINST SIMULATION DATA PERFORMED BY EARLIER MODEL

In the first instance ($n = 2, c = 0.06\ mm, s = 4\ mm, w = 0.03\ mm$) presented in Figure 8.8, the discharge coefficients of incompressible fluid performed by simulations and computed by Saikishan's model under the first tooth seem not to be related with Reynolds numbers. This means that in these particular flow and geometric conditions, the total losses occurring as the fluid flows under the first tooth and through the cavity remain almost constant irrespective of the fluid velocity. However, there are differences between the outcomes performed by simulations and created by Saikishan's model. Saikishan's model seems to predict that the total losses, when the fluid flows under the first tooth and through the cavity, are less than those performed by simulations. This finding indicates that Saikishan's model, conducted under his limited conditions, is not appropriate under these particular flow and seal geometric conditions. In order to predict more perfect leakage mass flow rate, it needs to compensate for the differences between the simulations and Saikishan's model for the entire range of Reynolds numbers.

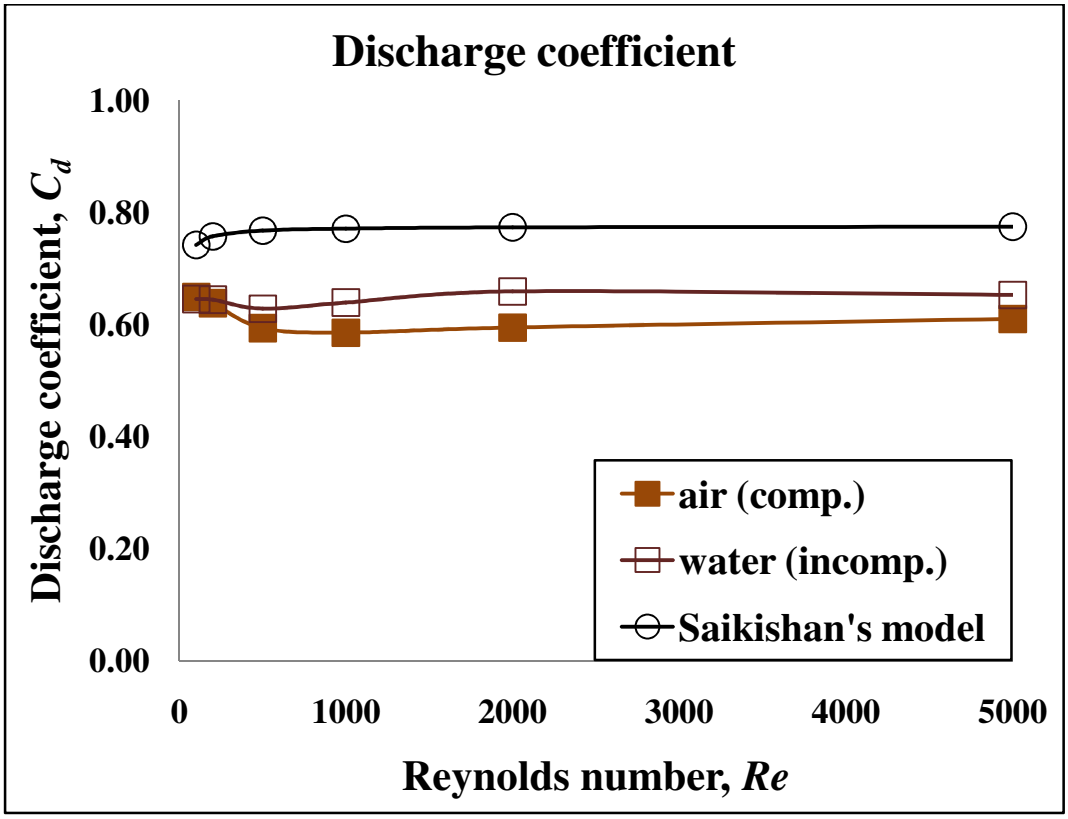

Figure 8.8. Comparison of discharge coefficient of predicted compressible and incompressible flows for first tooth of single cavity labyrinth seal with Saikishan's model (case #1–6 in Appendix A)

In Figure 8.9, it is found that the discharge coefficient of incompressible fluid under the second tooth is also different from that of Saikishan's model. The discharge coefficient of the incompressible fluid increases as identically as Saikishan's model but his outcomes are greater than those performed by simulations. It is likely because the total losses occurring through the cavity and under the second tooth are greater than those Saikishan expected. Saikishan considered the discharge coefficient under the second tooth as a function of only the carry-over coefficient ($z = 0.925\gamma^{0.861}$). However,

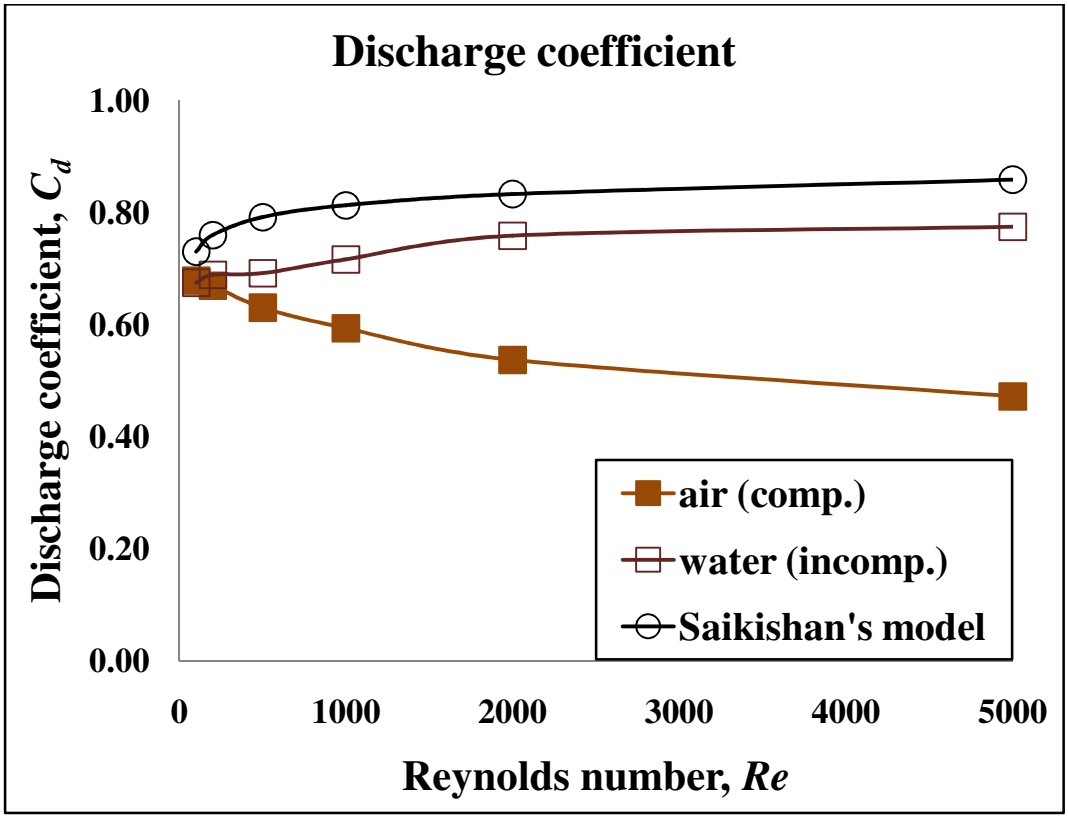

Figure 8.9. Comparison of discharge coefficient of predicted compressible and incompressible flows for second tooth of single cavity labyrinth seal with Saikishan's model (case #1–6 in Appendix A)

there seems to be other factors correlated with the discharge coefficient under the second tooth. Thus, it is necessary to find other factors associated with the discharge coefficient under the second tooth and incorporate them into the leakage model. Since the pressure ratio of the fluid decreases gradually as the fluid flows across each tooth and the flow of the fluid through the constriction becomes eventually choked, the discharge coefficient of the compressible fluid decreases despite an increase in the Reynolds numbers.

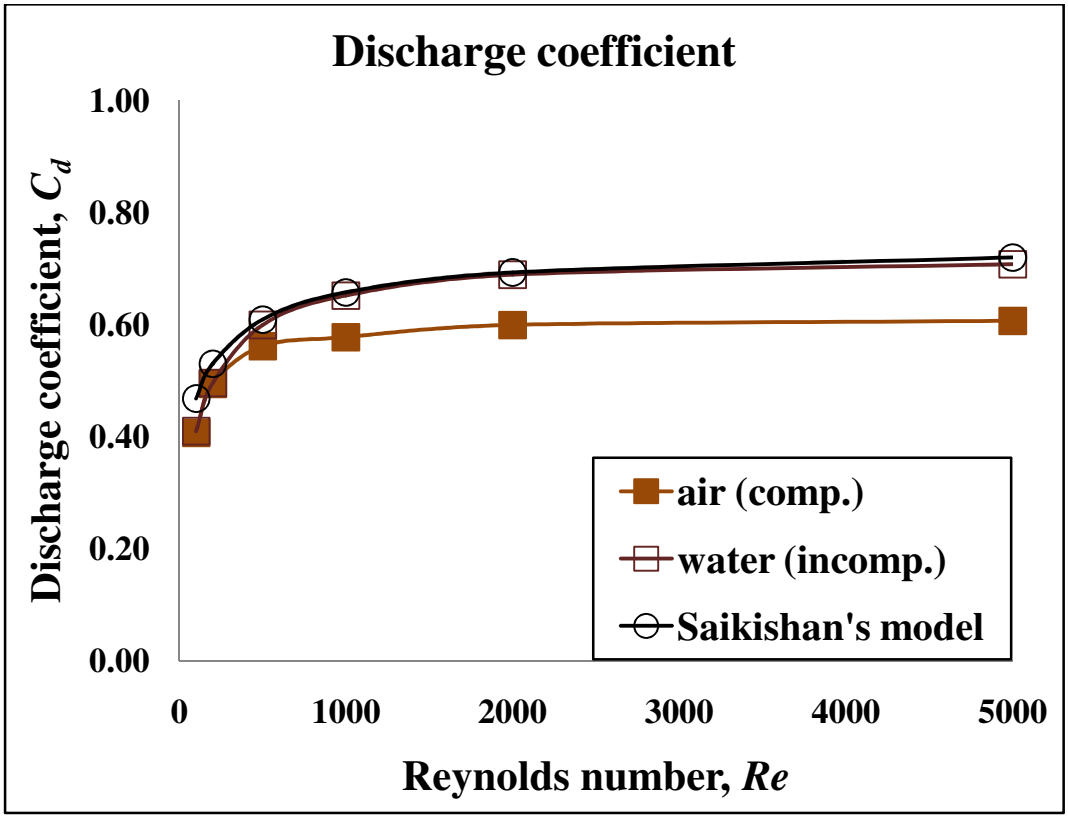

Figure 8.10. Comparison of discharge coefficient of predicted compressible and incompressible flows for first tooth of single cavity labyrinth seal with Saikishan's model (case #7–12 in Appendix A)

In the second instance ($n = 2, c = 0.06\,mm, s = 4\,mm, w = 1\,mm$) presented in Figure 8.10, the discharge coefficient of incompressible fluid under the first tooth exactly follows Saikishan's model. Hence, in these particular flow and seal geometric conditions, it can be concluded that the outcomes not only conducted in these studies but also deduced by Saikishan's model are accurately evaluated for estimating the prediction of the leakage mass flow rate through labyrinth seals.

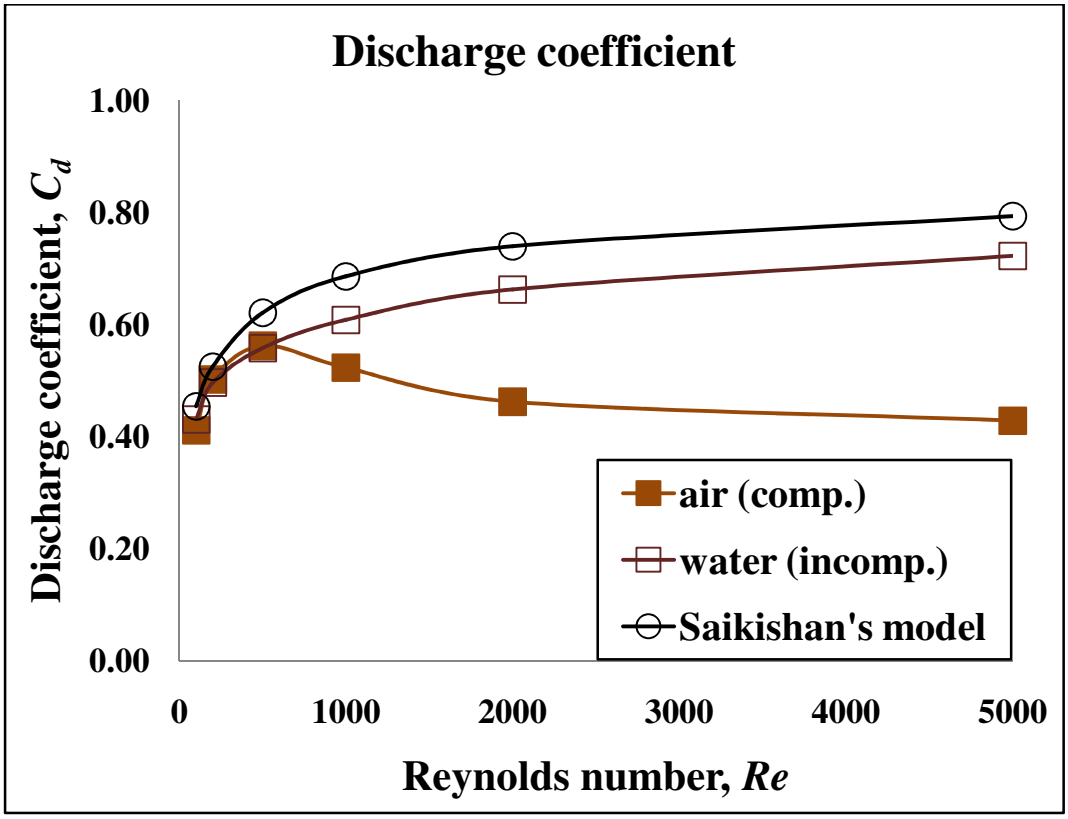

Figure 8.11. Comparison of discharge coefficient of predicted compressible and incompressible flows for second tooth of single cavity labyrinth seal with Saikishan's model (case #7–12 in Appendix A)

However, Figure 8.11 shows that the discharge coefficient of incompressible fluid under the second tooth is different from Saikishan's model. Since total losses occurring through the cavity and under the second tooth are greater than those expected by Saikishan, the outcomes performed by simulations are therefore less than those predicted by him. Since the discharge coefficient under the second tooth, reflected by Saikishan, is a function of only the carry-over coefficient ($z = 0.925\gamma^{0.861}$), the differences seem to appear. Thus, it needs to discover other factors related with the discharge coefficient under the second

tooth and include them into the leakage model. Because the pressure ratio of the fluid decreases gradually as the fluid flows across each tooth and the flow of the fluid through the constriction becomes eventually choked, the discharge coefficient of the compressible fluid decreases even though the Reynolds number increases.

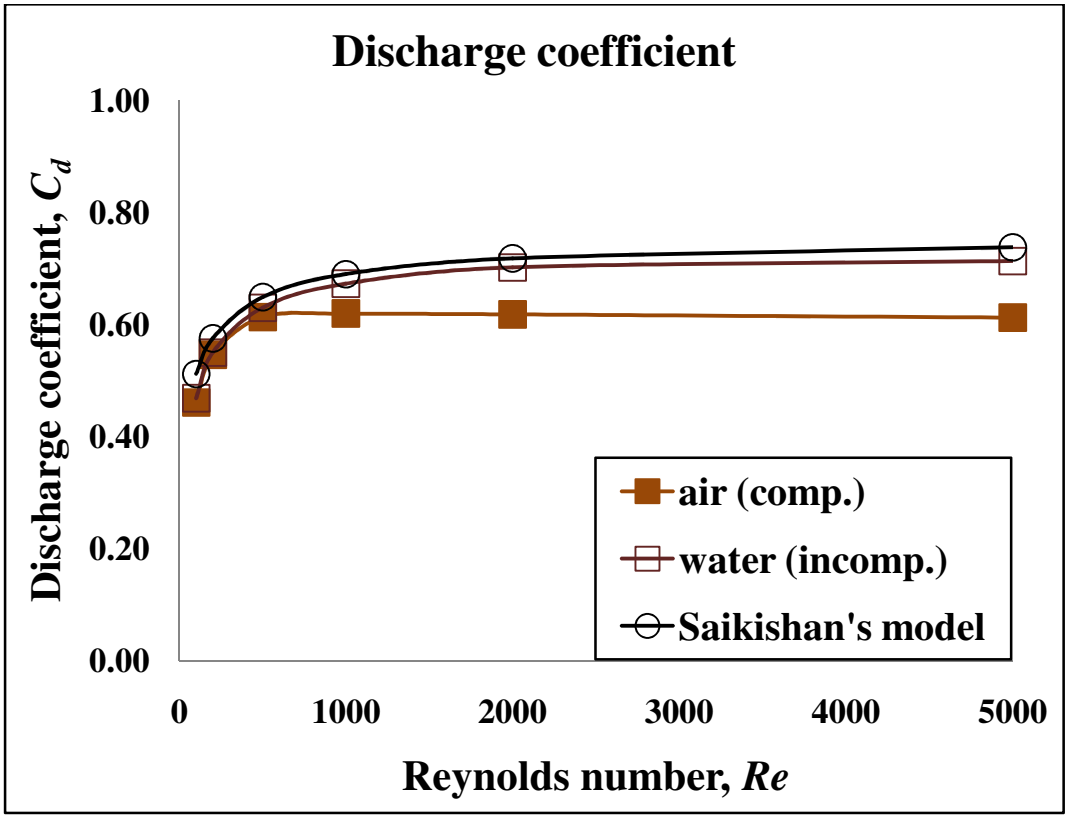

Figure 8.12. Comparison of discharge coefficient of predicted compressible and incompressible flows for first tooth of single cavity labyrinth seal with Saikishan's model (case #13–18 in Appendix A)

In the third instance ($n = 2, c = 0.09\ mm, s = 4\ mm, w = 1\ mm$) presented in Figure 8.12, the discharge coefficient of incompressible fluid under the first tooth almost

follows Saikishan's model. Hence, it can be safely said that the outcomes found in these studies and estimated by Saikishan's model are exactly evaluated in these given flow and seal geometric conditions; therefore, they are enough to predict leakage mass flow rate through labyrinth seals.

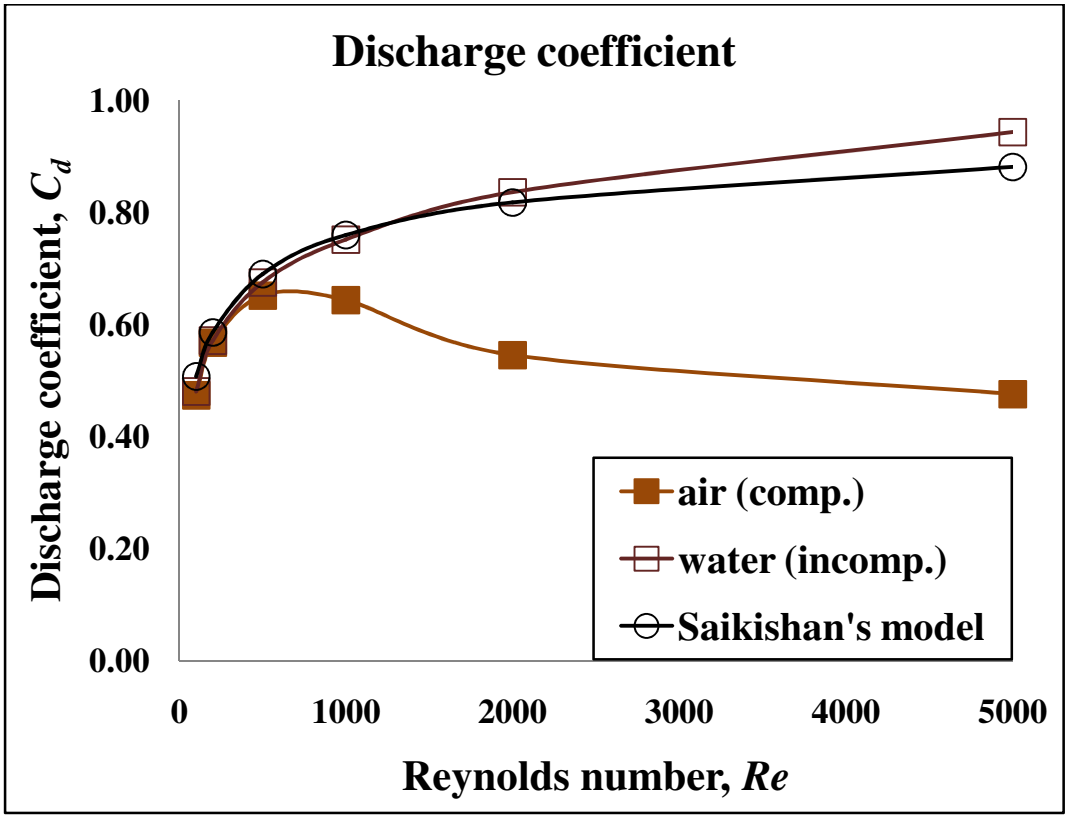

Figure 8.13. Comparison of discharge coefficient of predicted compressible and incompressible flows for second tooth of single cavity labyrinth seal with Saikishan's model (case #13–18 in Appendix A)

Figure 8.13 shows that at lower Reynolds numbers ($Re < 2000$), the discharge coefficient of incompressible fluid under the second tooth follows Saikishan's model;

however, at higher Reynolds number ($Re = 2000$), the discharge coefficient tends to deviate from Saikishan's model. Hence, it can be concluded that except at higher Reynolds number ($Re = 2000$), the outcomes found in these studies and deduced by Saikishan's model are exactly evaluated under these flow and seal geometric conditions in order to evaluate the prediction of the leakage mass flow rate through labyrinth seals.

Moreover, it is necessary to inspect what happened at higher Reynolds number ($Re = 2000$) and then compensate for the differences between the simulations and Saikishan's model at the Reynolds number ($Re = 2000$). Since the pressure ratio of the fluid decreases gradually as the fluid flows across each tooth and the flow of the fluid through the constriction becomes eventually choked, the discharge coefficient of the compressible fluid decreases regardless of an increase in the Reynolds number.

In the fourth instance ($n = 2, c = 0.15\ mm, s = 4\ mm, w = 0.4\ mm$) presented in Figure 8.14, the discharge coefficient of incompressible fluid under the first tooth exactly follows Saikishan's model. Hence, the outcomes not only performed in these studies but also conducted by Saikishan's model are so precisely evaluated that they are enough to estimate leakage mass flow rate through labyrinth seals for the given flow and seal geometric conditions.

However, the discharge coefficient of incompressible fluid under the second tooth is different from Saikishan's model as shown in Figure 8.15. This is likely because the total losses occurring through the cavity and under the second tooth are greater than those Saikishan predicted. Because the discharge coefficient under the second tooth is regarded as a function of only the carry-over coefficient ($z = 0.925\gamma^{0.861}$) by Saikishan,

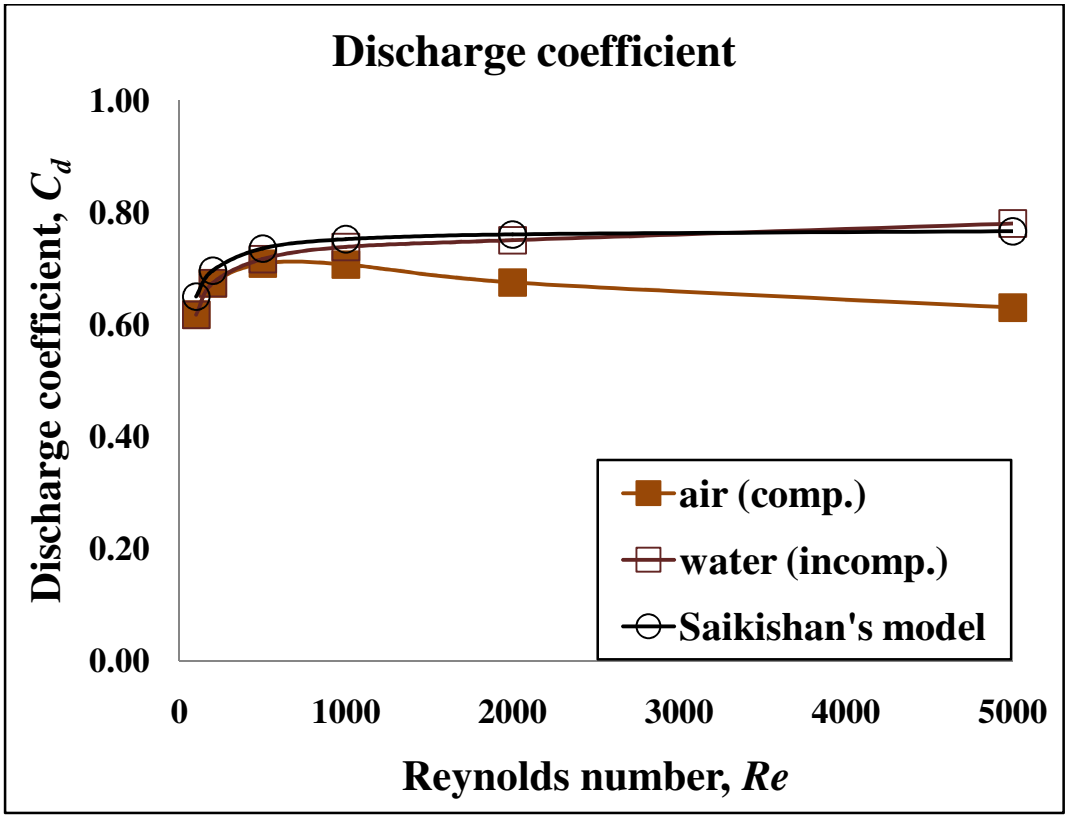

Figure 8.14. Comparison of discharge coefficient of predicted compressible and incompressible flows for first tooth of single cavity labyrinth seal with Saikishan's model (case #19–24 in Appendix A)

there exist the differences. Thus, it has to be noted that other factors can be associated with the discharge coefficient under the second tooth and that they are incorporated into the leakage model. Since the pressure ratio of the fluid decreases gradually as the fluid flows across each tooth, even if the flow of the fluid through the constriction does not become choked, the discharge coefficient of the compressible fluid decreases irrespective of an increase in the Reynolds numbers.

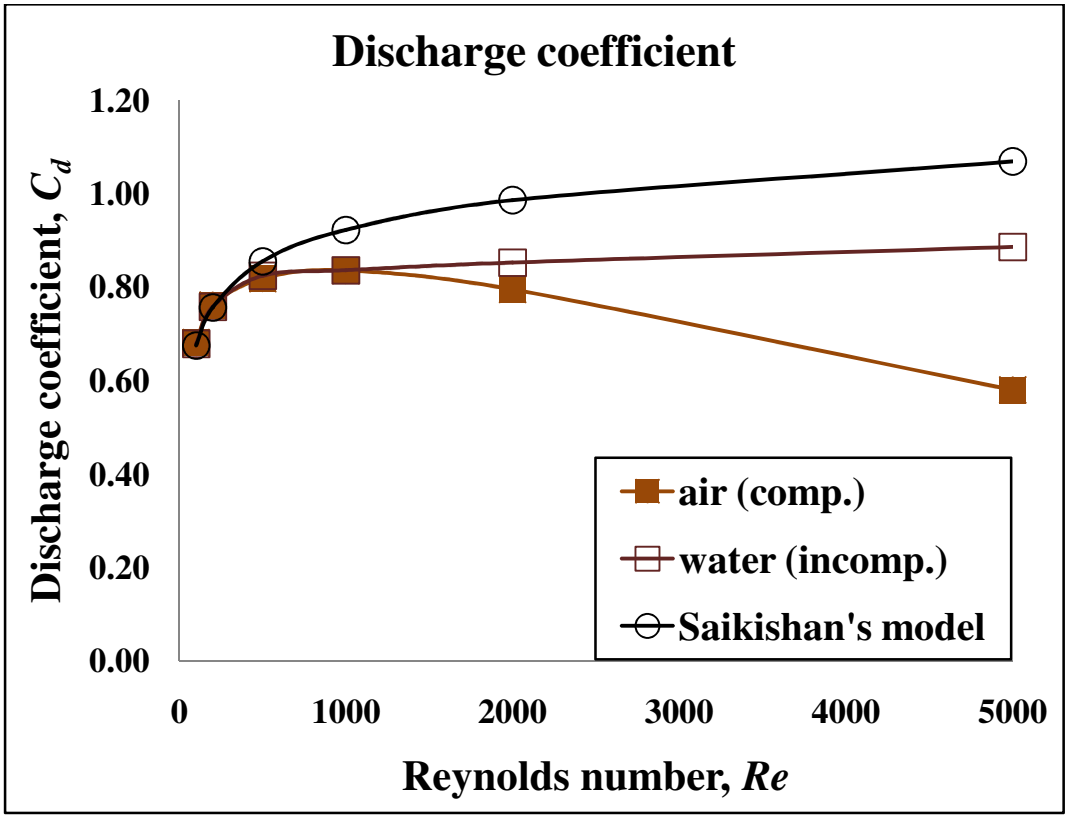

Figure 8.15. Comparison of discharge coefficient of predicted compressible and incompressible flows for second tooth of single cavity labyrinth seal with Saikishan's model (case #19–24 in Appendix A)

The last instance ($n = 4, c = 0.06\,mm, s = 4\,mm, w = 1\,mm$) presented in Figures 8.16, 8.17, 8.18, and 8.19 shows the outcomes for a multiple cavity labyrinth seal with four teeth. It can be seen in Figure 8.16 that the discharge coefficient of incompressible fluid under the first tooth is considerably different from that of Saikishan's model. Since the total losses occurring under the first tooth and through the cavity are less than those Saikishan expected, the outcomes conducted by simulations are greater than those predicted by Saikishan's model. This finding denotes that Saikishan's

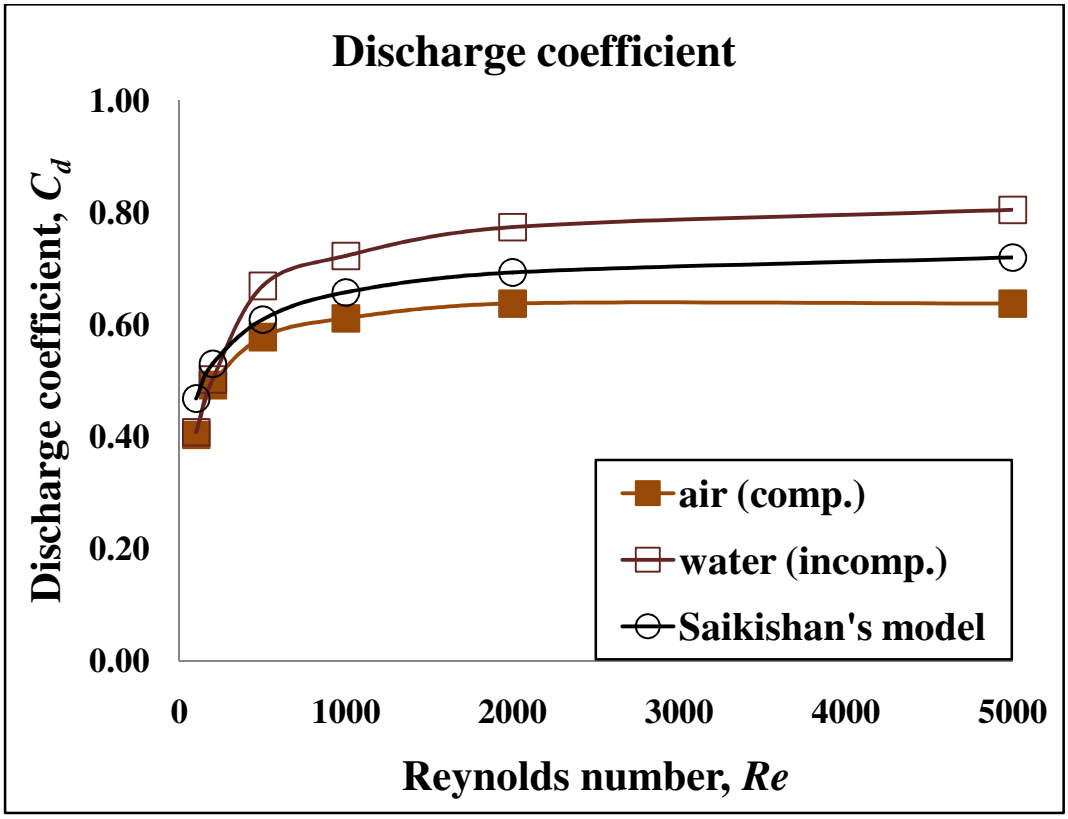

Figure 8.16. Comparison of discharge coefficient of predicted compressible and incompressible flows for first tooth of multiple cavity labyrinth seal with Saikishan's model (case #25–30 in Appendix A)

model, conducted under his limited conditions, is not appropriate under these particular flow and seal geometric conditions. Hence, it has to be noted that the differences between the simulations and Saikishan's model should be compensated for the entire range of Reynolds number in order to develop more accurate leakage model which can predict exact leakage mass flow rate.

Furthermore, there exit differences between the discharge coefficients of incompressible fluid under the subsequent teeth as shown in Figures 8.17, 8.18, and 8.19

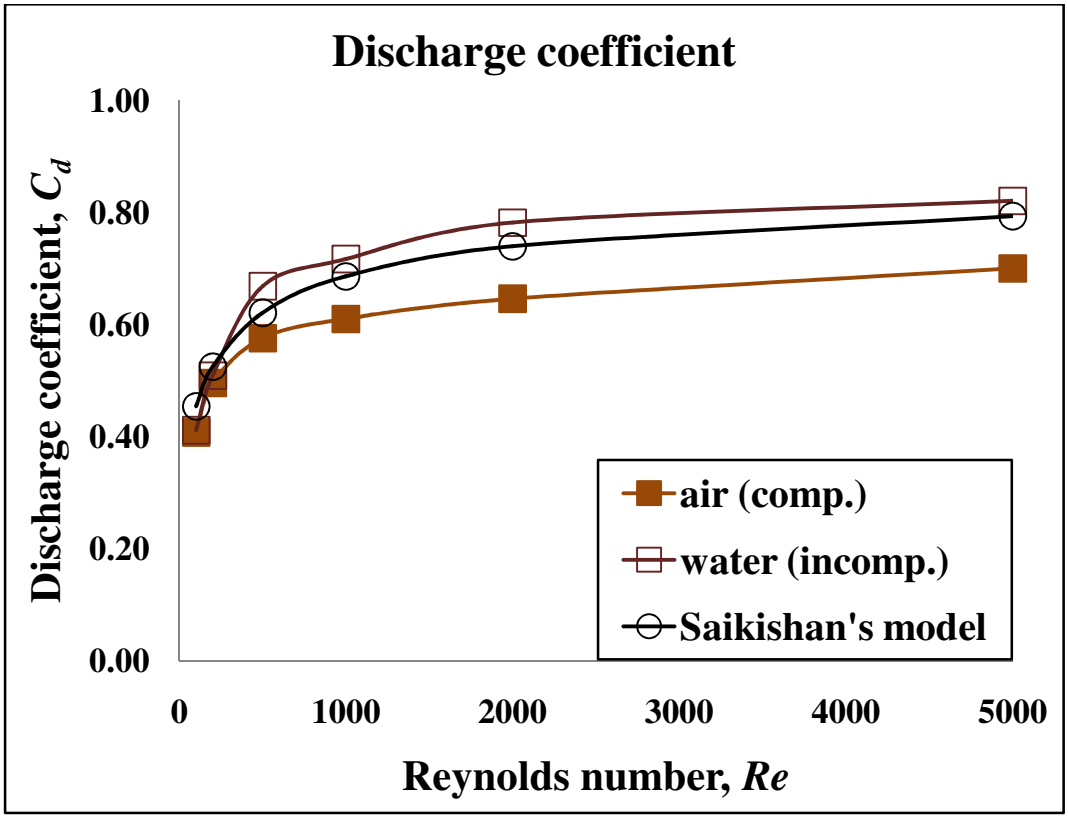

Figure 8.17. Comparison of discharge coefficient of predicted compressible and incompressible flows for second tooth of multiple cavity labyrinth seal with Saikishan's model (case #25–30 in Appendix A)

because Saikishan determined that the discharge coefficients through the subsequent teeth were a function of only the carry-over coefficients ($z = 0.925\gamma^{0.861}$). Hence, it is also necessary to find other factors associated with the discharge coefficient under the subsequent teeth and incorporate them into the leakage model.

Here, remarkable is the fact that in Figures 8.17, 8.18, and 8.19, as the fluid continuously flows to the downstream through each tooth within a labyrinth seal, the discharge coefficients of incompressible fluid tend to be equivalent with Saikishan's

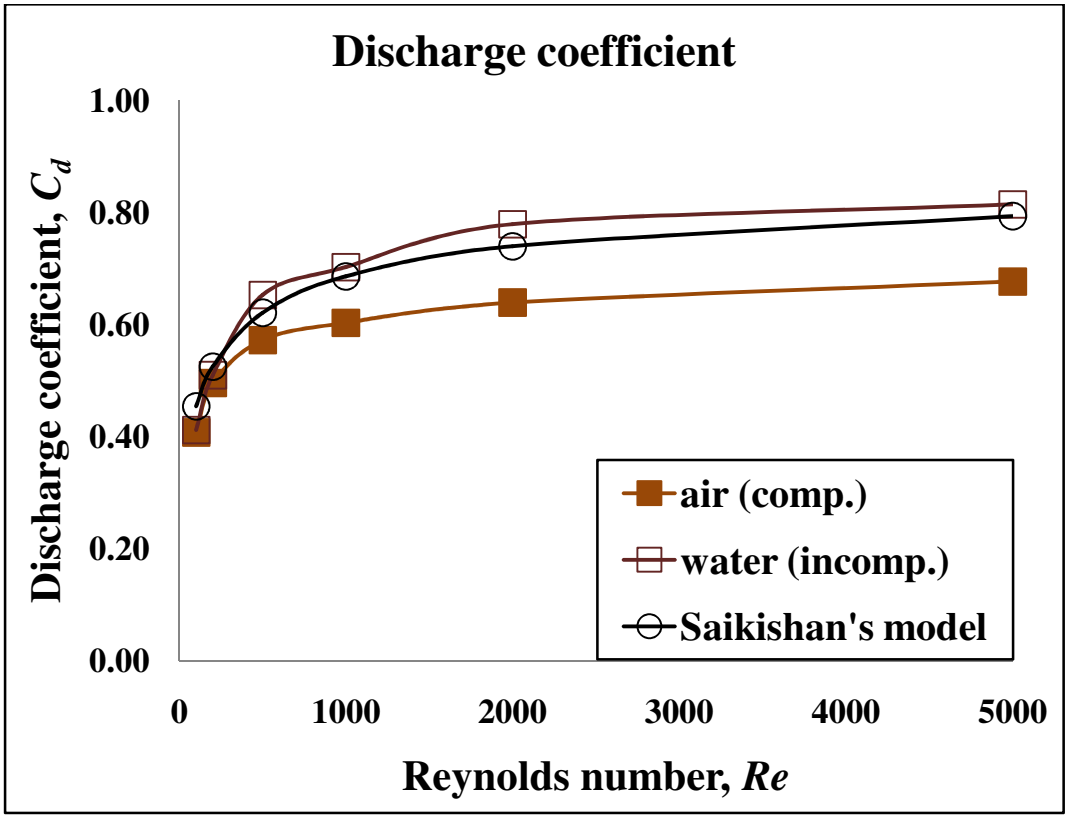

Figure 8.18. Comparison of discharge coefficient of predicted compressible and incompressible flows for third tooth of multiple cavity labyrinth seal with Saikishan's model (case #25–30 in Appendix A)

model. Therefore, it can be concluded that the outcomes found in these studies and predicted by Saikishan's model tends to become more exact as the fluid flows through each tooth within a multiple cavity labyrinth seal for the given flow and seal geometric conditions. Because the pressure ratio of the fluid decreases gradually as the fluid flows across each tooth and the flow of the fluid through the constriction becomes eventually choked, the discharge coefficient of the compressible fluid decreases although the Reynolds number increases.

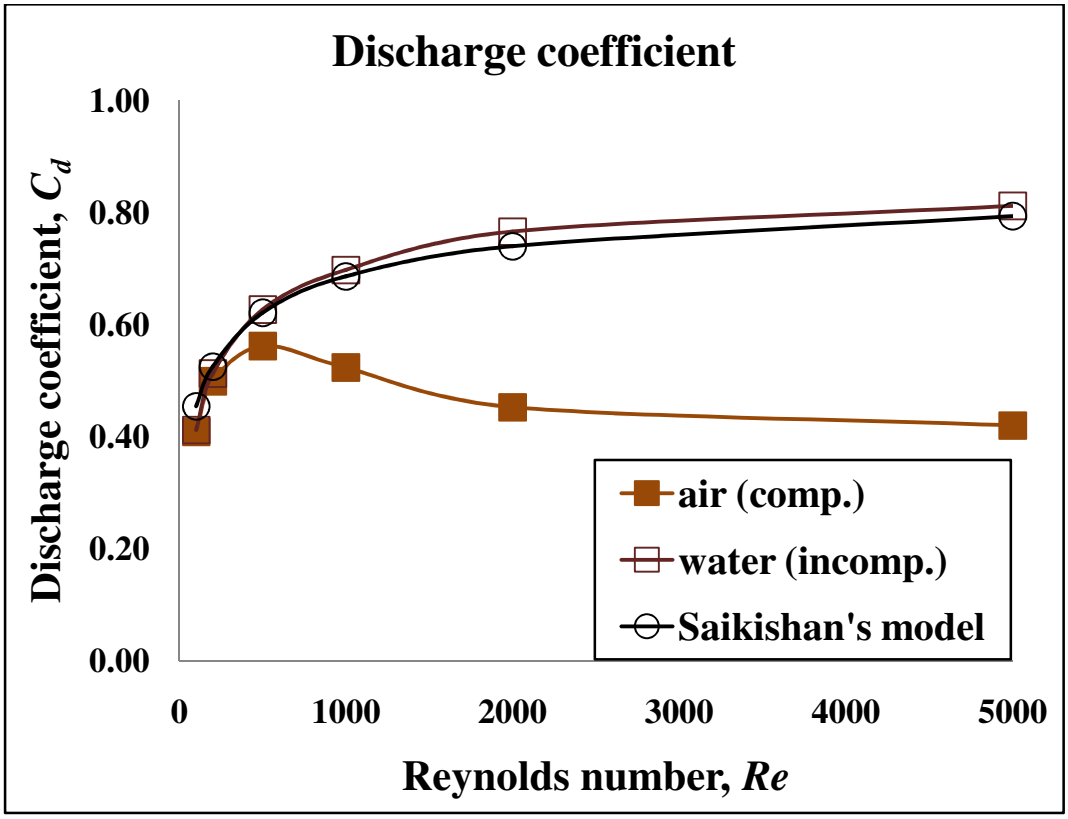

Figure 8.19. Comparison of discharge coefficient of predicted compressible and incompressible flows for fourth tooth of multiple cavity labyrinth seal with Saikishan's model (case #25–30 in Appendix A)

The validation of the discharge coefficient can be summarized as follows. Saikishan's model tends to be applied to his limited conditions only. When the fluid flows under the first tooth, the outcomes performed by simulations generally follow those predicted by Saikishan's model; however, under certain flow and seal geometry conditions, the outcomes by the simulations deviate from those by Saikishan. Hence, it needs to compensate for the differences in order to develop more accurate leakage model. Besides, as the fluid flows across subsequent teeth, the outcomes of simulations are also generally inclined to

deviate from Saikishan's model except the multiple cavity labyrinth seal. This is likely because Saikishan considered the discharge coefficients under the following teeth as a function of only the carry-over coefficient. Thus, it is necessary to find other factors related with the discharge coefficient under the following teeth and then incorporate them into the leakage model which can provide more accurate leakage mass rate through labyrinth seals. Taken together, it is recommended to study more simulations for future work to verify the accuracy of Saikishan's model as a method to compute the discharge coefficients across each tooth within single and multiple cavity labyrinth seals in more detail.

VALIDATION OF EFFECT OF COMPRESSIBILITY AGAINST SIMULATION DATA PERFORMED BY EARLIER MODEL

In order to develop a model which provides an exact leakage mass flow rate for compressible flows through labyrinth seals, Saikishan [15], [16], [17] discovered that the model developed for incompressible flows could be employed to arrive at reasonably accurate prediction as long as the individual tooth pressure ratios are greater than 0.7. However, since at low pressure ratios (less than 0.7) the model developed for incompressible flows deviated from CFD simulations, Saikishan considered the effects of compressibility and included the discharge coefficient compressibility factor into the model in order to compensate for the deviation between incompressible and compressible flows. Moreover, Saikishan found that the ψ-Pr relationship for air as a compressible flow could be modeled as a linear relationship.

$$\psi = 0.558\, Pr + 0.442 \tag{8.1}$$

Therefore, by utilizing the model developed for the carry-over coefficient and the discharge coefficient, Saikishan's algorithm could be developed to predict not only the leakage mass flow rate for incompressible and compressible flows but also the pressure distribution across labyrinth seals provided the inlet and outlet pressures are known.

$$\dot{m} = \psi C_{d_n} A\sqrt{2\rho_n(p_n - p_{n+1})} \qquad (1 \le n \le N) \tag{8.2}$$

for $0.0075 < c/s < 0.0375$, $0.0075 < w/s < 0.5$, $2.67 < w/c < 66.67$,

$0.75 < h/s < 4$, *and* $250 < Re < 15000$

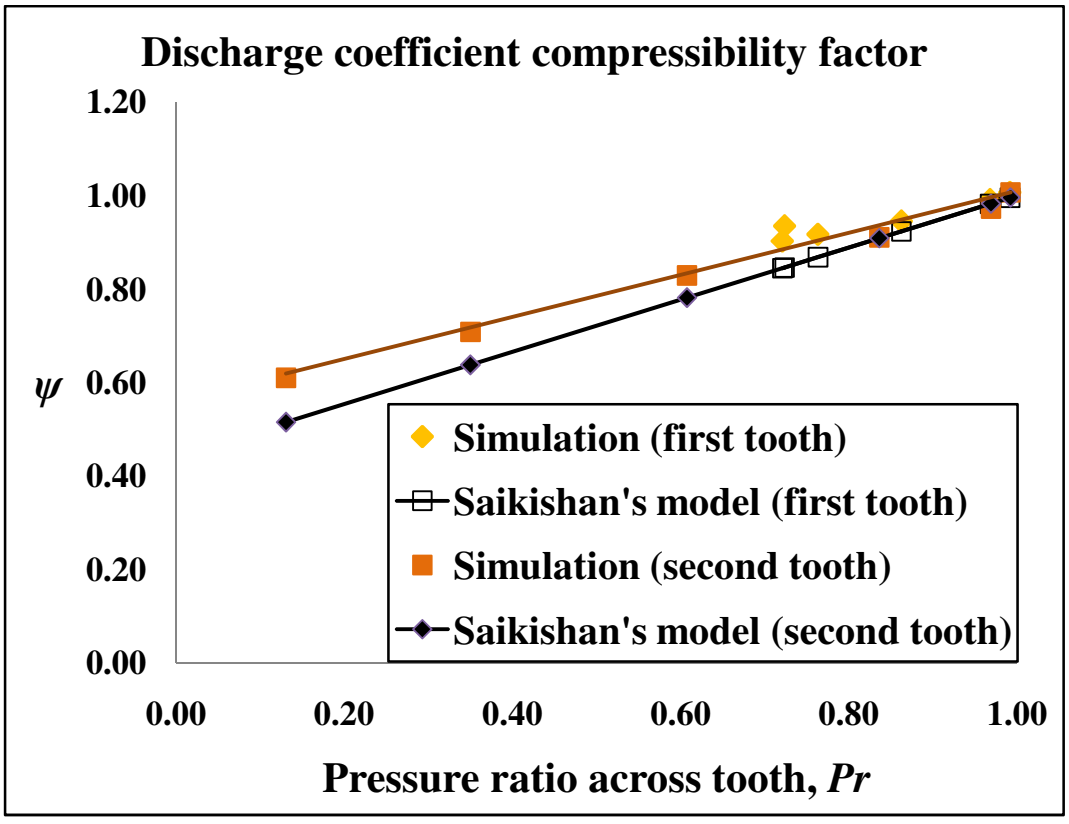

Figure 8.20. Comparison of discharge coefficient compressibility factor of predicted compressible flow of single cavity labyrinth seal (case #1–6 in Appendix A)

In the first instance ($n = 2, c = 0.06\,mm, s = 4\,mm, w = 0.03\,mm$) shown in Figure 8.20, as the pressure ratios of compressible fluid flowing through each tooth decrease, the discharge coefficient compressibility factor gradually deviates from that of Saikishan's model. In these particular flow and geometric conditions, as the pressure ratios of the compressible fluid decrease, it can be expected that more leakage mass flow rate than Saikishan predicted occurs based on Equation 8.2. Therefore, it is necessary to compensate for the differences between the simulations and Saikishan's model in order to estimate more perfect leakage mass flow rate through labyrinth seals.

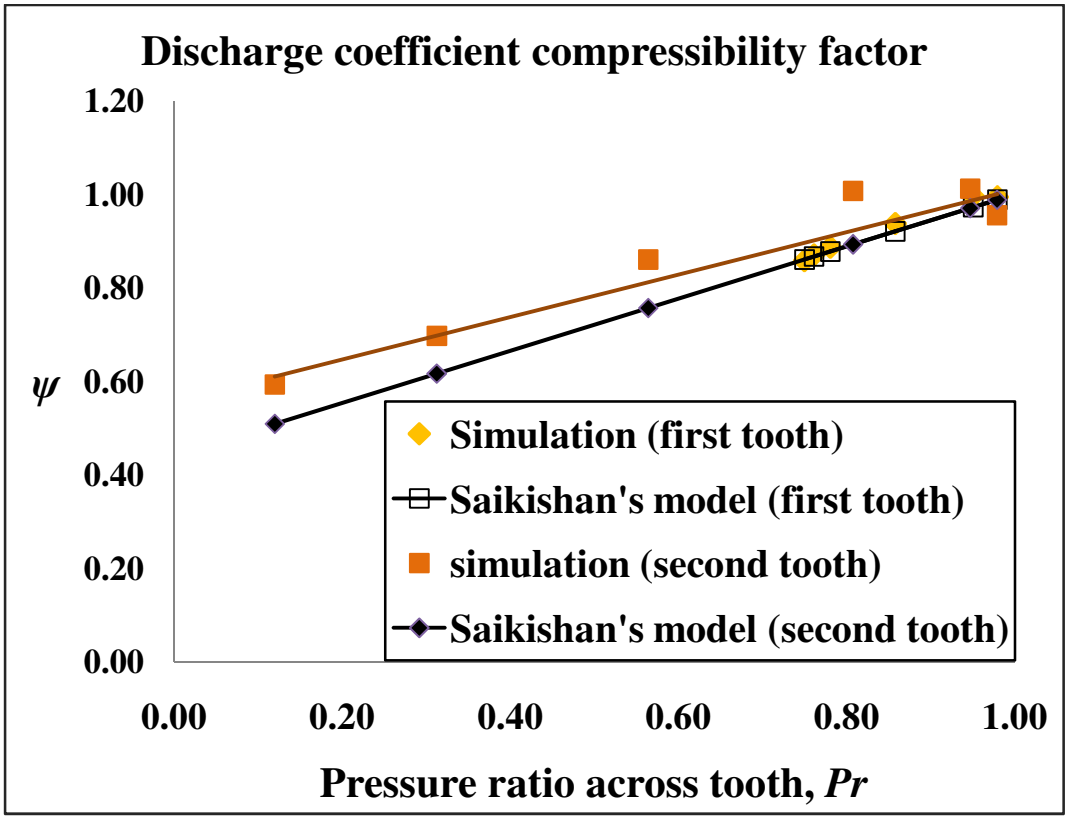

Figure 8.21. Comparison of discharge coefficient compressibility factor of predicted compressible flow of single cavity labyrinth seal (case #7–12 in Appendix A)

In the second instance ($n = 2, c = 0.06\,mm, s = 4\,mm, w = 1\,mm$) shown in Figure 8.21, as the pressure ratios of compressible fluid flowing through each tooth decrease, the discharge coefficient compressibility factor also gradually deviates from that of Saikishan's model. As the pressure ratios of the compressible fluid decrease in these given flow and geometric conditions, more leakage mass flow rate than Saikishan predicted happens through the labyrinth seal on the basis of Equation 8.2. Therefore, it has to be considered that the compressible fluid needs to be compensated for the differences between the simulations and Saikishan's model for the same reason mentioned in the first instance.

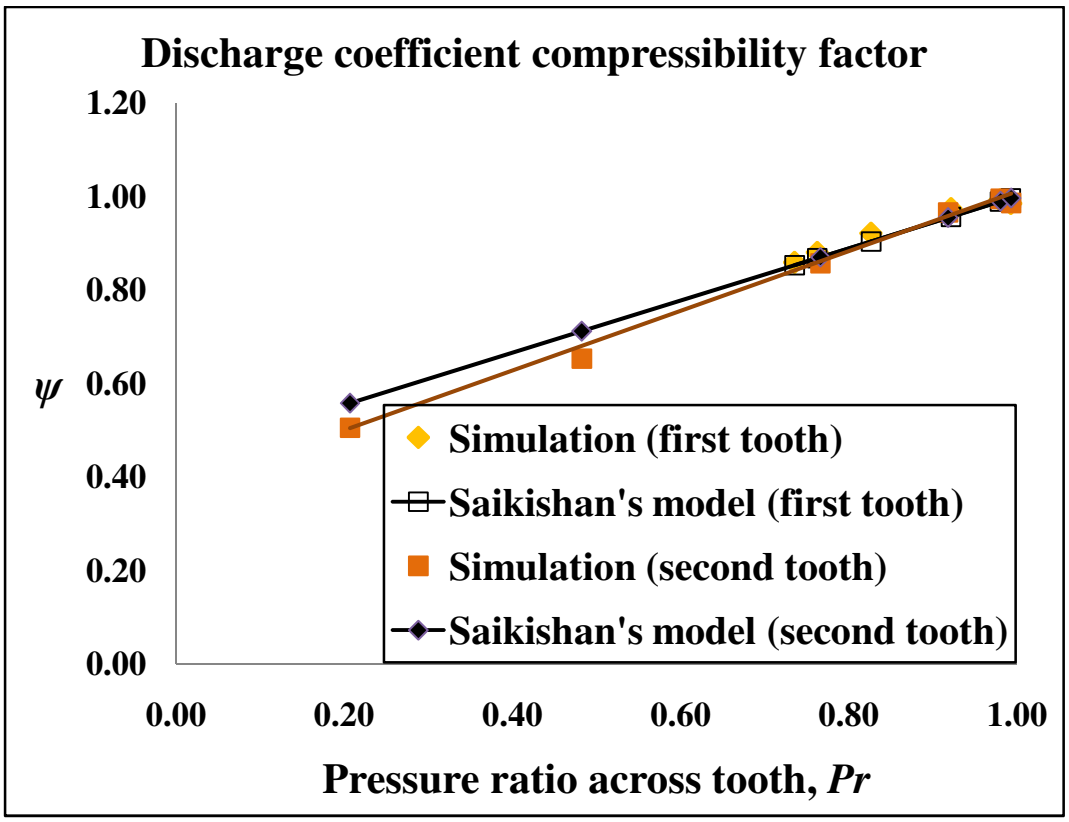

Figure 8.22. Comparison of discharge coefficient compressibility factor of predicted compressible flow of single cavity labyrinth seal (case #13–18 in Appendix A)

In the third instance ($n = 2, c = 0.09\ mm, s = 4\ mm, w = 1\ mm$) shown in Figure 8.22, the discharge coefficient compressibility factor is almost same as that of Saikishan's model as the pressure ratios of compressible fluid flowing through each tooth decrease. Therefore, it can be expected to obtain nearly exact leakage mass flow rate for the compressible fluid by applying Saikishan's model based on Equation 8.2 in these particular flow and geometric conditions exclusive of the relatively smaller pressure ratios ($Pr < 0.8$). However, it needs to be considered to compensate for the differences between the simulations and Saikishan's model for the same reason previously stated.

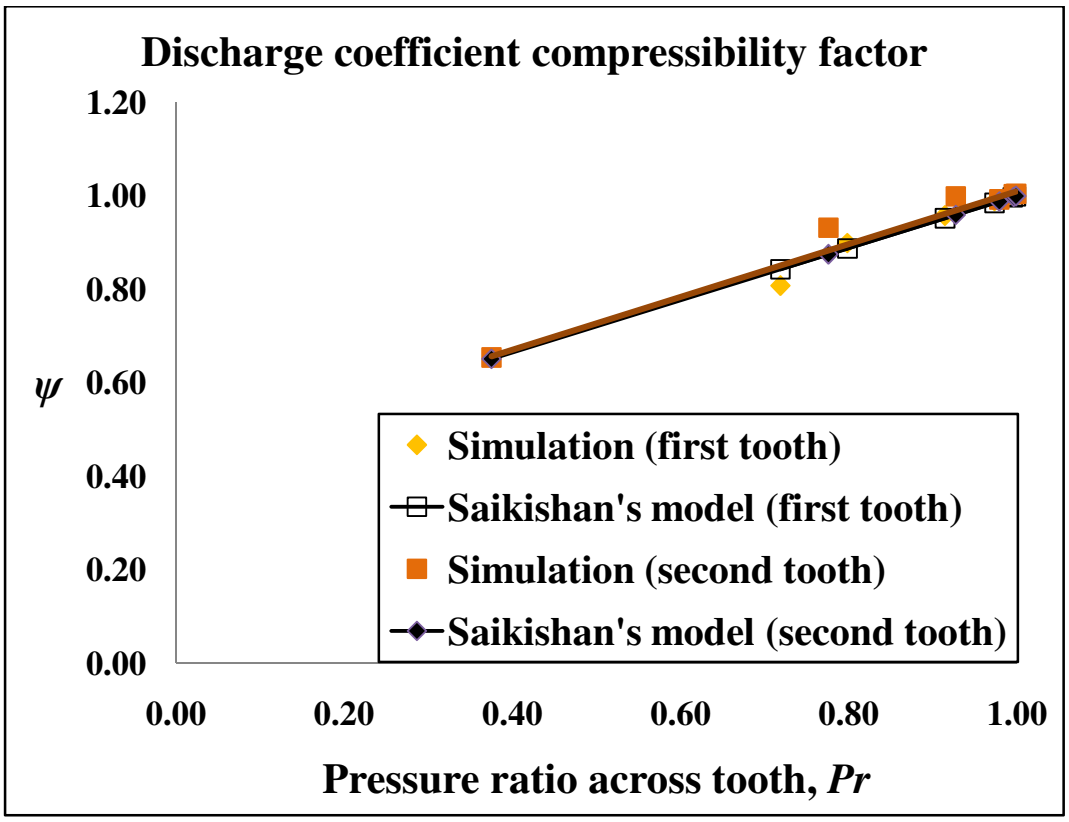

Figure 8.23. Comparison of discharge coefficient compressibility factor of predicted compressible flow of single cavity labyrinth seal (case #19–24 in Appendix A)

The fourth instance ($n = 2, c = 0.15\,mm, s = 4\,mm, w = 0.4\,mm$) shown in Figure 8.23 indicates that as the pressure ratios of compressible fluid flowing through each tooth decrease, the discharge coefficient compressibility factor is exactly same as that of Saikishan's model. Hence, by applying Saikishan's model based on Equation 8.2 in these particular flow and geometric conditions, it is possible to acquire precise leakage mass flow rate for the compressible fluid through labyrinth seals. However, to compensate for some deviations between the second tooth of the simulations and that of Saikishan's model, a modified ψ-Pr relationship including Saikishan's model is indispensible.

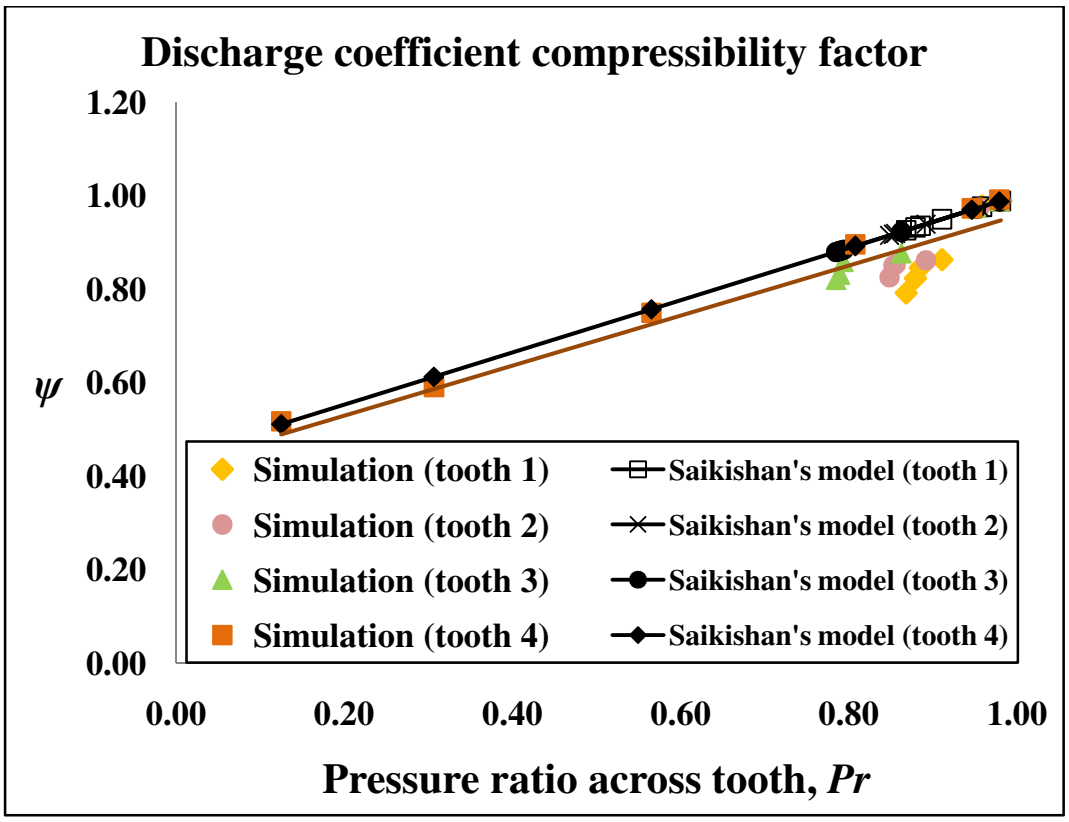

Figure 8.24. Comparison of discharge coefficient compressibility factor of predicted compressible flow of multiple cavity labyrinth seal (case #25–30 in Appendix A)

The last instance ($n = 4, c = 0.06\ mm, s = 4\ mm, w = 1\ mm$) shown in Figure 8.24 suggests that this is a multiple cavity labyrinth seal with four teeth. It can be observed from Figure 8.24 that the discharge coefficient compressibility factor is nearly equivalent to that of Saikishan's model as the pressure ratios of compressible fluid flowing through each tooth decrease. Hence, in these flow and geometric conditions, there is a possibility to procure accurate leakage mass flow rate for the compressible fluid by applying Saikishan's model on the basis of Equation 8.2. However, since there are also differences between the simulations and Saikishan's model, it is necessary to be considered to compensate for the differences.

In order to compensate for the differences between the simulations and Saikishan's model, it is necessary to consider all the instances at once to find a modified ψ-Pr relationship including Saikishan's model. As previously stated, the effects of compressibility are generally quantified by pressure ratio. In order to verify this idea of modeling the discharge coefficient compressibility factor purely based upon pressure ratio, Saikishan [14] performed simulations for different backpressures and Reynolds numbers for a labyrinth seal and found that pressures ratio across the tooth (not overall pressure ratio) was the only flow parameter which determined the discharge coefficient compressibility factor. Figure 8.25 represents the discharge coefficient compressibility factors of the compressible flow of both single and multiple cavity labyrinth seals. It is found from Figure 8.25 that the ψ-Pr relationship for air as a compressible fluid can be modeled as a modified linear relationship which includes Saikishan's model. Further, it is also found that the standard deviation of the curve fit is $\pm\ 0.033$ showing how much dispersion is from the line of best fit.

$$\psi = 0.530\ Pr + 0.464\ [\pm\ 0.033\ (Standard\ Deviation)] \qquad (8.3)$$

It is interesting to note that the relationship presented in Equation 8.3 is almost the same as that modeled by Saikishan (see Equation 8.1) even though there are slightly differences between the simulations and his model. Therefore, Equation 8.3 is better to be utilized as the relationship of the ψ-Pr rather than Equation 8.1 predicted by Saikishan when one needs to consider the effects of compressibility.

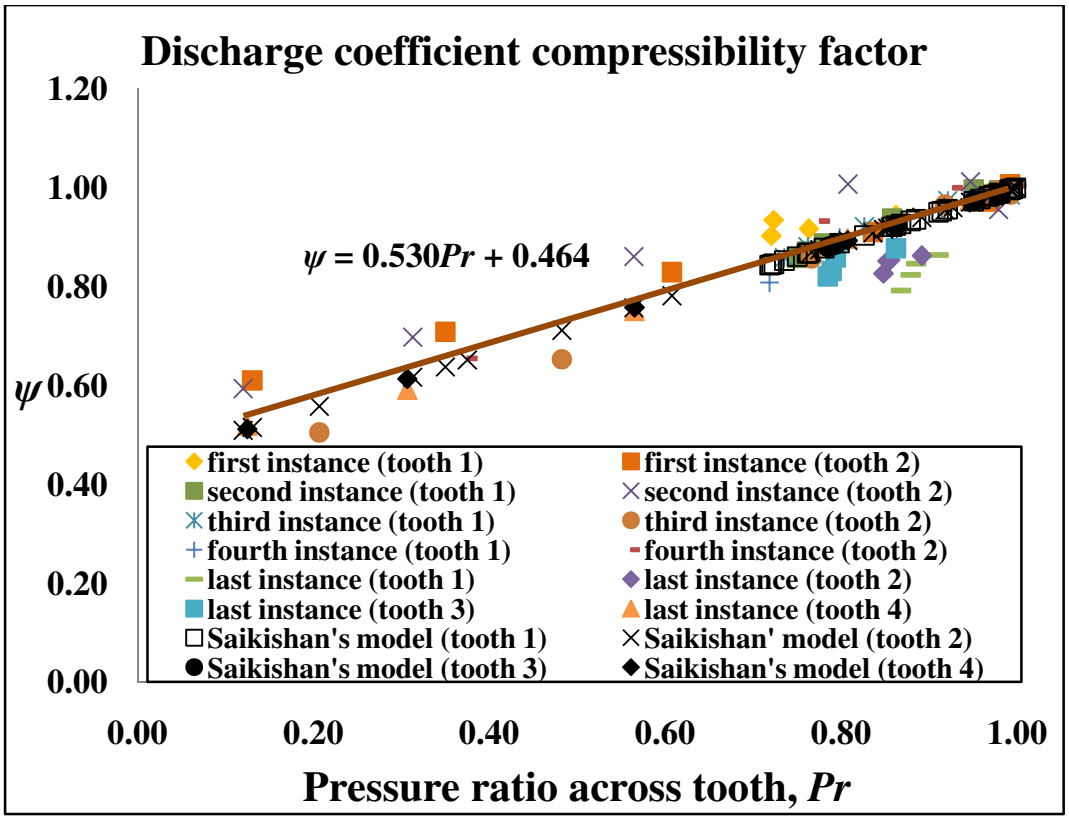

Figure 8.25. Comparison of discharge coefficient compressibility factors of predicted compressible flow of both single and multiple cavity labyrinth seals including Saikishan's model (case #1–30 in Appendix A)

CHAPTER IX

SUMMARY AND RECOMMENDED FUTURE WORK

The ensuing sections summarize the subjects and results presented in this thesis. This thesis discussed characteristics on the leakage models of see-through labyrinth seals, evaluated theoretical approaches for labyrinth seal leakage mass flow rate, and presented comparisons of these outcomes to those of another previous model. Four categories will be discussed in this chapter: motivation, methodology, findings, and recommended future work.

MOTIVATION

It is required to obtain accurate predictions of leakage mass flow rate through non-contact annular type labyrinth seals for the efficiency enhancement of turbomachinery. Since the analysis based on the bulk flow model simplified the Navier-Stokes equations and did not consider turbulence effects, the model could not predict the leakage mass flow rate in the various geometric configurations in the teeth although it could be utilized due to its small computational time. Furthermore, many researchers have attempted to attain models which can provide accurate predictions of the leakage mass flow rate through labyrinth seals, based on empirical approaches. However, these models are appropriate under certain flow conditions and are not applicable under certain other flow conditions.

Gerald L. Morrison and Adnan Al-Ghasem [13] discovered, while using Hodkinson' model to compute carry-over coefficients for windback seals, the carry-over coefficient

did not remain constant for the seal geometry as suggested by Hodkinson but varied according to the flow conditions such as pressure ratio. Moreover, Saikishan [14] developed his model by employing the models for the carry-over coefficient and discharge coefficient. Saikishan's model was developed to estimate the leakage mass flow rate for incompressible flow and compressible flow provided the individual tooth pressure ratios are greater than 0.7. In the case that the pressure ratios are less than 0.7, Saikishan considered the effects of compressibility and incorporated the discharge coefficient compressibility factor into his model to determine more exact leakage mass flow rate. Hence, it was necessary to carry out a direct comparison of the results of the model against other results performed under different operating conditions. This study verified not only the accuracy of the results conducted in this thesis but also the accuracy of the earlier model deduced by Saikishan and also indicated the range of flow and geometric conditions for which the results provided accurate prediction.

METHODOLOGY

This study performed several simulations by using the commercial CFD (Computational Fluid Dynamics) program, FLUENT since the program makes it possible to generalize the flow inside labyrinth seals. The standard κ-ε turbulence model was selected because it has been proven to exactly simulate the flow through the labyrinth seals collated with experimental data. This thesis analyzed both compressible and incompressible fluids and compared them by employing simulations in order to determine the leakage mass flow rate in the various geometric configurations in the tooth of see-through labyrinth seals.

TECPLOT 360 program was also applied to study the flow field within the labyrinth seals and compute the divergence angle of the jet in each cavity.

FINDINGS

CARRY-OVER COEFFICIENT

The carry-over coefficient, based on the divergence angle of the jet, was found to change with flow parameters with fixed seal geometry while earlier models expressed the carry-over coefficient solely as a function of seal geometry. It was also found that for both compressible and incompressible flows, the Reynolds number based on clearance was the only flow parameter which could influence the carry-over coefficient.

In the case of incompressible flow, based on the simulations for various seal geometries and operating conditions, it was found that as only c/w was decreased when radial clearance, tooth width, and tooth pitch were fixed, the turbulent dissipation of the kinetic energy of the incompressible flow in the cavity relatively increased with an increasing Reynolds number. Therefore, the carry-over coefficient of the incompressible flow tended not to significantly increase. Moreover, it was found that for a given Reynolds number, the carry-over coefficient of the incompressible flow strongly depended on c/w because not only the carry-over coefficient increased when both c/w and c/s were increased but the coefficient also decreased when only c/w was decreased for fixed c/s. In general, the lower the Reynolds number, the larger is the inertial force of the jet emerging from under the tooth and the smaller is the viscous force under the same tooth. The divergence angle of the jet becomes larger and this results in a smaller carry-over

coefficient at the lower Reynolds numbers. However, during transition from laminar to turbulent, the carry-over coefficient reduced initially and once the Reynolds number attained a critical value, the carry-over coefficient increased again.

In the case of compressible flow, performed by the simulations for various seal geometries and operating conditions, it was found that for a given Reynolds number, the carry-over coefficient of the compressible flow had been slightly increased if c/w and c/s were increased when tooth width and tooth pitch were fixed. It was also found that the carry-over coefficient of the compressible flow did not considerably change if only c/w was decreased when radial clearance, tooth width, and tooth pitch were fixed.

Furthermore, due to the fact that undissipated portion of the kinetic energy in the cavity associated with the carry-over coefficient, in certain flow and seal geometric conditions, it was more effective to employ compressible fluid as a working fluid and in other conditions, it seemed better to utilize incompressible fluid as a working fluid in order to reduce the leakage mass flow rate through labyrinth seals.

DISCHARGE COEFFICIENT

The discharge coefficient for compressible and incompressible flows through labyrinth seals was found to depend only on the Reynolds number based on clearance. It was also found that the discharge coefficient of the tooth in a single cavity labyrinth seal was equivalent to that in a multiple tooth labyrinth seal indicating that flow downstream had negligible effect on the discharge coefficient.

In particular, for compressible fluid, it was found that under certain flow and seal geometric conditions, the discharge coefficient of the compressible fluid did not increase

with an increase in the Reynolds number. It was correlated to the pressure ratio defined as the ratio of the inlet pressure to the outlet pressure of a tooth expressed in absolute values. The discharge coefficient was found to have a greater dependence on the pressure ratio rather than the Reynolds number. In order to examine the effect of the pressure ratio on the discharge coefficient of the compressible fluid, it needed to collate the relationship between the discharge coefficient and the pressure ratio for each tooth. It was also related to the fact that the flow of the fluid through the constriction became compressible and the flow eventually became choked. Choked flow was a restricted condition that occurred when the mass flow rate did not increase with a further decrease in the downstream pressure while the upstream pressure was fixed.

EFFECT OF COMPRESSIBLITY

The carry-over coefficient compressibility factor, φ, defined as the ratio of the carry-over coefficient of a cavity that includes effect of kinetic energy carry-over for compressible flow to that for incompressible flow through a labyrinth seal with the same geometry and at the same Reynolds number, was found to have two linear relationships with positive and negative slopes regarding the pressure ratios. It was found that this result was not associated with the seal geometry because c/w and c/s for both single and multiple cavity labyrinth seals were located within the nearly same ranges. Further, the φ-Pr relationship was found to be independent of the number of teeth regardless of single and multiple cavity labyrinth seals. Hence, the effect of the carry-over coefficient compressibility factor could be considered to be included into the leakage model.

The discharge coefficient compressibility factor, ψ, defined as the ratio of the discharge coefficient of flow of an ideal gas to the discharge coefficient for an incompressible fluid for the same tooth at the same Reynolds number, was found to be a linear relationship with pressure ratios across the tooth as Saikishan predicted. However, in certain flow and seal geometric conditions, Saikishan's model needed to be modified for the deviation appearing when the pressure ratios were decreased. Hence, a modified ψ-Pr relationship including Saikishan's model was presented in order to compensate for the deviation between the simulations and his model.

RECOMMENDED FUTURE WORK

1. There are certain limits of flow and seal geometric conditions in which this thesis can provide the estimation of the leakage mass flow rate.

   The limits are: $100 < Re < 5000$, $0.06 < c/w < 5$, $0.015 < c/s < 0.0375$, $0.0075 < w/s < 0.25$, $0.9625 < h/s < 0.985$

   compared with Saikishan's conditions: $250 < Re < 15000$, $0.015 < c/w < 0.3745$, $0.0075 < c/s < 0.0375$, $0.0075 < w/s < 0.5$, $0.75 < h/s < 4$.

   Developing a new model or modifying the limits developed in this work to accommodate most labyrinth seals would require much more simulations. The same can be said about higher Reynolds numbers and larger turbomachinery. However, this could be a probable future work.

2. The φ-Pr relationship is not associated with seal geometry. Nonetheless, it is recommended to study more simulations to define c/w dependence in order to verify the effects of seal geometry on the φ-Pr relationship.
3. The carry-over coefficient of incompressible flow, as the tooth width increases (w: $0.03/0.4\ mm \rightarrow 1\ mm$), presents a great contrast to that predicted by Saikishan's model although seal geometry of simulations exists within the range of his model. Therefore, it is recommended to study more simulations to verify not only the dependence on the wide tooth width in more detail but also the accuracy of Saikishan's model for the relatively wide tooth width.
4. Saikishan [14] considered that the discharge coefficient of a downstream tooth could be expressed as a function of only the carry-over coefficient of the preceding cavity. However, it is found that there exist other factors related with the discharge coefficient of a downstream tooth. Therefore, it is recommended to find the other factors which can influence the discharge coefficient of a downstream tooth.
5. These studies have dealt with air as compressible fluid and water as incompressible fluid. However, in certain applications, Carbon Dioxide (CO_2) and Helium (He) can be utilized as compressible working fluids and Oils (C_8H_{18} or $C_{12}H_{23}$) can also be employed as incompressible fluids. Therefore, it is recommended to study other compressible and incompressible fluids as working fluids.
6. These studies have modified the ψ-Pr relationship. However, it is necessary to compare this new relationship with other previous models which have both CFD simulations and experimental data. Therefore, it is recommended to study whether

the modified relationship is truly better to be employed to consider the effects of compressibility.

7. These studies are limited to tooth on stator, straight through labyrinth seals with rectangular cavities and unbeveled teeth. Thus, it is recommended to study the effects of cavity shapes, beveled teeth, staggered and tooth on rotor designs utilizing a similar approach as presented in this thesis.
8. These studies have been validated against one of earlier models which has only CFD simulations data. However, more experimental studies and exhaustive validation are recommended in order to acquire more exact prediction of the leakage mass flow rate.

REFERENCES

1. Gamal, A.M., 2007, "Leakage and Rotodynamic Effects of Pocket Damper Seals and See-Through Labyrinth Seals," Ph.D. Dissertation. Texas A&M University, College Station, U.S.A.

2. Hodkinson, B., 1939, "Estimation of the Leakage through a Labyrinth Gland," Proceedings of the Institution of Mechanical Engineers **141**, pp. 283–288.

3. Alford, J.S., 1965, "Protecting Turbomachinery from Self-Excited Rotor Whirl," ASME Transaction – Journal of Engineering for Power. pp. 333–334.

4. Martin, H., 1908, "Labyrinth Packings," Engineering, pp. 35–36.

5. Egli, A., 1935, "The Leakage of Steam through Labyrinth Seals," Trans. ASME, **57**, pp. 115–122.

6. Vermes, G., 1961, "A Fluid Mechanics Approach to the Labyrinth Seal Leakage Problem," ASME Transactions – Journal of Engineering for Power, **83** (2), pp. 161–169.

7. Childs, D.W., 1993, *Turbomachinery Rotodynamics – Phenomena, Modeling, and Analysis*, John Wiley & Sons, New York, U.S.A.

8. Gurevich, M.I., 1965, *Theory of Jets in an Ideal Fluid*, Translated by Street, R.L. and Zagustin, K., Academic Press, New York, U.S.A.

9. Zimmerman, H., and Wolff, K.H., 1987, "Comparison between Empirical and Numerical Labyrinth Flow Correlations," ASME 87-GT-86.

10. Vennard, J.K., and Street, R.L., 1982, *Elementary Fluid Mechanics*, John Wiley & Sons, New York, U.S.A.

11. Childs, D.W., and Scharrer, J., 1988, "Theory versus Experiment for the Rotordynamic Coefficient of Labyrinth Gas Seals: Part II – A Comparison to Experiment," Journal of Vibration, Acoustics, Stress and Reliability in Design, **110**, pp. 281–287.

12. Esser. D., and Kazakia, J.Y., 1995, "Air Flow in Cavities of Labyrinth Seals," International Journal of Engineering Science, **33** (15), pp. 2390–2326.

13. Morrison, G.L., and Al-Ghasem, A., 2007, "Experimental and Computational Analysis of a Gas Compressor Windback Seal," GT2007-27986, *Proceedings of ASME Turbo Expo 2007*, Montreal, Canada, May 14–17.

14. Suryanarayanan, S., 2009, "Labyrinth Seal Leakage Equation," M.S. Thesis, Texas A&M University, College Station, U.S.A.

15. Suryanarayanan S., and Gerald M., 2009, "Analysis of Flow Parameters Influencing Carry-Over Coefficient," GT2009-59245, *Proceedings of ASME Turbo Expo 2009*, Orlando, Florida, U.S.A., June 8–12.

16. Suryanarayanan S., and Gerald M., 2009, "Effect of Tooth Height, Tooth Width, and Shaft Diameter on Carry-Over," GT2009-59246, *Proceedings of ASME Turbo Expo 2009*, Orlando, Florida, U.S.A., June 8–12.

17. Suryanarayanan S., and Gerald M., 2009, "Labyrinth Seal Discharge Coefficient for Rectangular Cavities," 2009, FEDSM2009-78152, *Proceedings of FEDSM 2009*, Vail, Colorado, U.S.A., August 2–6.

18. Rhode, D.L., and Hibbs, R.I., 1993, "Clearance Effects on Corresponding Annular and Labyrinth Seal Flow Leakage Characteristics," Journal of Tribology, **115**, pp. 699–704.

19. Moore, J.J., 2003, "Three-Dimensional CFD Rotordynamic Analysis of Gas Labyrinth Seals," Journal of Vibration and Acoustics, **125** (4), pp. 427–433.

20. Vakili, A.D., Meganathan, A.J., Michaud, M.A., and Radhakrishnan, S., 2005, "An Experimental and Numerical Study of Labyrinth Seal Flow," GT2005-68224, *Proceedings of ASME Turbo Expo 2005*, Reno-Tahoe, Nevada, U.S.A., June 6–9.

21. Wittig, S., Schelling, U., Kim, S., and Jacobsen, K., 1987, "Numerical Predictions and Measurements of Discharge Coefficients in Labyrinth Seals," ASME 87-GT-188.

22. Jones, W.P., and Launder, B.E., 1972, "The Prediction of Laminarization with a Two-Equation Model of Turbulence," International Journal of Heat and Mass Transfer, **15**, pp. 301–314.

23. Launder, B.E., and Sharma, B.I., 1974, "Application of the Energy Dissipation Model of Turbulence to the Calculation of Flow Near a Spinning Disc," Letters in Heat and Mass Transfer, **1** (2), pp. 131–138.

24. Bardina, J.E., Huang, P.G., and Coakley, T.J., 1997, "Turbulence Modeling Validation, Testing, and Development," NASA Technical Memorandum 110446.

25. Patankar, S.V., 1980, *Numerical Heat Transfer and Fluid Flow*, Hemisphere Pub. Corporation, Taylor & Francis Group, New York, U.S.A.

26. Ferziger, J.H., and Peric M., 2001, *Computational Methods for Fluid Dynamics,* Springer-Verlag, Berlin Heidelberg, Germany.

APPENDIX A

Table A.1. Seal geometries applied for simulations of air

Case No.	No. of Teeth	Clearance (mm)	Pitch (mm)	Tooth Width (mm)	Tooth Height (mm)	Shaft Diameter (mm)
1	2	0.06	4	0.03	3.94	60
2	2	0.06	4	0.03	3.94	60
3	2	0.06	4	0.03	3.94	60
4	2	0.06	4	0.03	3.94	60
5	2	0.06	4	0.03	3.94	60
6	2	0.06	4	0.03	3.94	60
7	2	0.06	4	1	3.94	60
8	2	0.06	4	1	3.94	60
9	2	0.06	4	1	3.94	60
10	2	0.06	4	1	3.94	60
11	2	0.06	4	1	3.94	60
12	2	0.06	4	1	3.94	60
13	2	0.09	4	1	3.91	60
14	2	0.09	4	1	3.91	60
15	2	0.09	4	1	3.91	60
16	2	0.09	4	1	3.91	60
17	2	0.09	4	1	3.91	60
18	2	0.09	4	1	3.91	60
19	2	0.15	4	0.4	3.85	60
20	2	0.15	4	0.4	3.85	60
21	2	0.15	4	0.4	3.85	60
22	2	0.15	4	0.4	3.85	60
23	2	0.15	4	0.4	3.85	60
24	2	0.15	4	0.4	3.85	60
25	4	0.06	4	1	3.94	60
26	4	0.06	4	1	3.94	60
27	4	0.06	4	1	3.94	60
28	4	0.06	4	1	3.94	60
29	4	0.06	4	1	3.94	60
30	4	0.06	4	1	3.94	60

Table A.2. Seal geometries applied for simulations of water

Case No.	No. of Teeth	Clearance (mm)	Pitch (mm)	Tooth Width (mm)	Tooth Height (mm)	Shaft Diameter (mm)
1	2	0.06	4	0.03	3.94	60
2	2	0.06	4	0.03	3.94	60
3	2	0.06	4	0.03	3.94	60
4	2	0.06	4	0.03	3.94	60
5	2	0.06	4	0.03	3.94	60
6	2	0.06	4	0.03	3.94	60
7	2	0.06	4	1	3.94	60
8	2	0.06	4	1	3.94	60
9	2	0.06	4	1	3.94	60
10	2	0.06	4	1	3.94	60
11	2	0.06	4	1	3.94	60
12	2	0.06	4	1	3.94	60
13	2	0.09	4	1	3.91	60
14	2	0.09	4	1	3.91	60
15	2	0.09	4	1	3.91	60
16	2	0.09	4	1	3.91	60
17	2	0.09	4	1	3.91	60
18	2	0.09	4	1	3.91	60
19	2	0.15	4	0.4	3.85	60
20	2	0.15	4	0.4	3.85	60
21	2	0.15	4	0.4	3.85	60
22	2	0.15	4	0.4	3.85	60
23	2	0.15	4	0.4	3.85	60
24	2	0.15	4	0.4	3.85	60
25	4	0.06	4	1	3.94	60
26	4	0.06	4	1	3.94	60
27	4	0.06	4	1	3.94	60
28	4	0.06	4	1	3.94	60
29	4	0.06	4	1	3.94	60
30	4	0.06	4	1	3.94	60

APPENDIX B

Table B.1. Seal geometries utilized by Saikishan

Case No.	No. of Teeth	Clearance (mm)	Pitch (mm)	Tooth Width (mm)	Tooth Height (mm)	Shaft Diameter (mm)
1	2	0.03	4	0.03	4	60
2	2	0.06	4	0.03	4	60
3	2	0.09	4	0.03	4	60
4	2	0.15	4	0.03	4	60
5	2	0.06	8	0.03	8	60
6	2	0.06	4	0.03	3	60
7	2	0.06	4	0.03	8	60
8	2	0.06	4	0.03	16	60
10	2	0.06	4	0.2	4	60
11	2	0.06	4	0.4	4	60
12	2	0.06	4	0.6	4	60
13	2	0.06	4	1	4	60
14	2	0.06	4	2	4	60
15	2	0.03	4	1	4	60
16	2	0.09	4	1	4	60
17	2	0.15	4	1	4	60
18	2	0.15	4	2	4	60
19	2	0.06	4	0.03	4	180
20	2	0.06	4	0.03	4	300
21	8	0.06	4	0.03	4	60
22	1	0.03	–	0.2	4	60
23	1	0.06	–	0.4	4	60
24	1	0.09	–	0.6	4	60
25	1	0.15	–	1	4	60
26	1	0.03	–	0.4	4	60
27	1	0.15	–	2	4	60
28	1	0.03	–	0.6	4	60
29	1	0.03	–	1	4	60
30	1	0.06	–	2	4	60
31	1	0.03	–	2	4	60
32	1	0.06	–	0.4	3	60
33	1	0.06	–	0.4	8	60
34	1	0.06	–	0.4	4	180

Table B.1. Continued

Case No.	No. of Teeth	Clearance (mm)	Pitch (mm)	Tooth Width (mm)	Tooth Height (mm)	Shaft Diameter (mm)
35	2	0.03	4	0.2	4	60
36	2	0.09	4	0.6	4	60
37	4	0.06	4	1	4	60
38	2	0.06	4	0.4	8	60
39	2	0.03	4	0.4	4	60
40	2	0.06	4	0.4	4	180

APPENDIX C

STANDARD κ-ε TURBULENCE MODEL

The κ-ε model is one of the most common turbulence models. It is a two equation model, that means, it includes two extra transport equations to represent the turbulent properties of the flow. This allows a two equation model to account for history effects like convection and diffusion of turbulent energy.

The first transported variable is turbulent kinetic energy, κ. The second transported variable in this case is the turbulent dissipation, ε. It is the variable that determines the scale of the turbulence, whereas the first variable, κ, determines the energy in the turbulence.

There are two major formulations of κ-ε models [22], [23]. That of Launder and Sharma is typically called the "Standard" κ-ε Model. The original impetus for the κ-ε model was to improve the mixing-length model, as well as to find an alternative to algebraically prescribing turbulent length scales in moderate to high complexity flows.

The κ-ε model [24] has been shown to be useful for free-shear layer flows with relatively small pressure gradients. Similarly, for wall-bounded and internal flows, the model gives good results only in cases where mean pressure gradients are small; accuracy has been shown experimentally to be reduced for flows containing large adverse pressure gradients. One might infer then, that the κ-ε model would be an inappropriate choice for problems such as inlets and compressors.

for turbulent kinetic energy, κ

$$\frac{\partial}{\partial t}(\rho\kappa) + \frac{\partial}{\partial x_i}(\rho\kappa u_i) = \frac{\partial}{\partial x_j}\left[\left(\mu + \frac{\mu_t}{\sigma_\kappa}\right)\frac{\partial \kappa}{\partial x_j}\right] + P_\kappa + P_b - \rho\varepsilon - Y_M + S_\kappa \quad \text{(C. 1)}$$

for dissipation, ε

$$\frac{\partial}{\partial t}(\rho\varepsilon) + \frac{\partial}{\partial x_i}(\rho\varepsilon u_i) = \frac{\partial}{\partial x_j}\left[\left(\mu + \frac{\mu_t}{\sigma_\varepsilon}\right)\frac{\partial \varepsilon}{\partial x_j}\right] + C_{1\varepsilon}\frac{\varepsilon}{\kappa}(P_\kappa + C_{3\varepsilon}P_b) - C_{2\varepsilon}\rho\frac{\varepsilon^2}{\kappa} + S_\varepsilon \quad \text{(C. 2)}$$

$$\mu_t = \rho C_\mu \frac{\kappa^2}{\varepsilon} \quad \text{(C. 3)}$$

$$P_\kappa = -\rho\overline{u_i' u_j'}\frac{\partial u_j}{\partial x_i} \quad \text{(C. 4)}$$

$$P_\kappa = \mu_t S^2 \quad \text{(C. 5)}$$

$$S \equiv \sqrt{2S_{ij}S_{ij}} \quad \text{(C. 6)}$$

$$P_b = \beta g_i \frac{\mu_t}{Pr_t}\frac{\partial T}{\partial x_i} \quad \text{(C. 7)}$$

Where, Pr_t is the turbulent Prandtl number for energy and g_i is the component of the gravitational vector in the ith direction. For the standard and realizable models, the default value of Pr_t is 0.85. The coefficient of thermal expansion is also defined as

$$\beta = -\frac{1}{\rho}\left(\frac{\partial \rho}{\partial T}\right)_p \quad \text{(C. 8)}$$

A set of constants recommended by Jones and Launder [22] after examination of a considerable body of experimental data is

$C_{1\varepsilon} = 1.44$, $C_{2\varepsilon} = 1.92$, $C_\mu = 0.09$, $\sigma_\kappa = 1.0$, $\sigma_\varepsilon = 1.3$

APPENDIX D

FINITE VOLUME METHOD

The finite volume method is a method for representing and evaluating partial differential equations in the form of algebraic equations. Similar to the finite difference method or finite element method, values are calculated at discrete places on a meshed geometry. “Finite volume” refers to the small volume surrounding each node point on a mesh. In the finite volume method, volume integrals in a partial differential equation that contain a divergence term are converted to surface integrals, using the divergence theorem. These terms are then evaluated as fluxes at the surfaces of each finite volume. Because the flux entering a given volume is identical to that leaving the adjacent volume, these methods are conservative. Another advantage of the finite volume method is that it is easily formulated to allow for unstructured meshes.

Discretization using the finite volume method can be illustrated by considering the unsteady 2-D transport equation for a scalar quantity, ϕ

$$\int_V \frac{\partial \rho \phi}{\partial t} dV + \oint \rho \phi \vec{v} \cdot d\vec{A} = \oint \Gamma_\phi \nabla \phi \cdot d\vec{A} + \int_V S_\phi \, dV \qquad \text{(D. 1)}$$

ρ	Density
$\vec{v}$	Velocity vector
$\vec{A}$	Surface area vector
Γ_ϕ	Diffusion coefficient for a scalar quantity, ϕ
$\nabla \phi$	Gradient of a scalar quantity, ϕ
S_ϕ	Source of per unit volume of a scalar quantity, ϕ

$$\frac{\partial \rho \phi}{\partial t} V + \sum_{f}^{N_{faces}} \rho_f \vec{v}_f \phi_f \cdot \vec{A}_f = \sum_{f}^{N_{faces}} \Gamma_\phi \nabla \phi_f \cdot \vec{A}_f + S_\phi V \quad \text{(D. 2)}$$

N_{faces} Number of faces enclosing cell

ϕ_f Value of a scalar quantity, ϕ, convected through a face, f

$\rho_f \vec{v}_f \phi_f \cdot \vec{A}_f$ Mass flux through a face, f

$\vec{A}_f$ Area of a face, f

$\nabla \phi_f$ Gradient of a scalar quantity, ϕ, at a face, f

V Cell volume

APPENDIX E

SIMPLE ALGORITHM

In computational fluid dynamics, SIMPLE algorithm is a widely used numerical procedure to solve the Navier-Stokes equations. SIMPLE is an acronym for Semi-Implicit Method for Pressure Linked Equations. The SIMPLE algorithm was developed by Prof. Brian Spalding and his student S. V. Patankar at Imperial College, London in the early 1970s. Since then it has been extensively used by many researchers to solve different kinds of fluid flow and heat transfer problems. Many popular books on computational fluid dynamics discuss the SIMPLE algorithm in detail [25], [26]. This algorithm forms the basis of Commercial CFD (Computational Fluid Dynamics) packages. A modified variant is the SIMPLER algorithm (SIMPLE Revised), that was in 1979 introduced by Patankar.

If a steady-state problem is being solved iteratively, it is not necessary to fully resolve the linear pressure-velocity coupling, as the changes between consecutive solutions are no longer small. The SIMPLE algorithm:

- An approximation of the velocity field is obtained by solving the momentum equation. The pressure gradient term is calculated using the pressure distribution from the previous iteration or an initial guess.
- The pressure equation is formulated and solved in order to obtain the new pressure distribution.
- Velocities are corrected and a new set of conservative fluxes is calculated.

The basic steps in the solution update are as follows:

1. Set the boundary conditions.
2. Compute the gradients of velocity and pressure.
3. Solve the discretized momentum equation to compute the intermediate velocity field.
4. Compute the uncorrected mass fluxes at faces.
5. Solve the pressure correction equation to produce cell values of the pressure correction.
6. Update the pressure field: $p^{k+1} = p^k + urf \cdot p'$, where urf is the under-relaxation factor for pressure.
7. Update the boundary pressure corrections, p'_b.
8. Correct the face mass fluxes: $\dot{m}_f^{k+1} = \dot{m}_f^* + \dot{m}'_f$
9. Correct the cell velocities: $\vec{v}^{k+1} = \vec{v}^* - \frac{Vol\nabla p'}{\vec{a}_P^v}$, where $\nabla p'$ is the gradient of the pressure corrections, $\vec{a}_P^v$ is the vector of central coefficients for the discretized linear system representing the velocity equation and Vol is the cell volume.
10. Update density due to pressure changes.

VITA

Jeng Won Woo was born and raised in Seoul, Republic of Korea. He earned his Bachelor of Science in mechanical engineering at Yonsei University, Republic of Korea in 2000. After graduation, he worked at COSMOIT Company for about 3 years instead of his compulsory military services and then at Doosan Heavy Industries & Construction Company for over 2 years. At COSMOIT Company, he was involved in developing bank automation machinery and counterfeit currency counters. Also, at Doosan Heavy Industries & Construction Company, he conducted performance and system designs of thermal power plants, executed test operations, and settled trouble shooting occurring at thermal power plants.

He came to the United States of America to pursue graduate studies in mechanical engineering at Texas A&M University, College Station, Texas, in the Fall of 2008. He worked in the Turbomachinery Laboratory under the guidance of Dr. Gerald L. Morrison. His research has concentrated on the labyrinth seals to reduce the leakage mass flow rate caused by the pressure difference between each stage in the turbomachine. He received a Master of Science in mechanical engineering at Texas A&M University in May 2011.

Jeng Won Woo can be contacted through Texas A&M University's Department of Mechanical Engineering at the following address:

Texas A&M University

Department of Mechanical Engineering

c/o Dr. Gerald L. Morrison

3123 TAMU, College Station, TX 77843-3123, U.S.A.